Cerebral CT- and MRI perfusion: Techniques and clinical application in iNPH

Doerthe Constantinescu Ziegelitz

Department of Radiology

Institute of Clinical Sciences

Sahlgrenska Academy at University of Gothenburg

UNIVERSITY OF GOTHENBURG

Cover illustration: Coronal T1, sagittal T2 and trans-axial CBF map of an iNPH patient.

Cerebral CT- and MRI perfusion: Techniques and clinical application in iNPH

doerthe.ziegelitz@vgregion.se

ISBN 978-91-628-9372-9

Printed in Gothenburg, Sweden 2015
Kompendiet, Aidla Trading AB

„Wer A sagt, der muß nicht B sagen. Er kann auch erkennen, daß A falsch war.“

(Svensk översättning: Har man sagt A, behöver man inte säga B. Man kan istället inse att A var felaktig.)

Bertolt Brecht (1898-1956)

Für meine Eltern

Cerebral CT- and MRI perfusion: Techniques and clinical application in iNPH

Doerthe Constantinescu Ziegelitz

Department of Radiology, Institute of Clinical Sciences
Sahlgrenska Academy at University of Gothenburg
Göteborg, Sweden

ABSTRACT

Idiopathic normal pressure hydrocephalus (iNPH) is a disorder of the elderly, defined by slowly progressive impairment of gait and balance, cognitive decline, and incontinence. Disturbance of the cerebrospinal fluid (CSF) dynamics results in ventriculomegaly without intracranial pressure increase. Treatment by CSF diversion is successful in about 80% of the cases. Better preoperative identification of non-responders is required.
The pathophysiology of iNPH is obscure, but linked to cortical and especially subcortical cerebral blood flow (CBF) reductions. The association between perfusion and the severity of the clinical features is not clearly established and a predictive perfusion pattern has not been identified.
CT-perfusion (CTP) and Dynamic susceptibility contrast MRI perfusion (DSC MRI) offer advantages compared to traditional perfusion techniques, but are so far not of significant use in iNPH.
The aim of this thesis was to compare CTP and DSC MRI in iNPH and to study their potential role as investigational techniques by exploring the pre- and postoperative CBF changes, how these correlate to the severity of the symptoms and, subsequently, the prognostic value of CBF.
Fifty-one patients with suspected iNPH and 24 age-matched healthy individuals (HI) were recruited. At baseline all subjects had CTP and DSC MRI on 2 consecutive days. Patients repeated the perfusion measurements 3 months after shunting. Probable iNPH was diagnosed corresponding to the European-American iNPH guidelines and clinical performance was scored according to a recently published scale. After drop-outs, omission secondary to unsuccessful imaging and exclusion of non iNPH patients, 20 HI and 21 patients with complete preoperative imaging remained. One patient died prior to shunting. Postoperative DSC MRI was successful in all 20 cases and CTP in 17. Deconvolution generated absolute CBF estimates that eventually were normalized against an internal reference. Region of interest analysis was used for evaluation. Seventy-five percent of the patients were shunt responders. Correction of partial volume effects (PVE) of the arterial input function increased the accuracy of DSC MRI in HI. Despite PVE correction the linear

relationship on the group level and the agreement between the modalities was limited. In iNPH, preoperative global and regional perfusion deficits, most pronounced in the periventricular white matter (PVWM), were measured by DSC MRI and, in spite of a limited spatial coverage, also by CTP. After shunting, DSC MRI and CTP demonstrated CBF restoration in responders in all anatomical regions and remaining hypoperfusion in the PVWM of non-responders. Postoperative metallic valve artefacts restricted the DSC MRI evaluation to one hemisphere, but were no issue in CTP. A valid prognostic CBF threshold was not identified. Regional and global CBF correlated with the severity of symptoms of iNPH. Patients with higher preoperative perfusion performed better in clinical tests and a lower preoperative perfusion resulted in a more marked postoperative improvement. Although the agreement of CTP and DSC MRI is limited, both methods contain perfusion information. The good general consistency of the results of CTP and DSC MRI measurements in the same material indicates reliability of both methods. DSC MRI and CTP might be used as investigational tools in iNPH.

Keywords: *Idiopathic normal pressure hydrocephalus, Dynamic susceptibility contrast MRI, Computed tomography perfusion, Cerebral perfusion*

ISBN: 978-91-628-9372-9

SAMMANFATTNING PÅ SVENSKA

Normaltryckshydrocefalus är en sjukdom som vanligtvis drabbar äldre personer. Tillståndet karakteriseras av en störning av hjärnvätskans (likvor) cirkulation, vilket leder till en vidgning av de vätskeförande hålrummen i hjärnan utan att nämnvärt höja trycket innanför skallbenet. Orsaken till sjukdomen är oklar, varför den kallas ”idiopatisk”. De typiska symptomen vid idiopatisk normaltryckshydrocefalus (iNPH) är långsamt tilltagande gång- och balansrubbningar, kognitiv svikt och urininkontinens. Sjukdomen behandlas genom att avleda likvor via en så kallad shunt, dvs. en permanent slang som löper från hjärnans hålrum under huden till bukhålan, där likvor tas upp av kroppen. Behandlingsresultaten är goda i ungefär 80 % av fallen, men det vore önskvärt att kunna förutse vilka 20 % av patienterna som inte kommer att svara på denna behandling.

Även om alla bakomliggande faktorer till detta tillstånd inte är kartlagda, så är iNPH förknippad med generellt och regionalt nedsatt blodflöde i hjärnan. Det har inte entydigt visats att den nedsatta genomblödningen har ett samband med symptomens svårighetsgrad och man har hittills inte kunnat förutsäga behandlingsresultaten med hjälp av blodflödesmätningar.

Datortomografi (DT) och magnetisk resonanstomografi (MR) kan användas för att mäta genomblödningen (perfusion) av hjärnan. Dessa metoder har en del fördelar i jämförelse med andra mättekniker, men har hittills inte eller endast i mycket begränsad omfattning använts i samband med iNPH.

Syften med denna avhandling var att jämföra DT- och MR-baserade perfusionsmätningar och undersöka om de kan användas som verktyg inom iNPH forskning och klinik. Målet var att utforska om man kan mäta störningarna i perfusionen hos iNPH-patienter och relatera störningarna till symptomens svårighetsgrad och om perfusionsmätningarna kan användas för att förutse effekten av shuntbehandlingen.

Femtioen patienter med möjlig iNPH och 24 friska kontrollpersoner ur samma åldersgrupp inkluderades i studien. Patienterna och kontrollerna genomgick en DT- och en MR-baserad perfusionsmätning med en dags mellanrum. Tre månader efter operation upprepades dessa undersökningar i patientgruppen. Diagnosen sannolik iNPH ställdes preoperativt om de Europeisk-Amerikanska kriterierna för detta var uppfyllda och patienternas handikapp bedömdes med hjälp av en nyligen utvecklad skala. En del patienter avbröt sitt deltagande i studien, andra fick uteslutas p.g.a. ofullständigt bildmaterial eller p.g.a. att diagnoskriterierna inte var uppfyllda. Tjugo friska kontroller och 21 iNPH-patienter hade bedömbara preoperativa bildsekvenser och kunde vara kvar i studien. Efter operation hade 20 patienter användbara MR-baserade perfusionsmätningar och 17 av dessa

också en bedömbar DT-undersökning. Absoluta blodflödesvärden beräknades och normaliserades vid behov mot blodflödesvärdet i bakre hjärnbarken. Utvärderingen av perfusionen gjordes genom att mäta blodflödet i utvalda, avgränsade regioner av hjärnan. Hos 75 % av patienterna förbättrades symptomen avsevärt efter operationen och dessa representerar den shunt-positiva gruppen.

Korrektionen av så kallade partiella volymseffekter, som stör när man mäter blodflödet i en tillförande artär i hjärnan, resulterade i en bättre mätnoggrannhet av MR-metoden i ett försök med friska kontrollpersoner. Trots denna korrektion visade de CT- och MR-baserade mätmetoderna dock en begränsad linjär relation och dålig överensstämmelse. Före shuntinläggningen uppmättes med hjälp av DT, som täckte endast ett litet område av hjärnan, och med MR hos iNPH patienterna en generell och regional nedsättning av perfusionen, som var mest uttalad i den vita substansen närmast hjärnans hålrum. Efter operation visade DT- och MR-baserade perfusionsmätningar en återhämtning av blodflödet i den shunt-positiva gruppen, medan patienter som inte svarade på behandlingen hade en oförändrat reducerad perfusion i den vita substansen nära hjärnans hålrum. Shunten orsakade störningar vid mätningar med MR, men inte med DT. Något specifikt blodflödesmönster som kunde förutse behandlingseffekten identifierades inte.

Hjärnans perfusion uppvisade ett samband med iNPH-besvärens intensitet. Patienter med bättre preoperativ perfusion klarade kliniska tester bättre och patienter som hade en sämre perfusion förbättrades tydligare efter shuntinläggningen.

Även om de DT- och MR-baserade metoderna inte ger samma värden, speglar båda hjärnans genomblödning. Förändringen av perfusionen hos iNPH-patienterna och sambandet mellan perfusion och symptomatologi kunde visas med både DT och MR. Denna överensstämmelse gör att båda teknikerna kan anses som tillförlitliga och användbara inom iNPH-forskningen.

LIST OF PAPERS

This thesis is based on the following studies, referred to in the text by their Roman numerals.

I. Ziegelitz D, Starck G, Mikkelsen IK, Tullberg M, Edsbagge M, Wikkelsø C, Forssell-Aronson E, Holtås S, Knutsson L.
Absolute quantification of cerebral blood flow in neurologically normal volunteers: dynamic susceptibility contrast MRI-perfusion compared with computed tomography (CT)-perfusion.
Magn Reson Med. 2009 Jul; 62(1):56-65

II. Ziegelitz D, Starck G, Kristiansen D, Jakobsson M, Hultenmo M, Mikkelsen IK, Hellström P, Tullberg M, Wikkelsø C.
Cerebral perfusion measured by dynamic susceptibility contrast MRI is reduced in patients with idiopathic normal pressure hydrocephalus.
J Magn Reson Imaging. 2014 Jun; 39(6):1533-42

III. Ziegelitz D, Arvidsson J, Hellström P, Tullberg M, Wikkelsø C, Starck G.
In patients with idiopathic normal pressure hydrocephalus postoperative cerebral perfusion changes measured by dynamic susceptibility contrast MRI correlate with clinical improvement.
Submitted and accepted for publication in JCAT 2015

IV. Ziegelitz D, Arvidsson J, Hellström P, Tullberg M, Wikkelsø C, Starck G.
Pre- and postoperative cerebral blood flow changes in patients with idiopathic normal pressure hydrocephalus measured by CT-perfusion
Submitted

CONTENT

ABBREVIATIONS

AD	Alzheimer's disease
ADC	Apparent diffusion coefficient
AIF	Arterial input function
AVIM	Asymptomatic ventriculomegaly with features of normal pressure hydrocephalus on MRI
CBF	Absolute cerebral blood flow
CBV	Cerebral blood volume
CNS	Central nervous system
Cr	Creatine
CSF	Cerebrospinal fluid
CT	Computed tomography
CTP	CT-perfusion
CTTC	Concentration-to-time curve
CVR	Cerebrovascular reactivity
DESH	Disproportionately enlarged subarachnoid space hydrocephalus
DSC MRI	Dynamic susceptibility contrast MRI
DTI	Diffusion tensor imaging
DWI	Diffusion weighted imaging
EA	European-American

EI	Evans’ index
ELD	Extended lumbar drainage
ETV	Endoscopic third ventriculostomy
fMRI	Functional MRI
FOV	Field of view
FT	Fourier transform
GE	Gradient echo
gCBF	Global cerebral blood flow
GM	Grey matter
HI	Healthy individuals
ICP	Intracranial pressure
iNPH	Idiopathic normal pressure hydrocephalus
m	Months
MRI	Magnetic resonance imaging
MRS	Magnetic resonance spectroscopy
MTT	Mean transit time
NAA	N-acetylaspartate
NAWM	Normal appearing white matter
NPH	Normal pressure hydrocephalus (iNPH+ sNPH)

oSVD	Block-circulant singular value decomposition
PET	Positron emission tomography
Pixel	Picture element
PSP	Progressive supranuclear palsy
PVE	Partial volume effects
PVWM	Periventricular white matter
R2	Transversal relaxation rate (s-1)
RAVLT	Rey auditory verbal learning test
rCBF	Relative cerebral blood flow
regCBF	Regional cerebral blood flow
rrCBF	Relative, regional cerebral blood flow
Ro	CSF outflow resistance
ROI	Region of interest
SAE	Subcortical arteriosclerotic encephalopathy
SAS	Subarachnoid space
SE	Spin echo
sNPH	Secondary normal pressure hydrocephalus
SNR	Signal to noise ratio
SPECT	Single photon emission computed tomography

SVD	Singular value decomposition
T1	Longitudinal relaxation time (ms)
T2	Transversal relaxation time (ms)
VOF	Venous output function
Voxel	Volume element
VPS	Ventriculoperitoneal shunt
WM	White matter
y	Years

1 INTRODUCTION

Idiopathic normal pressure hydrocephalus (iNPH) is a condition of unknown cause in the elderly, characterized by ventricular dilatation and a gradual onset of gait impairment, imbalance, cognitive deterioration and urinary disturbances. Shunting of the cerebrospinal fluid system relieves the complaints in the vast majority of cases. Without treatment the symptoms progress and the patients deteriorate. iNPH is underdiagnosed, as the symptoms and imaging findings might be confused with "normal aging" or misinterpreted as some other neurological disorder such as Alzheimer's disease or subcortical arteriosclerotic encephalopathy. Patients with iNPH tend also to be undertreated as it is difficult to estimate the benefit of the surgical procedure in relation to its risks. The identification of a bio- or imaging marker that can predict the outcome after shunting would therefore be helpful.

Although the pathophysiology of iNPH is still not fully understood, there is widespread agreement that subcortical hypoperfusion is an important contributing factor. However, the association between the level of perfusion and the severity of the clinical features of iNPH is not clearly established and a perfusion pattern predictive of good shunt outcome has not been identified.

Perfusion measurements in the iNPH patient group have mostly been performed by Xenon computed tomography, single photon emission computed tomography and positron emission tomography. Newer perfusion techniques like dynamic susceptibility contrast MRI (DSC MRI) and computed tomography perfusion (CTP) have so far not been of any significant use in iNPH. Both these techniques offer methodological advantages, such as inert tracers, better spatial resolution and sensitivity for deep anatomical structures. These factors might be favorable for measurements of perfusion in iNPH.

The aim of this thesis was to compare DSC MRI and CTP in iNPH and to study their potential role as investigational techniques by exploring:

- the pre- and postoperative cerebral blood flow changes,
- the correlation between blood flow and symptomatology and
- the prognostic value of blood flow.

2 PERFUSION

2.1 General considerations

The term" perfusion" describes the capillary blood flow in tissue. Since many neurological diseases are associated with changes in the cerebral blood flow (CBF), the study of brain perfusion can contribute to diagnosis, lesion characterization and follow-up of treatment results.

The measurement of perfusion requires a technique, an indicator and a model.

The different imaging-based techniques build upon one of three possible principles and use an exogenous or endogenous indicator:

* Dynamic imaging of the distribution of a tracer that is restricted to the vasculature at first pass. The corresponding techniques are magnetic resonance imaging (MRI) and computed tomography (CT).

* Static monitoring of the absorption of a diffusible tracer, used in single photon emission computed tomography (SPECT), positron emission tomography (PET) and stable Xenon computed tomography (Xenon CT).

* Direct imaging of blood motion, applied in intravoxel incoherent motion and arterial spin labeling.

For the calculation of the perfusion parameters 3 main models exist:

1) The maximum slope model

This model was initially applied to perfusion measurements with intra-arterially, almost instantaneously administered microspheres as indicators. As microspheres are captured at the level of the capillaries, they are "extracted" at first pass. The rate, i.e. the slope, of the indicator accumulation curve and the perfusion of a region define the total amount of microspheres gathered in that area[1].

2) The equilibrating indicator model

This model is mainly implemented when diffusible tracers are used, like in SPECT and stable Xenon CT. It is supposed that equivalence is achieved between the tracer concentrations in the brain tissue of different areas and the blood in accordance to the perfusion in those regions. By determination of the concentration of the tracer in blood and tissue, the CBF for each picture element (pixel) can be calculated[1] .

3) The central volume principle

In this model regional vascular structures are viewed as separate volumes through which the whole amount of an introduced indicator eventually passes[2-6]. Ideally, the injection of the indicator bolus is infinitely short and arrives instantaneously at time 0 at tissue level, with a total amount C_0 of indicator. The residue function, R(t), describes the fraction of the indicator present in the vascular network of the tissue at each time point after the injection and is a decreasing function of time. The tissue concentration of the indicator as function of time, $C_t(t)$, is proportional to CBF:

$C_t(t) = CBF \cdot C_0 \cdot R(t)$

The tissue residue function scaled with CBF, CBF·R(t), is called the tissue impulse response function.

In vivo, using intravenous tracer injection, the bolus is not instantaneous or infinitely narrow, but delivered to the brain tissue in a dispersed form and with delay, as the tracer first has to be carried through the minor circulation. By monitoring the concentration-to-time curve (CTTC) of the indicator in a supplying cerebral artery, $C_a(t)$, the actual distribution of the tracer over time can be measured. This curve is called the arterial input function (AIF). The tissue CTTC becomes the convolution of the tissue impulse response function with the AIF:

$C_t(t), = CBF \cdot C_a(t) \otimes R(t)$

By deconvolution of the AIF and the tissue CTTC, which are measurable variables, the tissue impulse response function is determined. At time point zero R(0) = 1 by definition, and thus, the initial/maximum height of the impulse response function equals the CBF.

Deconvolution can be performed in different ways.

One approach is the model-dependent or parametric deconvolution, in which the indicator is assumed to have a specific behavior or the vascular structure to have a certain appearance. Some known residue function models of the vasculature are the “box-shaped” (parallel capillaries with equal lengths and transit times, the “gaussian” (parallel capillaries with a Gaussian distribution of lengths and mean transit time) and the “exponential” (the vasculature is a single, well mixed compartment)[1,4]. The applied analytical function mirrors the vascular model. A risk associated with this technique is, that an inconsistent signal pattern, caused by a pathological process, might be forced to match the expected, physiological model. However, Mouridsen et al.[7] have proposed the use of a Bayesian estimation algorithm and a vascular model of heterogeneous capillary flow, which seem to outperform the singular value decomposition methods (SVD)[8].

The SVD method is one of several different deconvolutions that are model-independent or non-parametric. As the name states, no theory about the

underlying nature of the vasculature is established. However, also in this approach regularization is necessary, e.g. to suppress noise, oscillations and negative values. The SVD[3,4] is the most widely used method in this group and performed in the time domain. Deconvolution in the frequency domain is done by the transform approach, e.g. the Fourier transform (FT)[9,10]. While model independent FT generally is considered being very sensitive to noise and to underestimate CBF at high flow rates[3,4], SVD is also biased with regard to noise[11] and affected by delay of the AIF. The latter problem has been corrected by introducing the block-circulant SVD (oSVD) by Wu et al.[12]. Other proposed concepts to perform non-parametric deconvolution use a statistical [13-15] or an algebraic approach[4,16,17].

2.2 Dynamic susceptibility contrast MRI-perfusion

MRI-based perfusion techniques are attractive because they do not expose the patients to ionizing radiation.

MRI offers various approaches for the measurement of cerebral perfusion. The perfusion can be performed with an exogenous/non-diffusible or endogenous/diffusible tracer. If exogenous contrast agents are used, the perfusion study can be done in the steady state or dynamically with either T1- or T2 weighted imaging sequences.

Dynamic susceptibility contrast MRI perfusion (DSC MRI)[18] is the most widely used technique. DSC MRI tracks the first pass of a tracer through the vessles of the brain by means of a fast, dynamic spin echo (SE) or gradient echo (GE) sequence, generating T2 or T2* weighted images, respectively. The tracer, a paramagnetic gadolinium-based chelate, is administred at high rate intravenously and remains in the intravascular space, if the blood-brain-barrier is not disrupted. This compartmentalization results in microscopic susceptibility gradients which reach beyond the vascular space into the adjacent tissue. The gradients cause the local protons to dephase, thereby increasing their transverse relaxation rate (ΔR_2 or ΔR_2*), visible as signal loss. The degree of signal loss depends on the amount of tracer in each pixel, i.e. the perfusion, and on the magnetic field strengt of the MRI machine. Further, the SE sequence is sensitive to the microvasculature, while measurements by a GE sequence are equally sensitive for all vessel sizes above 4 µm[19]. This implies, that the signal drop in SE sequences is much smaller, which has to be met by doubling the amount of contrast used in GE-based perfusion. DSC MRI is most often performed using T2* weighted imaging, because of its inherent higher signal-to-noise ratio (SNR).

The signal loss over time is registered pixel-wise and then mathematically converted into a CTTC. This conversion is built upon the assumption, that there is

a) a proportionality between the contrast agent concentration in tissue (C) and the T2* relaxation rate change [$\Delta R_2^* = kC$] [20]
b) an exponential relationship between the signal change (S_c = post-contrast signal; $S_{0=}$ baseline signal) and the product of echo time (TE) and the T2* relaxation rate change. [$S_c(t) = S_0 e^{-TE\Delta R2^*}$] [21]

The concentration of the contrast agent is given by combining assumptions a and b:

$$C(t) = -\frac{1}{kTE} \ln\left(\frac{S_c(t)}{S_0}\right)$$

Usually *k*, a proportionality constant, is unknown and the concentration is given in arbitrary units.

For optimal signal decrease during bolus passage at 3T, a single dose of gadobutrol (Gd-BT-DO3A, Gadovist ®, 1.0, Schering AG, Berlin, Germany) or gadobenate dimeglumine (Gd-BOPTA, Multihance®, Bracco, S.p.A., Milan, Italy) is sufficient, due to the higher gadolinium concentration or higher T2* relaxivity of these tracers, respectively[22]. At lower magnetic field strenght, a double dose of a contrast agents with low or a single dose of a tracer with high gadolinium concentration is recommended[23,24]. According to the guidelines from the European Society of Urogenital Radiology (ESUR) regarding contrast media safety and nephrogenic systemic fibrosis (NSF) macrocyclic gadolinium-chelates, e.g. gadobutrol, can be administred even to patients with the highest stage of chronic kidney failure, as long as no additional gadolinum-based contrast is given within the following 7 days[25] .

Figure 1. Five "snapshots" out of 1440 source images of the DSC MRI sequence, used in this work. Shown is the slice at the level of the lateral ventricles. Images (a-e) are taken at different time points during the first passage of the tracer, which causes a signal loss on T2 weighted scans. Image (a) represents a baseline image prior to the arrival of the bolus. Baseline is about 40 s long. Image (b) is taken shortly after bolus arrival, (c) at the maximum signal drop and image (d) during wash-out of the bolus. This bolus passage takes about 15 s. Image (e) shows the status after the bolus passage, when the signal has almost returned to baseline.*

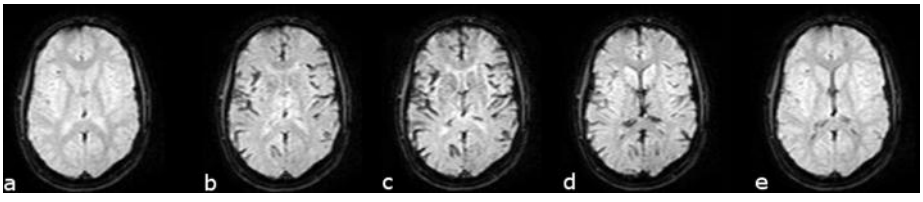

The contrast agent is administrated by a power injector and followed by a saline chase injection. An injection rate of 5ml/s is often used in order to prevent any additional broadening of the CTTC beyond the effect of dispersion caused by the passage of the indicator through the heart and lungs[26]. Broader AIF lead to an underestimation of the CBF [27,28].

As explained in the above section about the central volume principle, the impulse response function is estimated by deconvolution of the AIF and the tissue CTTC, and the CBF is determined as the maximal height of the estimated impulse response function.

The absolute cerebral blood volume (CBV) is most accurately described by integrating the area under the tissue impulse response function or by integrating the area of the tissue CTTC after a gamma variate fitting[29,30].

The mean transit time (MTT), i.e. the mean value for a distribution of transit times of all blood components through a given brain volume, is determined according to the central volume theorem, i.e. MTT= CBV: CBF [2,5,6].

CBF refers to the total blood flow in the capillaries per unit tissue mass, measured in ml/ (min ·100g). CBV describes the volume of blood per unit tissue mass, measured in ml/ 100g. CBF and CBV are estimated voxel wise, i.e. per volume element, and therefore, the measurements are converted to perfusion rates per unit mass of tissue by using an estimate for the tissue density of brain, typically 1.05 g/ml [10]. MTT is measured in seconds (s).

Due to the fact that the indicator is only distributed in the blood plasma and not the full blood volume, the CBF and CBV values have further to be corrected for differences in hematocrit between large vessels (as the AIF) and the capillaries. There is no consensus about the correct factor. In the normalization proposed by Rempp et al.[10], a large vessel hematocrit of 0.45 and a small vessel hematocrit of 0.25 were applied.

A PET study [31] reported the average values (±SD) for CBF, CBV and MTT listed in table 1 and noted that "CBF and CBV decreased with age approximately 0.5% per year".

Table 1. PET-based absolute mean perfusion estimates according to Leenders et al.[31] in a group of 34 healthy volunteers age range 22-82y

	Grey matter Mean ± SD	White matter Mean ± SD
CBF ml/ (min ·100g)	54.5 ±12.3	22.2 ± 4.9
CBV ml/100g	5.2 ± 1.4	2.7 ± 0.6
MTT s	5.7	7.3

Standard DSC MRI usually does not offer true absolute quantification of CBF and CBV. The reported grey-to-white matter (GM/WM) ratios are normally quite appropriate, but the CBF and CBV values are usually higher in comparison with the gold standard of PET-measurements and the reproducibility of DSC MRI perfusion only moderate[32,33]. The inaccuracy of the AIF is the major problem in this context. Partial volume effects (PVE)[34,35], arterial signal saturation at peak concentration[36] and local geometric distortion[37] lead to an underestimation of the AIF and a subsequent overestimation of CBF and CBV. Among these influencing factors, PVE are especially crucial.

To increase the accuracy and repeatability of the AIF, different criteria to identify the optimal AIF and automated methods to select a global AIF have been proposed[10,38,39]. Further, to minimize the underestimation of CBF secondary to dispersion, the concept of local or regional AIF in close proximity to the tissue of interest has been studied[40-42].

Another issue regarding the accuracy of the perfusion measurements is related to the fact that the transverse relaxivity of intravascular and extravascular protons during the passage of the bolus differ, which violates the assumptions of proportionality between contrast agent concentration and ΔR_2^*[43-45]. This effect probably contributes to the overestimation of perfusion by DSC[46].

The echo time in DSC MRI is a tradeoff between a prolonged TE that is optimal for the signal at tissue level and shorter TE values that offer an optimal AIF without saturation and a better SNR at baseline[36,46].

The temporal resolution of T2* weighted DSC MRI should not be lower than 1.5s. A reduced sampling rate might return an inaccurate form of the CTTC and an underestimation of the CBF[27].

The perfusion values of each pixel are used to create grey scale parametric perfusion maps which also can get color-encoded for easier visual assessment.

Due to the above mentioned quantification problems, DSC MRI-based perfusion estimates are usually presented as relative values. The CBF estimate of a certain region of interest (ROI) is divided by the perfusion value of an internal reference, e.g., a ROI in the contra-lateral white matter (WM), which results in a relative CBF value (rCBF)[47].

2.3 CT-perfusion

CT-perfusion (CTP) was described already by L. Axel[48] 1980, but first after the development of spiral CT systems in the 1990s and the associated faster image acquisition, CT perfusion started to spread.

In CTP, like in DSC MRI and other bolus tracking techniques, a rapid intravenous injection of a contrast agent is followed by monitoring the first pass of the tracer through the cerebral vasculature by dynamic imaging. In CTP the iodinated contrast agent causes an increase in attenuation, which is registered pixel by pixel. If the tracer remains within the vasculature, a linear relationship exists between the attenuation and the contrast agent concentration, which facilitates quantitative measurements. The registered density-to-time curve in each pixel can readily be converted into a CTTC. Based on this curve absolute CBF, CBV, MTT estimates can be calculated [48]. However, in CTP the measured density change is much weaker than the signal change in DSC MRI perfusion with a resulting low SNR for CTP.

The earliest cerebral CTP studies[49,50] calculated CBF based on the maximum slope model and required high injection rates of 10-20 ml/s. To achieve such high injection rates a venous catheter with a large diameter (14 gauge) had to be placed, a demanding procedure in elderly people and in an acute clinical setting. Further, the risk of extravasation of contrast during bolus injection was increased at these rates. Even at high injection rates the basic assumptions of the maximum slope model, i.e. the maximum gradient of the tissue CTTC has to be reached before venous outflow starts, is violated in CTP [51]. Consequently, CBF is underestimated and if the maximum slope model is used at low injection rates also the GM/WM ratio will be corrupted[1].

The introduction of a commercially available deconvolution technique improved the computation of the perfusion parameters and permitted for the use of more acceptable injection rates of 3-5 ml/s [52,53] that can be achieved using smaller venous catheters, sized 18-22 gauge. The method was validated against the microsphere method in animals [54-57] and stable Xenon CT and $H_2{}^{15}O$ PET in humans [17,58,59].

In accordance with DSC MRI, the most wide spread model for the calculation of perfusion parameters is the central volume principle [2,5,6] in combination with a model-free deconvolution method, guaranteeing the most accurate

results at low injection rates of iodinated contrast material according to Wintermark et al. [1].

Several non-parametric deconvolution approaches are in theory applicable to CTP, e.g. an algebraic method[4,16,17], SVD[3,4], oSVD[12], FT[10]. A model dependent deconvolution method, the Bayesian estimation algorithm[7,8] , was originally proposed for DSC MRI but can be applied to CTP and has shown promising accuracy and delay insensitivity, outperforming oSVD[60].

As stated in the central volume theorem[2,5,6] CBV, MTT and CBF are related by a simple equation and if two of these variables are known, the third can be calculated. In CTP, there are, compared to DSC MRI perfusion, more kinetic models determining in which order the perfusion parameters are to be derived.

a) Most kinetic models start by calculating the CBV.

   For the estimation of CBV the area under the tissue CTTC can be divided by the area under a venous, purely vascular, CTTC (VOF)[1,48]. According to the mass conversation principle, the area under the CTTC for artery, tissue and vein ought to be constant. However, the observed contrast enhancement represents only the vascular compartment, which in the brain parenchyma only constitutes a small fraction of a pixel. The tissue CTTC is thus influenced by PVE from nerve cells, axons, myelin sheets, etc. and the area under the curve underestimated. The VOF, if measured correctly in a large venous sinus, usually at the confluence sinuum, is free from PVE. The VOF can therefore be used to calculate the vascular fraction of the tissue CTTC. If the area under the AIF is referenced to the area under the VOF and, thus, without PVE, the corrected AIF might also be used as denominator in the above mentioned fraction[61].

   Alternatively, CBV is defined as the area under the impulse response function, which in theory is equivalent to the above mentioned tissue/VOF CTTC integrals. The tissue/VOF CTTC integrals can however be influenced by recirculation effects and overestimate CBV and appear to be more sensitive to noise, which is filtered out by deconvolution when CBV is defined as the area under the impulse response function[62].

b) Some schemes that calculate CBV as the area under the tissue CTTC divided by the area under the VOF advocate the computation of MTT as a second step.

   Wintermark et al.[1] define the MTT as the weighted mean of the transit-time distributions of the tissue impulse response function. According to Östergaard et al.[4] and Weisskoff et al.[63] this definition

cannot be applied to DSC MRI and CTP, as these techniques do not measure the concentration of the tracer leaving the parenchyma, but instead the concentration remaining in the tissue. Subsequently, a transport function for venous output is not available, which would be the prerequisite for the MTT calculation as described by Wintermark et al.[1]

Other researchers estimate MTT as the ratio of the area under the impulse response function and the maximum height of that curve[54,56,64].

c) When CBV is calculated as the area under the impulse response function, usually CBF is the second perfusion variable to be determined by measurement of the maximum height of the impulse response function[52].

In similarity to DSC MRI the CBF and CBV values have to be corrected for the difference in hematocrit between large and small vessels and are expressed as rates per unit mass of tissue[10].

Perfusion parameters are usually presented as grey scale and color-encodes maps for visual assessment.

Figure 2. CTP-based color-encoded CBF, CBV and MTT maps at the level of the basal ganglia

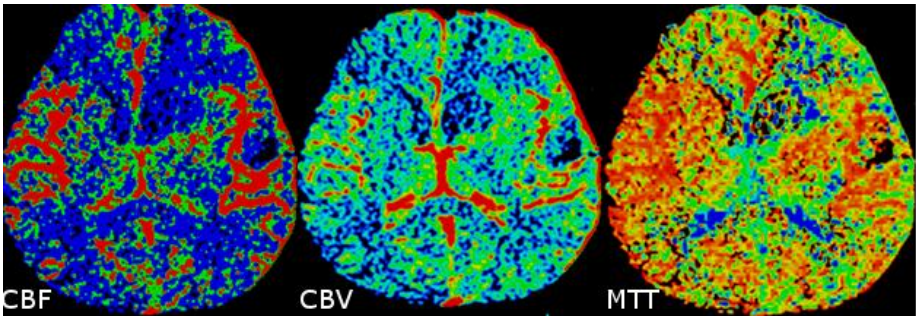

The cranio-caudal anatomical coverage of a CTP study is dependent on the width of the CT detector. The 16-detector row scanner used in this work can screen a 2 cm slab, which might contain two 10 mm or four 5 mm thick sections. With a 64- detector row scanner from the same manufacturer the generated slab measures 4 cm. The combination of a wide detector and the toggling-table technique, in which the scanner table moves back and forth between two adjacent cine views, extends the coverage at the cost of lower

temporal resolution[65,66]. Finally, the latest 320-detector row scanners offer a combined time-resolved CT angiography and CTP of the whole brain[67,68].

Iodinated contrast material serves as tracer, which is usually safe, but the glomerular function, estimated from the serum creatinine value, should, ideally, be known, especially in older patients and in those with diabetes or other risk factors for contrast medium induced renal failure. In patients with severe renal failure, contrast media may be contraindicated, unless the procedure is considered life-saving[69].

Keeping the total amount of iodine constant, higher contrast agent concentrations result in increased maximum enhancement of vessels and parenchyma and an improvement of the SNR and of the accuracy of the perfusion estimates[23,70]. The use of highly concentrated contrast agents allows reducing the volume of the bolus, which shortens the administration time, and, thereby, the risk of CTTC truncation and erroneous perfusion estimates is diminished[71]. Further, the width of the CTTCs is decreased, which in analogy to DSC MRI, improves the accuracy of the perfusion values. However, the increased viscosity of a highly iodinated contrast medium results in an injection pressure rise limiting the iodine delivery rate, which might counteract the positive effects of a higher iodine concentration[72].

At constant injection rates, the administration of equal bolus volumes of 300 or 400 mg iodine /ml[73] or increasing the bolus volume beyond 30 ml of 300 mg iodine/ml[74] does not result in significantly different quantitative perfusion values, calculated either by the maximum slope model[73] or the central volume principle[74].

Like in DSC MRI, sparse data sampling during CTP influences the form of the CTTC and thereby the quantitative perfusion estimates. Usually tissue CBF and CBV get overestimated and MTT underestimated. The optimal temporal resolution of CTP is 0.5-2 seconds. However, sampling intervals of 3 to 4 seconds, which are common when using the toggling-table technique, can be partly compensated for by increasing the administered volume of the contrast agent[74].

Wintermark et al.[75] showed that a reduction of the tube voltage from the initially used 120kV to 80kV generated a better contrast enhancement and an improved contrast between grey matter (GM) and WM at a lower radiation dose, without significantly increasing the image noise. Photons in an 80-kV X-ray spectrum are closer to the K-edge of iodine, which results in an increased photoelectric effect at this tube voltage.

CTP performed with a 512×512 matrix and a field of view (FOV) of 250mm has a much better in-plan spatial resolution than DSC MRI. Yet, even in CTP the AIF might be affected by PVE, which can be accounted for by scaling with a VOF free from PVE[61]. The location of the AIF has no significant

impact on the quantitative or qualitative results of CTP, as long as the AIF is not placed distal to an occlusion or significant stenosis[76-78] and the AIF and especially the VOF with the maximal peak enhancement are selected[77,79]. Automated post-processing of CTP data, avoiding operator dependent choices of AIF, VOF and other variables, can aid to reduce the inter-observer variability[80].

A disadvantage of CTP is the exposure of patients to radiation. The published effective doses vary depending on the image acquisition parameters and the CT scanner. Perfusion scans of high temporal resolution (0.5-1 seconds) usually generate effective doses slightly higher than a plain head CT on a similar scanner[56,74,81]. Comprehensive protocols for 320-detector row scanners can amount to a total effective dose of 11.2 mSv[82]. Yet, when a temporal resolution of 4 seconds is chosen, the reported effective dose for a whole brain conventional CT, time-resolved CT angiography and CTP in one acquisition is equivalent to a routine head CT[83].

2.4 Summary DSC MRI and CTP

The results of DSC MRI and CTP are influenced by technique inherent limitations like low SNR and PVE and by the choice of imaging parameters, for example temporal resolution, tracer characteristics and scan duration. Further, the applied method of perfusion calculation is of great importance. The accuracy and reliability of the perfusion parameters, tested on phantoms and patients, vary considerably among different post-processing algorithms[71,84-86]. Direct comparison of absolute perfusion estimates cannot be done among different software programs and even relative values contain errors[84] .

Therefore, standardization of perfusion analysis and consensus regarding imaging protocols are desirable, not only for research purposes but also regarding clinical decision making, e.g., perfusion thresholds defining the penumbra or the grade of primary brain tumors.

3 CEREBROSPINAL FLUID AND COMPLIANCE

Cerebrospinal fluid (CSF)

The CSF is located within the ventricular system of the brain, the central canal of the spinal cord and in the subarachnoid space (SAS) surrounding both the brain and the spinal cord. It bears up the weight of the brain and spinal medulla, protects the central nervous system (CNS) from the effects of trauma, maintains a balanced chemical environment for the CNS and is a variable in the intracranial pressure (ICP) regulation.

It is widely believed, that CSF is mainly produced by the choroid plexuses of the ventricles even if alternate sites of CSF formation exist, e.g. the ependyma, the cerebral pial surface, the interstitial fluid and the SAS. Whether the alternate sites contribute on a constant basis to the CSF production or only gain importance under non-physiological circumstances is unclear[87,88]. One theory claims that the water component of the CSF (99 %) forms a functional unit with the interstitial fluid, which is regulated by osmotic and hydrostatic forces at the CNS capillaries[89].

The composition of CSF differs from plasma regarding ion concentrations, cell count and amount of glucose. Diffusion, active transports and free passage of water have a part in the CSF formation[87]. In young human adults the production rate of CSF is 0.41ml/min (approximately 500 ml/day)[90], quite constant and not pressure-dependent below an ICP of 200mm water. The production and the content of the CSF are controlled in detail by the autonomic nervous system, humoral regulations and, in the case of increased intraventricular pressure, by the pressure gradient over the blood-brain-barrier. However, vasoconstriction, hypotension and the interference of drugs with active transport mechanisms can cause a down regulation of the CSF formation[88].

The CSF net flow is promoted by the cardiac cycle and rapid respiratory waves, and it moves from the lateral ventricles through the interventricular foramina into the 3rd ventricle and further down through the cerebral aqueduct into the fourth ventricle. From here CSF passes through the midline aperture into the cisterna magna and via the lateral apertures into the pontine cisterns. From the basal cisterns some CSF spreads caudally into the spinal canal and the remaining CSF flows rostrally within the basal cisterns. From there, CSF continues to flow into the narrow SAS around the brain and upwards, towards the superior sagittal sinus.

Traditionally, the CSF outflow from the SAS is supposed to occur through a dual system: Drainage along cranial and spinal nerve sheaths into lymphatic vessels and via the arachnoid granulations within the lumen of the venous sinuses and the epidural venous plexus in the spine.

The mechanism of the lymphatic outflow is not completely understood, but in animal studies the olfactory nerve pathway, followed by the optic and acoustic nerve regions have regularly shown communication between the SAS and the lymphatic system[91].

The CSF drainage routes via the arachnoid granulations are assumed to be especially important later in life, indicated by their increasing number and size with age[87,91]. The exact mechanism of the CSF absorption at the arachnoid granulations is still debated. In humans these structures do not show free communications between the SAS and the venous sinuses, although CSF, containing substances of varying molecular weight and lipid solubility, is drained this way. It is hypothesized that a pressure dependent vacuolization in the arachnoid granulations, together with active transport and diffusion might explain the process of resorption[87,92,93]. In the spine the CSF absorption is larger in the prone position during activity than in the resting, supine position, presumably as gravity induces increased pressure gradients[94].

Other proposed CSF resorption sites are the leptomeningeal vessels[87] and periventricular capillaries[89,95,96]. In rats the transependymal CSF resorption increases in relation to the severity of the induced hydrocephalus[97].

Recently, a glymphatic system has been proposed in which extracellular proteins are cleared from the interstitium to the CSF. CSF enters the parenchyma along the arterial, para-vascular space, interchanges with interstitial fluid, which leaves the brain along para-venous tracks. The transfer through the parenchyma depends on water transport via the astrocytic aquaporin-4 water channels. Trauma and ischemia seem to affect these water channels negatively, thereby reducing the clearance of waste products from the brain[98,99].

The normal, total CSF volume in adults is about 150 ml and the turnover rate of CSF is between three to five times per day in young adults. During aging the liquor spaces increase secondary to loss of parenchyma and the choroid plexa as well as the arachnoid granulations degenerate. Consequently, the turnover rate in this population decreases[87,88,90].

Compliance

Traditionally, a malfunctioning CSF resorption at the level of the arachnoid granulations was thought to cause the ventriculomegaly in communicating

hydrocephalus. However, such an outflow obstruction should rather result in the dilatation of the SAS than in ventriculomegaly[100].

Instead, it has been shown that an increased intraventricular CSF pulse pressure without elevation of the mean CSF pressure can cause communicating hydrocephalus[101,102].

The pulse pressure is the intermittent ICP rise during systolic arterial inflow into the cranial cavity, prior to the expulsion of CSF and venous blood from the cranium. The latter keeps the total intracranial volume constant. The size of the pulse pressure depends on the compliance of the thecal sac and the intracranial vascular system[103]. Compliance is defined as the property of a material to deform/ change in volume when exposed to pressure and is decreased in NPH[96,104-108].

A consequence of the reduced compliance in NPH is an increase in pulse pressure and in cerebral venous pressure, which will reduce the compliance further.

According to Bateman[106], an increase in venous pulse pressure prevents CSF absorption via the arachnoid granulations. Instead CSF is cleared via the transependymal pathway.

Compliance decreases with age[109] or secondary to conditions that render the intracranial arteries stiffer. Both factors are present in iNPH, which affects the elderly and is associated with a higher frequency of hypertension and cerebrovascular WM disease[110-114].

CSF infusion leads to a decrease in compliance and CSF diversion increases the compliance as a slight overdrainage induces a compensatory increase of the venous and capillary blood volume and, subsequently, a dilatation of the veins[100,106].

4 IDIOPATHIC NORMAL PRESSURE HYDROCEPHALUS

4.1 Definition

iNPH, a disease of the elderly, can be described as an active dilatation of the ventricular system of unknown cause and without intraventricular obstruction or increased ICP. Clinically, the disorder is characterized by a subcortical symptomatology of slowly progressive impairment of gait, balance, continence and cognition. If the patient presents with a history of intracranial infection, subarachnoid or intraventricular hemorrhage several months to years prior to the development of normal pressure hydrocephalus, the syndrome is classified as secondary (sNPH) and believed to be caused by leptomeningeal fibrosis.

4.2 Symptoms

Disturbance of the gait is often the first symptom to be noted and the main complaint of the patients. The gait is hypokinetic, characterized by short, broad-based, shuffling steps with low foot-floor elevation and an outward rotation of the toes and occasional freezing[115,116]. Apart from the gait also other motor functions are impaired, which can result in brady- and hypokinesia of the upper extremities and the face, a reduced ability to turn from side to side in bed or to rise from a supine to a sitting position[117,118].

Patients often experience their imbalance and postural difficulties as a tendency to lean or fall backwards, which is related to an abnormal subjective visual vertical perception[119].

Urinary urgency, increased frequency of urination and urgency incontinence dominate among lower urinary tract symptoms in iNPH[120] and develop usually later than the other symptoms, or not at all[121].

Applying the classification system for organic psychiatric disorders[122] iNPH patients present initially with astheno-emotional disturbances (concentration and memory difficulties, fatigue, irritability and/or emotional lability), followed by emotional-motivational problems (apathy , emotional indifference, lack of drive) and /or somnolence-sopor-coma disorders (impaired wakefulness, general slowing and dampening of cognitive, emotional, conative and motor processes)[123] . Cerebrovascular comorbidity aggravates the neuropsychological impairment[121].

4.3 Epidemiology

The most recent and so far largest community-based prevalence study of iNPH, by Jaraj et al.[124], evaluated retrospectively CT scans and clinical performance of 1238 Swedish elderly. Probable iNPH was defined, in concordance with the European-American diagnostic guidelines[125], as ventricular dilatation without signs of cortical atrophy, impaired gait and either cognitive disturbance and/ or incontinence. The reported prevalence was 0.2% in those aged 70–79 years and 5.9% in patients aged 80 years and older. According to the authors' calculations, 2 million European citizens above the age of 70 years may suffer from iNPH.

The prevalence in earlier studies has varied between 0.1 and 2.9%[126-130]. The populations of those studies were in general younger than in the work by Jaraj et al.[124], which probably explains the lower prevalence values. In addition, variations of the results are also due to methodological differences and the use of non-uniform diagnostic criteria.

4.4 Diagnosis

4.4.1 Diagnostic criteria

The existence of diagnostic criteria enables the distinct definition of a study population, which is essential for research findings to be comparable. This was, however, not the case for iNPH until Japanese guidelines for the clinical diagnosis of iNPH were published in 2002 , supplemented by a summary in English 2004[131] and followed by European-American (EA) guidelines in 2005 [125,132]. The Japanese management guidelines in full length, in English, became available in 2008[133] and a second, updated version in 2012[134]. Although the Japanese and EA guidelines differ to some extent, their existence and gradually increasing worldwide acceptance, are improving the comparability of study results.

In both guidelines the diagnosis of iNPH is based on the medical history, clinical data, imaging findings on CT or MRI and on physiological data, and the likelihood of the iNPH diagnosis is graded. The criteria of the EA guidelines are summarized in table 2.

Table 2. Summary of the diagnostic criteria of iNPH according to the European-American guidelines[125]

	Probable iNPH	Possible iNPH
Clinical history	Insidious onset of symptoms; after age of 40 y; duration of at least 3 to 6 m; no known cause; progressive over time; absence of other conditions that might explain symptoms	May have a subacute or indeterminate onset; begin at any age; have lasted less than 3 m or indeterminately; follow conditions that are unlikely causally related; non- or not clearly progressive; not entirely attributable to other conditions
Clinical findings	Impaired gait/balance (mandatory) combined with either or both of disturbed cognition and continence	Incontinence and/or cognitive impairment in the absence of a gait or balance disturbance; Alternatively; gait disturbance or dementia alone
Imaging	EI > 0.30, not entirely caused by atrophy; No obstruction to CSF flow; One of the following supportive features 1. Enlargement of temporal horns not entirely caused by hippocampus atrophy 2. Callosal angle ≥40 degrees 3. Altered periventricular water content not attributable to arteriolosclerosis or demyelination 4. Flow void in aqueduct or 4th ventricle	EI > 0.30; No obstruction to CSF flow; Cerebral atrophy potentially explaining ventricular size; Structural lesions potentially influencing ventriculomegaly are accepted
Physiological data	CSF opening pressure of 5–18 mm Hg (or 70–245 mm H2O)	Opening pressure measurement not available or pressure outside the range of probable INPH
Improbable or unlikely iNPH: 1. No ventriculomegaly 2. Increased ICP 3. No component of the clinical triad of INPH 4. Symptoms are explained by other conditions		

According to the EA criteria the patients´ age at disease onset should be >40y, but the typical iNPH patient has reached retirement when the symptoms become noticeable, as also indicated by the above cited prevalence studies (section 4.3). According to the Japanese guidelines the patient has to be >60y old to meet the criteria of iNPH.

ICP can be measured in different ways and in different compartments, but in the context of hydrocephalus and benign intracranial hypertension lumbar CSF pressure is usually assessed. Optimally, monitoring should be performed over a period of at least 30 minutes, registering pressure and pulse amplitudes. Instantaneous measurements of the height of the CSF column may be inaccurate due to CSF pressure variations over time[135]. According to a consensus of experts the expected "normal ICP" in iNPH, defined as

baseline lumbar opening pressure in the supine position, should be between 60 and 240 mm H_2O or 4.4 to 17.6 mmHg[136], which in the EA-guidelines, by the same experts, was translated to 70–245 mm H_2O or 5–18 mm Hg. These values are somewhat higher than the ICP reference interval of 106-194 mm H_2O or 7.8-14.3 mm Hg (defined as 5th to 95th percentiles), reported in healthy elderly with a mean age of 70y[137] and in the young and middle-aged[138]. The CSF opening pressure has to be ≤ 200 mmH_2O, when implementing the Japanese guidelines.

4.4.2 Scales

For pre- and postoperative grading of the general impairment or the severity of specific symptoms in iNPH a number of different scales have been developed and are in use[139-143]. The lack of a uniform scale hampers the comparison of research results between different medical centers. In an attempt of standardization, Hellström et al.[144] proposed a new scale, in which the clinical performance of iNPH patients is estimated in total and in the 4 domains that exhibit the most characteristic features of the disease; gait, balance, continence and neuropsychology. Ordinal or continuous measurements are performed, balancing feasibility and accuracy, and for all domains normality is clearly described.

At our NPH center, a neurologist, a neuropsychologist and a physiotherapist share the task of scoring the patients´ performance, applying the parts of the above mentioned scale[144] that they are trained for.

4.4.3 Supplementary tests

Marmarou et al.[136] concluded in their evidence-based guidelines for the use of supplementary, pre-surgical tests, that a "single standard for the prognostic evaluation of INPH patients was lacking". However the use of supplementary tests could increase the prognostic accuracy to more than 90%.

The spinal tap test, a supplementary test during which 40-50 ml of CSF are withdrawn, simulates shunting. According to the guidelines136, a "positive" test result, i.e. when the patient shows significant clinical improvement after the CSF removal, can be of prognostic value, but a negative test cannot exclude patients from surgery due to the low sensitivity of the test. In agreement with this recommendation, the negative predictive value of this test was low (18%) in the European iNPH Multicenter Study[145]. At the same time, the positive predictive value of the spinal tap test was merely slightly higher (88%) than the positive outcome rate (84%) after selecting patients for shunt surgery based only on clinical performance and imaging[145]. Thus, the spinal tap test did not notably add to the prognostic accuracy.

CSF outflow resistance (Ro) can be measured in different ways, for example by the Katzman infusion test[146] or the bolus method[147], and the reported thresholds defining an increased Ro, i.e., the dysfunctional absorption of CSF, vary depending on the used methodology. In a sample of healthy elderly the median Ro was 8.6 mm Hg/mL/min and the 90th percentile 17.4 mm Hg/mL/min[137], whereas in iNPH patients Ro is usually increased[148,149]. In the guidelines[136] the accuracy of Ro is described as higher than that of the CSF tap test, why the determination of Ro might be of complementary prognostic value when the tap test is negative. The somewhat higher accuracy of Ro estimates was confirmed in the European iNPH Multicenter Study[150]. This study further showed that neither Ro nor a combination of CSF tap test and Ro should exclude patients from shunt surgery.

According to the guidelines[136], the supplementary test with the highest sensitivity (50-100%) and highest positive predictive value (80-100%) is the prolonged external lumbar drainage (ELD) of more than 300ml over several days by an intrathecal catheter, but this test requires hospitalization of the patients and is accompanied by an increased risk of complications like CSF overdrainage and infection of the CNS.

Marmarou et al.[136] also evaluated cisternography and the continuous recording of ICP variables, like the frequency and shape of so called B waves, and concluded that these techniques do not aid in the identification of iNPH shunt responders.

However, recordings of ICP pulsatility[151] have shown that increased wave amplitudes indicate favorable outcome after shunting with a positive predictive values of >90%. The negative predictive value of this variable was likewise >90%. The major drawback of this type of supplementary test is its invasive nature and need for hospitalization.

4.4.4 Imaging

General considerations

Imaging in the work up of iNPH is today mainly performed by CT and MRI. Imaging at its best is meant to

1) support or rule out the diagnosis of iNPH
2) establish differential diagnoses
3) aid in the treatment control
4) predict shunt-responsiveness

Like other biomarkers, imaging markers ought to represent objective findings which can be measured accurately and reproducibly as indicators of a pathogenic process and should disclose or predict the incidence and outcome of the disease and the effects of treatment. The search for such an imaging

marker for iNPH is still ongoing and summarized in the paragraphs below about imaging features of iNPH.

Possible differential diagnoses regarding iNPH are subcortical arteriosclerotic encephalopathy (SAE), Alzheimer's disease (AD), multi infarct dementia, Parkinson´s disease and age-related changes of the brain. These conditions usually demonstrate brain atrophy and WM changes that can also be found in iNPH patients and especially central atrophy might be mistaken for or difficult to differentiate from hydrocephalus.

In most aspects of iNPH imaging MRI is superior to CT. Without exposure to radiation, MRI allows a much more detailed soft tissue characterization and a better visualization of the ventricular system and can, contrary to CT, easily demonstrate flow in the cerebral aqueduct or the 4th ventricle, which is one of the EA diagnostic criteria for probable iNPH[125].

Further, MRI also offers non-morphological imaging like diffusion weighted sequences including diffusion tensor imaging, functional MRI, phase contrast MRI (PC-MRI), magnetic resonance spectroscopy and magnetic resonance elastography (MRE), which are potentially of diagnostic and prognostic value. The only advanced image sequence that can be implemented in both CT and MRI studies, is the measurement of cerebral perfusion.

In cases in which the suspicion of iNPH is already fairly high, the imaging method of choice is usually an MRI examination. Yet, usually, the first radiological examination is an unenhanced brain CT study. This might be ordered to support the possible diagnosis of iNPH and to rule out differential diagnoses, but is more often done for other clinical reasons than suspected iNPH, e.g. trauma, ischemic events, vertigo, and then reveals radiological signs of iNPH as an incidental finding.

Treatment control can be done by either CT or MRI. At our clinic an unenhanced brain CT is routinely performed within 24 h after shunt-insertion, to inspect the shunt position and to rule out complications as for example intracranial hemorrhage. Also routinely, postoperative MRI examinations are done after 3 months, together with a neurological clinical follow up. In patients with adjustable shunts, the opening pressure of the shunt system might change within the magnetic field during the examination why the shunt settings have to be checked with conventional radiographic imaging prior to and after the MRI investigation.

The investigation of mechanical shunt dysfunction includes the inspection and palpation of the accessible parts of the shunt and an X-ray of the shunt system to search for tube disconnections. Sometimes a radionuclide shuntography controlling the shunt patency[152] or an infusion test is performed. In cases of shunt obstruction Ro is elevated[153]

Ventricular dilatation

In both the EA and the Japanese diagnostic criteria for iNPH[125,134], imaging has to provide proof of ventricular enlargement by demonstrating an Evans' index (EI)[154] larger than 0.3. The EI is the ratio between the maximal width of the frontal horns and the maximal inner diameter of the skull, established in the same trans-axial slice of either a CT or an MRI examination. However, depending on the angulation of the trans-axial slices and the slice chosen for the measurement, the EI can vary in the same patient[155]. Further, an increased EI as an isolated finding can indicate any type of hydrocephalus as well as central atrophy. Therefore, the EI is only a rough marker of ventriculomegaly and in iNPH this index has been shown to be of no predictive value prior to shunt therapy[156,157].

Another marker of ventriculomegaly is dilatation of the temporal horns and the 3rd ventricle. In iNPH these findings should not entirely be attributable to atrophy, as stated in the diagnostic guidelines, and the 4th ventricle is usually relatively normal. Temporal horn dilatation secondary to hydrocephalus is indicated by a rounded and blunt instead of a sharp, triangular form of the horns and apparent normal volume of the hippocampi. The latter is suggested by normal sized parahippocampal fissures[158]. Regarding the 3rd ventricle, an enlargement in combination with downward bulging of the ventricular floor and/or an elevation of the corpus callosum[159] also favors hydrocephalus rather than central atrophy. In a recent study, Virhammar et al.[157] have demonstrated that dilated temporal horns, but not a dilated 3rd ventricle, have a significant predictive value regarding good outcome after shunting. But, as is true for the EI, even measurements of the temporal horns and the 3rd ventricle are influenced by how they are carried out.

The relationships between clinical outcome after shunting and the change or absence of change of the size of the ventricular system are still under investigation. Nevertheless, the correlation between postoperative performance and ventricular volume in NPH does not seem to be as strong as in high-pressure hydrocephalus[160]. Volumetric measurements instead of index measurements might be necessary to establish the facts of the matter[161].

Aqueduct

To demonstrate the absence of a macroscopic CSF outflow obstruction at or caudally to the level of the cerebral aqueduct, mid-sagittal, thin T1 or preferably T2 weighted MRI images, are of great value. A T2 weighted sequence like the constructive interference in steady state (CISS) protocol, decreases the CSF flow artifacts and nicely delineates the ventricular contour and possible septa. If no overt obstruction is seen, an aqueductal stenosis might be indicated by a funnel shaped enlargement of the proximal aqueduct or a diffuse decrease of the aqueductal caliber.

Further, the form of the aqueduct might help in the differentiation of hydrocephalus and central atrophy as a distal dilatation of the aqueduct was detected in one third of patients with communicating hydrocephalus but not in cases of central atrophy[159].

Several pathophysiological theories regarding iNPH include the concept of a hyperdynamic aqueductal CSF flow[100,106,151,162], which can be assessed by MRI.

On T2 or proton weighted spin echo sequences, low signal in regions of flow, the so called "flow void phenomenon" can be observed; the higher the velocity of the protons, the higher the amount of signal void. In iNPH, on sagittal images, the extent of the flow void phenomenon of CSF across the cerebral aqueduct has been reported to be more pronounced than in normal controls and patients with other types of dementia[163-165]. Yet, this finding is not pathognomonic for iNPH[166]. The grading of the phenomenon is subjective and dependent on the MRI parameters, e.g., the slice thickness, the TE. Nevertheless, the flow void phenomenon suggests that the aqueduct is not completely obstructed which can strengthen the imaging-based diagnosis of iNPH in combination with other findings.

In order to find an aqueduct associated imaging marker CSF dynamics have also been studied in a quantitative way by phase-contrast MRI. This method quantifies the phase shifts of moving protons relative to protons in stationary tissue and can generate measurements of CSF velocity (cm/s), flow (cm3/s) and stroke volume (mean flow during systole and /or diastole). However, the measurements vary depending on the MRI machine and the software used why each imaging center needs to establish its own reference values. As summarized by Tanaris et al.[167] and shown by contradictory reports[168,169], evaluation of CSF dynamics have so far not been proven to be of diagnostic or predictive value. In reference to Scollato et al.[170], who found that the stroke volume in untreated iNPH patients varies depending on the time elapsed after onset of symptoms, future studies on CSF dynamics will have to determine the best timing for the measurements. Further, this time point should be identical for the responder and the non-responder group in prognostic studies.

Callosal angle

In the EA diagnostic guidelines[125], a corpus callosum angle of $\geq 40^0$ is listed as one of the supportive features for iNPH. No reference was presented, but to that date only pneumoencephalography-based studies had reported the diagnostic value of a corpus callosum angle $<120^0$ in normal pressure hydrocephalus[171,172]. Ishii et al.[166] reintroduced the measurement of the corpus callosum angle to MRI. The angle was assessed in the coronal plane at the level of the posterior commissure, perpendicular to a line connecting the

anterior with the posterior commissure. An angle $<90^0$ differentiated iNPH from AD and normal controls with an accuracy of 93%, a sensitivity of 97%, and a specificity of 88%. A combination of the two markers, corpus callosum angle ($<90^0$) and an EI (>0.3), resulted in an accuracy of 96%, a sensitivity of 97%, and a specificity of 94%. Recently, Virhammar et al.[173] tested the prognostic value of the corpus callosum angle and found that shunt responders had significantly smaller angles than non-responders, with an optimal cut-off at 63^0.

White matter changes

Another supporting imaging finding according to the EA guidelines[125] is the "evidence of altered brain water content, including periventricular signal changes on CT and MRI not attributable to microvascular ischemic changes or demyelination".

In both humans and animals the neuropathological changes in hydrocephalus comprise, among others, microscopic interstitial edema, various degrees of ependymal damage, microvascular infarcts, axonal stretching and loss, and gliosis in the periventricular region[174]. Measurements of T1 and T2 relaxation times[175], and the apparent diffusion coefficient[176] in the periventricular WM (PVWM) in NPH patients have proven the existence of edema in vivo. It is believed that the edema signals transependymal CSF absorption[95], but stagnation of extracellular fluid on its antegrade way to the ventricles has also been proposed as a possible cause for the finding[174]. MRI is much more sensitive than CT in depicting the edema, which typically is seen as smooth periventricular caps and rims that in T2 weighted MR images are hyperintense and on CT have a low attenuation. However, pure periventricular edema is not often seen in NPH[177] and it is usually impossible to differentiate from other types of PVWM changes that may co-occur[178]. In fact, the occurrence and extent of the periventricular and also of deep WM changes is significantly higher in iNPH patients as compared to healthy elderly controls[113] and, simultaneously, hypertension is overrepresented in the iNPH group[111,112]. Therefore, iNPH and vascular encephalopathy seem to coexist in at least a subgroup of patients and possibly even share pathophysiological mechanisms[110,113,114]. Although the severity of the WM changes correlates with the preoperative performance and although the extent of the WM changes is reduced postoperatively in patients with good clinical outcome, WM lesions can neither be used as a diagnostic nor a prognostic imaging marker[114,140,179].

Subarachnoid space (SAS)

A central imaging-based diagnostic iNPH criterion in the Japanese guidelines[134] is ventriculomegaly with "narrowing of the sulci over the high

convexity and midline surface, and dilatation of the Sylvian fissure and basal cisterns"[180,181]. This finding has been termed disproportionately enlarged subarachnoid space hydrocephalus (DESH) and is best seen in the coronal plane on MRI in the posterior part of the brain[182]. DESH has been suggested to be the manifestation of CSF retention in the inferior parts of the brain due to a CSF circulation block in the SAS at/ or cranial to the basal cisterns[180,181]. This imaging marker can help to discriminate iNPH from AD and vascular dementia, which instead demonstrate enlarged sulci over the high convexity due to temporal/parietal or general cortical atrophy and also show a more limited and proportional widening of the Sylvian fissure[180,181]. DESH without clinical symptoms of iNPH has been named asymptomatic ventriculomegaly with features of iNPH on MRI (AVIM) and might be a preclinical state of iNPH[128,183]. In Japan, in a prospective cohort study of elderly people Iseki et al.[128] found a prevalence of AVIM of 1.5% and Akiguchi et al.[184] observed an almost identical prevalence of 1.6% in Austria. In iNPH patients DESH has been identified as a significant predictor of positive shunt outcome [157].

The "cingulate sulcus sign", described as a narrowing of the posterior part of this sulcus on paramedian sagittal MRI images, probably bears analogy to the tight high convexity sulci in DESH. In a small study this sign was only observed in the iNPH group, but not in patients with progressive supranuclear palsy (PSP) or AD[185]. In the same study also the "upper midbrain profile sign", i.e. a concave form of the superior aspect of the mesencephalon, was evaluated and present in the majority of iNPH and PSP patients. In PSP this sign represents atrophy of the midbrain. In iNPH however, the midbrain is decreased in size as compared to healthy controls preoperatively[186] but increases in diameter after shunt insertion[187], which should be interpreted as a sign of compression by the enlarged basal cisterns[180].

Focally dilated sulci at the lateral or medial aspects of the hemispheres in NPH patients are proposed to represent sulci that communicate with the basal cisterns or the Sylvian fissure but otherwise are surrounded by blocked SAS. After shunting, these sulci might decrease in size, suggesting that they represent so called "transport sulci" [158,181,188].

In clinical praxis, the width of parts of the SAS is graded by subjective evaluation; taking into account the age of the patient. For research purposes an objective grading process is needed. Therefore, the width of the sulci is measured either quantitatively or on an ordinal scale. Virhammar et al.[157] reported an inter-rater reliability of 0.89 (intraclass coefficient) for the grading of the Sylvian fissure by a continuous variable and Cohen's kappa coefficient ranged from 0.36 to 0.64 for categorical variables describing the width of the sulci.

Magnetic resonance spectroscopy (MRS)

MRS is a well-established method for studying metabolites in the brain noninvasively, but the number of MRS studies in iNPH is limited and the use of different techniques and variations regarding the size and placement of the voxels of interest complicate the comparison of the findings.

The concentration of N-acetylaspartate (NAA), an indicator of neuronal state and function, was reduced in the thalami of iNPH patients in a study by Lundin et al.[189], indicating that the thalamus as a regulator of basal ganglia function might play a part in the generation of the symptoms. No other significant metabolic alterations, as compared to healthy controls, were found in the thalamus or the PVWM. Postoperatively, the NAA concentration in the thalamus remained low and unchanged in clinically improved patients, which had not been anticipated. In the PVWM choline and myo-inositol concentrations increased, which was seen as a sign of tissue repair[190]. Lenfeldt et al.[191] reported a decreased periventricular NAA/Creatine (Cr) ratio in patients with INPH, when compared with controls, but it was significantly higher in patients who improved after lumbar drainage. They interpreted the low ratio as secondary to decreased NAA levels due to neuronal dysfunction in frontal WM. Lundin et al.[189] questioned that interpretation in light of their own quantitative results, arguing that Cr, a marker of energy metabolism and part of especially astrocytes, does not represent a stable denominator, which can introduce statistical problems.

In a sNPH group Shiino et al.[192] found a link between preoperative higher NAA/Cr and NAA/choline ratios and good outcome after surgery, which together with the results of Lenfeldt et al.[191] might motivate further studies of these metabolites as potential outcome predictors.

In an MRS study of cortical and subcortical regions of the medial frontal lobes in an iNPH patient group the only significant results were an increased NAA/Cr ratio after shunting and correlations between NAA/Cr and cognition, both pre-and postoperatively[193].

Because of the periventricular hypoperfusion (please see the paragraph concerning perfusion in iNPH below) and the neuropathological changes observed in NPH patients and animal models[174], lactate as marker for anaerobic glycolysis has been searched for in the PVWM and within the CSF in iNPH and sNPH patients. However, the results have been contradictory and their interpretation is disputed[189,191,194-196].

Functional MRI (fMRI)

fMRI measures micro-level blood flow changes in response to activation of neuronal synapses. Lenfeldt et al.[197] were the first to apply fMRI to iNPH and showed that improved motor function after prolonged lumbar drainage was

reflected by bilaterally increased activation of the supplementary motor cortex. They hypothesized that CSF diversion improves the communication between central anatomical regions and the cerebral cortex.

Diffusion weighted MRI (DWI)/ Diffusion tensor imaging (DTI)

Diffusion of water in the brain is restricted by natural barriers and altered under pathological conditions. Diffusion imaging, using DTI, provides the means to determine the magnitude and directionality of water diffusion in vivo. Directionality is mainly an issue within the WM. Non-directional measures of diffusion are the apparent diffusion coefficient (ADC) and the mean diffusivity, which are equivalent. Directionality is usually described by axial (longitudinal) diffusivity, radial (perpendicular) diffusivity and fractional anisotropy (FA). Axial diffusivity and FA are considered to reflect axonal integrity. Radial diffusivity and the non-directional diffusion measures indicate myelin and tissue damage.

Several recent DTI studies of iNPH, sNPH as well as acute hydrocephalus have found increased FA along the corticospinal tract[198-203] and some FA normalization after shunt insertion[198,201,203]. By means of increased FA along the corticospinal tract Hattori et al.[200] were even able to differentiate iNPH patients from patients with AD or Parkinson´s disease with a comparable degree of ventriculomegaly.

It has been speculated that the directionality is increased as a result of white matter tract compression caused by the enlarged lateral ventricles and that the corticospinal tract has an important part in the generation of gait disturbance in iNPH. An alternative explanation is the degeneration of association and commissural WM fibers crossing the corticospinal tract, which also would result in a higher directionality within the latter[200].

In line with this, the commissural fibers of the corpus callosum have repeatedly shown decreased FA and increased mean diffusivity/ ADC[199,203-206]. The lower the FA values in the corpus callosum the more severe were the observed gait disturbances in a study by Koyama et al.[205].

Lenfeldt et al.[206], in their DTI study, found decreased FA in the periventricular, frontal WM, indicating disturbed axonal integrity. As the phenotype of iNPH is mainly subcortical and the concerned frontal WM areas contain corticostriate motor circuits, it has been assumed that the motor symptoms in iNPH are secondary to a disturbed motor planning process rather than to deficient primary motor efferents[206].

The results of ADC measurements in PVWM regions have been somewhat inconsistent[176,206-210], which might depend on methodological differences.

Nevertheless, these studies confirm, that the periventricular region is part of the pathophysiological process in iNPH.

Perfusion

Because of findings of a higher frequency of cerebrovascular WM lesions and pathological changes in the intracranial arteries and SAS of the iNPH patient group[110,211], the vasculature was proposed to be part of the pathogenesis.

A large number of perfusion studies have been performed, using the ^{133}Xenon clearance technique, various forms of SPECT, stable Xenon CT or PET. Among the techniques still in use, CBF studies by SPECT suffer from poor spatial resolution, tissue depth dependent sensitivity and have difficulties to quantify perfusion. In Xenon CT, the number of examined sections is limited and the inhalation of Xenon may have anesthetic effects that might influence the CBF measurements. PET, the reference method for perfusion studies, has the disadvantage of requiring an arterial catheter to measure the tracer concentration and is available only at centers with a cyclotron. Further, measurements of CBF in specific anatomic structures need MRI co-registration.

Apart from trying to cast some light on the pathophysiological aspect, the aims of perfusion studies have been to find a pathognomonic perfusion pattern for iNPH and an effective means of selecting shunt candidates. Owler and Pickard[212] reviewed the literature of NPH perfusion between 1969 and 2000 and found rather inconsistent study results, attributable to methodological and technical issues. Their main conclusion was that the global pretreatment CBF (gCBF) in NPH is decreased and that frontal regions are most likely to be affected. However, it remained unclear whether the CBF reduction represented the cause or an effect of NPH, and correlations between CBF and severity or duration of the symptoms were lacking. Further, perfusion parameters did not convince as diagnostic or predictive imaging biomarkers. For future projects Owler and Pickard[212] recommended the use of high resolution PET or MRI, the introduction of standards, conjoined studies of CBF and metabolism and a special attention for the PVWM.

A summary of baseline findings in blood flow associated NPH studies performed since 2000, as well as outcome of spinal tap test or shunting is presented in tables 7-9 in the Appendix. Among the listed investigations are only three DSC MRI perfusion studies[208,213,214] and no CTP study. The DSC MRI- investigations concentrated on the analysis of CBV and were assessed by visual inspection of the parametric maps[213,214] or had only measurements in a single slice at the level of the cella media[208].

Like the perfusion studies prior to 2000, also subsequent investigations have been lacking standardization of methods and scales for the clinical evaluation. The research results have to some extent been contradictory, for the most part regarding the status of autoregulation/ cerebrovascular reactivity (CVR) and the diagnostic and prognostic value of CBF. A CBF threshold that defines an irreversible brain damage and consequently can predict poor outcome after shunting has not been defined.

Due to their sensitivity for deep structures and relatively good spatial resolution, studies performed with MRI co-registered PET or DSC MRI have been able to show reduced perfusion in the basal ganglia, thalamus and the PVWM in iNPH[208,215-217], thus reproducing the findings of earlier stable Xenon CT experiments[218,219] and in line with the subcortical symptomatology of iNPH.

Among the studies, which addressed the correlation between CBF/rCBF and clinical symptoms pre-or postoperatively, there are several that found higher/increasing levels of cortical perfusion to be associated with less severe symptoms[220-223]. Only the investigation by Owler et al. [216] demonstrated a relationship between the CBF of subcortical anatomical regions and the clinical performance, which would be expected in a disease of a subcortical phenotype. However, the PVWM was not one of the areas associated with the symptomatology, although it is part of a known CBF reduction in iNPH and a site of interest regarding the pathophysiology of the disease.

A postoperative CBF/rCBF increase has been noted in most studies[104,220,221,223-226] but not all [208,227-229].

Bateman has made extensive efforts to prove the existence of a reduced, reversible compliance in iNPH, especially of the venous system[104-107,230].

Only one study, by Miyamoto et al.[228], investigated regional CBF (regCBF) and metabolism simultaneously. While no significant change of regCBF or regional oxygen extraction fraction was noticed in responders in the frontal lobe, putamen and thalamus, the regional cerebral metabolic rate of oxygen increased postoperatively in these regions, which might be interpreted as a sign of metabolic downregulation rather than of pure ischemia. Instead, in non-responders the regional oxygen extraction fraction decreased after shunting and regCBF and the cerebral metabolic rate of oxygen did not show any significant changes, which might indicate a true ischemic component.

As MRI and CT are already part of the diagnostic work up in iNPH patients, DSC MRI and CTP, sequences that are fast and easily performed, could without effort be incorporated into the standard imaging protocol. Yet, CTP has not been evaluated in the context of iNPH and the existing 3 studies using DSC MRI suffer from a number of limitations and have not demonstrated that this technique can assess the expected CBF and rCBF changes in iNPH.

4.4.5 CSF Biomarkers

Apart from the above described neuroimaging findings of a disturbed metabolism in iNPH (CBF and MRS) also analyses of CSF markers have repeatedly shown signs of dysfunctional periventricular and cortical metabolism and axonal degeneration[231-233]. The restoration of neurofilament protein (reflecting degeneration of large, myelinated axons) and tau protein (a marker of cortical axonal degeneration) to normal levels after shunt insertion are indications of an improved axonal and cortical neuronal activity[231,233]. Further, CSF markers have been proposed to aid in differentiating iNPH from other dementias. Sulfatide (a marker of demyelinisation) was suggested to distinguish between NPH and SAE[234] and phospo-tau (a marker of tangle formation) between AD and iNPH[235]. Neurofilament protein, phospho-tau, and amyloid beta 42 (linked to AD pathology and to the presence of plaques) in combination appeared to differentiate INPH, SAE, and HI[231]. Still, the validity of the proposed CSF biomarkers has not yet been confirmed.

In contrast to what is found in AD, in iNPH a general reduction of amyloid precursor protein (APP) fragments was reported[232], apparently contradicting the hypothesis that AD and iNPH possess an interrelated pathogenesis[236].

4.5 Treatment and outcome

Since Hakim and Adams introduced the concept of NPH[237] the insertion of a shunt system has been the therapy of choice. Because of ethical reasons comparison of operative and conservative treatment of iNPH has not been an option, explaining the limited evidence for surgical intervention and the limited knowledge of the natural history of iNPH.

There is only one double-blind randomized study investigating the effect of shunt surgery on the clinical performance[238]. The patients operated on fulfilled the criteria for iNPH, but also for SAE, had negative supplementary tests and could be described as having an unfavorable pre-surgical risk-to-benefit ratio, which justified the methodological approach of the study. All patients received either an open or an initially ligated shunt. Subjects with a patent shunt improved significantly regarding motor and cognitive function, while those who had a ligated shunt remained clinically unchanged.

The standard treatment today is the implantation of a ventriculoperitoneal shunt (VPS). A clinical history of peritonitis, multiple previous abdominal operations, severe obstipation or the presence of truncal obesity might result in the choice of a ventriculoatrial shunt[239]. If an iNPH patient presents with a

contraindication for intraventricular shunts, for example seizures, a lumbo-peritoneal shunt can be used. Rarely, when no other options remain, a ventriculopleural shunt is considered[239]. The discussion of choice of valve and opening pressure is beyond the scope of this text. It can just be mentioned that adjustable valves potentially are preferable as they allow managing problems associated with under- and overdrainage non-operatively[239].

The risk-to-benefit ratio is a concept that has to be taken into account as not every patient diagnosed with iNPH should be operated on. The patients' coagulation and immune status, comorbidity, clinical performance and age are factors that may influence the benefit-to-risk ratio negatively[239]. Further, there are still no means to tell which iNPH patients among those who are candidates for surgery, who have not yet developed irreversible brain damage[191,208,240], and thus will respond to the shunting procedure.

A systematic review[241] of the literature between 1966 and 2010 demonstrated, on average, a positive outcome in 71% of the cases at 3 months as well as 1 year after shunt insertion. Long-term outcome after at least 3 years was still favorable in 65% of the patients.

The reported total mortality was 1% (range 0-11%). The main complications were intracerebral hemorrhage or stroke (average 0.4%; range 0- 18%), infections (average 3%; range 1- 10%), subdural effusions/hematomas (average 6.3%; range 2- 47%) and new onset seizures (average 0.7%; range 0- 8%). Shunt-revision due to mechanical shunt obstruction was on average necessary in 16% (range 5-53%) of the patients.

Since 2006 the percentage of improved patients at 3 months and 1 year has increased to >80% and mortality and revision rates have decreased to 0.2% and 13 %, respectively. This positive trend is probably due to improved hospital care including anesthesia, surgical techniques and shunts as well as rehabilitation. Further, the introduction of the benefit-to-risk analysis and the optimized use of supplementary tests might have led to a better selection of patients.

The short-term (1 year) functional improvement does not persist in all patients in the long-term (>1 year). This is usually not due to shunt induced problems but to the progression of coexisting cerebro- and cardiovascular disease[145,242]. However, also the short-term outcome is negatively influenced by comorbidity[243].

In 2004, the minimum incidence of iNPH in Norway was estimated to 5.5/ 100000/ year [126], and during 1995-1998 and 2002-2006 the reported annual incidence of shunt surgery for NPH in Scandinavia was approximately 1/ 100000[244,245]. This illustrates the undertreatment of this patient group. As the life expectancy is increasing and iNPH is a disease of the elderly, the

frequency of surgical treatment has to increase. Not only in order to improve the patients' quality of life[246], but also to improve health economy. The costs for 24/7 care of a disabled iNPH patient exceed markedly the costs associated with shunt insertion.

Endoscopic third ventriculostomy (ETV) has been presented as an alternative therapeutic approach[247] based on the theory that iNPH is caused by reduced intracranial compliance and increased pulse pressure[100,106] instead of a primary disturbance of CSF circulation. The treatment of the latter requires external CSF diversion, while ETV increases the systolic CSF escape from the 3rd ventricle, which reduces the intraventricular pulse pressure and increases the intracranial compliance. Outcome reports have been contradictory, but a more recent, prospective, randomized study pointed towards better outcome rates for VPS than for ETV[248].

An approved pharmacological treatment does not exist for iNPH. Some studies have been performed testing the application of acetazolamide, a carbonic anhydrase inhibitor, which is supposed to reduce the CSF production. The preliminary results have been encouraging[249,250].

A comparison of outcome after shunting with outcome according to the natural course is meaningful only if the iNPH subgroups are diagnosed based on the same criteria and expected to be equivalent. The 3 studies performed according to this methodological set up[169,251,252] concordantly demonstrated that the natural course of iNPH is associated with symptom progression over time. Andrén et al.[251] even showed that clinical decline is only partially reversible if shunting is delayed.

4.6 Pathophysiology

There is no generally accepted pathophysiological concept for iNPH and to establish a causative connection between the multiple physiological changes observed in iNPH is challenging. The overrepresentation of cerebrovascular disease, the coexistence of other diseases like AD and the synchronicity of cerebral changes associated with normal aging complicate the understanding of the disease process further.

The main findings of iNPH have been described above, in the sections 3 and 4, and several of the existing pathophysiological theories have been mentioned[100,106,110,217,236].

Figure 3, created by Prof. Carsten Wikkelsø, is an attempt to illustrate their possible relationship.

The hypothetical pathogenesis of iNPH is delineated as a vicious cycle:

- Decreased intracranial compliance and malfunctioning CSF dynamics contribute to the macroscopic image of communicating hydrocephalus.
- Subsequently, subcortical dysfunctional metabolism and hypoperfusion develop, sometimes combined with failure of WM autoregulation, as evidenced by the above mentioned neuroimaging studies and findings of disturbed oxygen metabolism[228,253,254].
- The associated structural changes are demonstrated by functional and morphological MRI findings and histopathological examinations of humans and animals.
- These tissue changes lead to a further decrease of the intracranial compliance and complete the cycle.

CSF diversion enables the escape from this vicious cycle by increasing the compliance and lowering of the Ro.

There are numerous hypotheses trying to explain the subcortical hypoperfusion in iNPH in more detail than depicted in figure 3. Some of the suggested mechanisms are tissue distortion, watershed ischemia, vascular diseases, and interstitial fluid pressure increase and periventricular accumulation of vasoactive metabolites, summarized in the discussion part of a study by Momjian et al .[215].

Figure 3. The main pathophysiological aspects of iNPH (Courtesy of Prof. Wikkelsø)

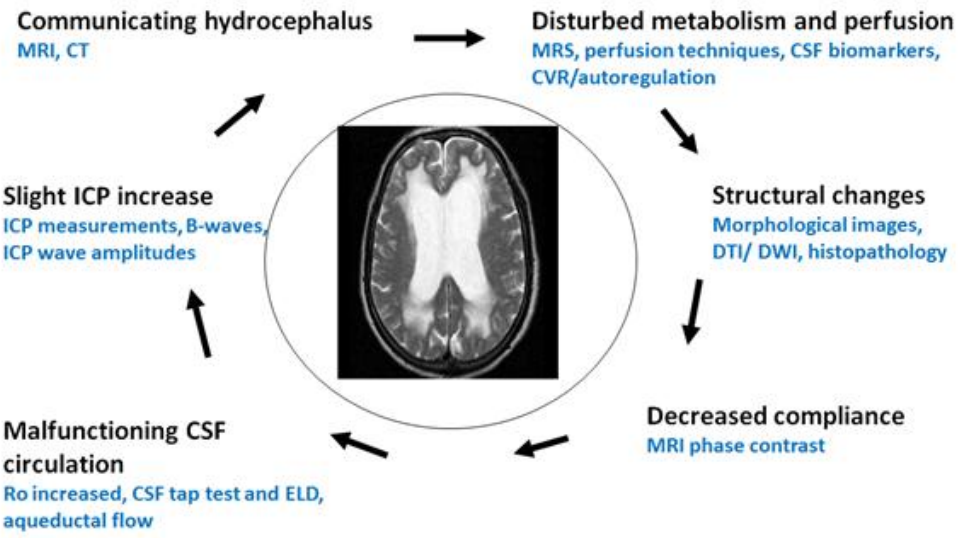

For abbreviations please see page iv.

5 AIMS OF THE THESIS

General aim

To study the potential role of dynamic susceptibility contrast MRI (DSC MRI) and CT-perfusion (CTP) as investigational techniques in idiopathic normal pressure hydrocephalus (iNPH).

Specific aims

Paper I

To assess the accuracy of DSC MRI perfusion values calculated with an arterial input function (AIF) rescaled by use of a venous output function (VOF) at 1.5T and test if the approach improves the correlation with CTP.

Paper II

To measure the preoperative perfusion in iNPH patients in comparison with healthy controls with DSC MRI, to try the hypothesis that a reduced preoperative, relative cerebral blood flow (rCBF) in iNPH correlates with the severity of the clinical symptoms and can predict shunt outcome.

Paper III

To study the correlation between the clinical improvement of iNPH patients after shunt insertion, and the regional cortical and subcortical postoperative rCBF changes as measured by DSC MRI.

Paper IV

To determine the pre- and postoperative regional and global CBF in iNPH by means of CTP, and to test if these results agree with the findings of a previous DSC MRI-based assessment of the same patient group, and controls.

6 SUBJECTS AND METHODS

6.1 Subjects

The recruitment process stretched over 3 years, from September 2005 until December 2008. An overview of the inclusion and exclusion process of patients and control subjects is given in figure 4.

iNPH patients

Fifty-one patients with suspected iNPH, who were referred to the Hydrocephalus Unit at Sahlgrenska University Hospital for preoperative assessment, were consecutively and prospectively included.

During 3 consecutive days these patients were extensively examined in order to establish the correct diagnosis and to collect data with focus on the clinical performance and the cerebral perfusion status.

The work up consisted of neuropsychological, physiotherapeutic and neurological examinations, basic blood tests and measurements of the ICP. When necessary, supplementary diagnostic tests were performed.

Patients had CT and MRI (a detailed description of the imaging protocols is found in the section below) and the morphological MRI series were used to either support the diagnosis of iNPH or suggest a differential diagnosis.

In thirty-two patients the diagnosis of probable iNPH based on the iNPH Guidelines[125,136] was established , while19 patients suffered from other disorders like SAE, aqueductal stenosis, foramen Monro obstruction or multi-infarct dementia.

Three patients with probable iNPH withdrew their written consent, and 6 had to be excluded because of unsuccessful MRI, i.e. incomplete imaging series or poor image quality.

Thus, 23 patients with probable iNPH completed the preoperative study protocol.

One patient had died prior to shunt surgery.

All other patients received a programmable ventriculoperitoneal shunt, either a Codman Hakim™ Valve (Codman Johnson & Johnson, New Jersey 08933, USA) or a Strata™ Valve (Medtronic PS Medical, Santa Barbara, USA), placed in either the right frontal lobe or the right parieto-occipital region. One patient developed a postoperative subdural hematoma, which was treated conservatively.

Three months after the shunt insertion patients were re-evaluated with the same battery of neuropsychological, physiotherapeutic, neurological and radiological examinations as preoperatively.

Patients, who improved substantially, i.e. five iNPH scale scores points or more, were considered shunt responders[144]. Those with an iNPH scale score change of less than 5 points were allocated the non-responder group.

Healthy individuals

Twenty-four, age- and sex-matched volunteering healthy individuals (HI), born between 1929 and 1942, were randomly recruited from the population registry of the City of Gothenburg and the Swedish retired people's organization. The recruitment of the last HI occurred after the evaluation process of Paper I had started. The control subjects had basic blood test and were examined by an experienced neurologist. Volunteers with hypertension and mild anti-hypertensive or antidepressive medication were accepted as controls. Exclusion criteria were major neurological disorders, psychiatric illness, nephropathy, drug or alcohol abuse, contrast agent hypersensitivity and claustrophobia.

One HI withdrew the written consent and one control subject was excluded because of an unsuccessful MRI. Thus, the control group comprised 22 HI.

Paper I

The last HI, number 22, was recruited to the project after the evaluation process for Paper I had started, and could subsequently not be a control subject for this paper. Thus, 21 HI (9 women, with mean age 70 years, and 12 men, with mean age 72 years) provided the data. One of these was identified as outlier during data analysis and, subsequently, was excluded. The applied ROIs were not extremely detailed and comparison was not performed between groups, but between different post-processing methods, which were employed to identical DSC MRI perfusion data. Therefore, minor motion artefacts and neurological problems of lesser grade in 3 HI were regarded as acceptable.

Paper II

After the addition of the one HI who was recruited late (see Paper I), 22 HI and 23 iNPH patients with apparently successful preoperative MRI were included. As the data evaluation was built on detailed, hand drawn ROIs, not even minor motion artefacts were tolerable. Imaging analysis demonstrated minor motion issues in 3 HI and major movements at bolus arrival in 2 of the iNPH patients, which prompted their exclusion. The group comparison of HI with iNPH patients also demanded the omission of 3 HI who had shown

minor neurological deficits following the neurological and radiological examination. Thus, 16 HI and 21 iNPH patients provided the reported data.

Paper III

This work was a postoperative follow-up survey of iNPH patients, who constituted the patient group of Paper II. However, one of the 21 patients included in Paper II had died prior to shunt insertion. One patient, with a minor postoperative, right-sided subdural hematoma was not excluded, since only the left hemisphere was evaluated in all patients. Consequently, 20 iNPH patients were analyzed in Paper III.

Paper IV

In this study the CTP data of the same patient group as in Paper III was investigated pre-and postoperatively. Out of the 20 iNPH patients from Paper III with successful MRI, 18 also had a CT of satisfactory quality**.** The postoperative CTP with the right-sided subdural hematoma was omitted from the postoperative assessment as ROIs were evaluated bilaterally. Thus, 18 pre- and 17 postoperative CTP examinations were finally included in Paper IV.

Among the 16 HI, who constituted the reference group of Paper II, 6 were randomly chosen to serve as control subjects in Paper IV.

Table 3. Demographic and clinical data as well as Evans' index and Wahlund's rating score for white matter changes for all subjects who were included in Papers II , III and IV

	HI (n=16) Paper II	**iNPH dead prior to op (n=1) Paper II**	**Respon-ders (n=15) Papers II, III**	**Non-responders (n=5) Papers II, III, IV**	**HI (n=6) Paper IV**	**Respon-ders (n=13) Paper IV**
Age in years, mean (range)	71 (64-82)	65	71 (59-82)	69 (55-80)	71 (68-74)	71 (59-82)
Sex, men/women	10/6	man	8/ 7	4/ 1	4/2	6/ 7
Hypertension, yes/no	1/15	no	5/ 10	2/ 3	0/6	3/ 10
Symptom duration in months, mean (range)		36	36 (7-168)	22 (18-24)		39 (7-168)
Pre-op iNPH scale score, mean (range)		47	48 (8-92)	65 (38-94)		46 (8-92)
Post-op iNPH scale score, mean (range)			68 (39-98)	62 (37-93)		67 (39-99)
Pre-op EI, mean (±SD)	0.28 (±0.05)	0.41	0.40 (± 0.05)	0.42 (±0.04)	0.28 (±0.02)	0.41 (± 0.06)
Post-op EI, mean (±SD)			0.37 (± 0.6)	0.41 (± 0.03)		0.38 (± 0.06)
Pre-op WM score, mean (±SD)	5 (± 4.1)	11	5.9 (± 4.6)	7.2 (± 5.8)	6.8 (± 1.7)	6 (± 4.9)
Post-op WM score, mean (±SD)			5.8 (± 4.7)	6.6 (± 6.3)		5.9 (± 5)

Figure 4. Flow chart of the subjects

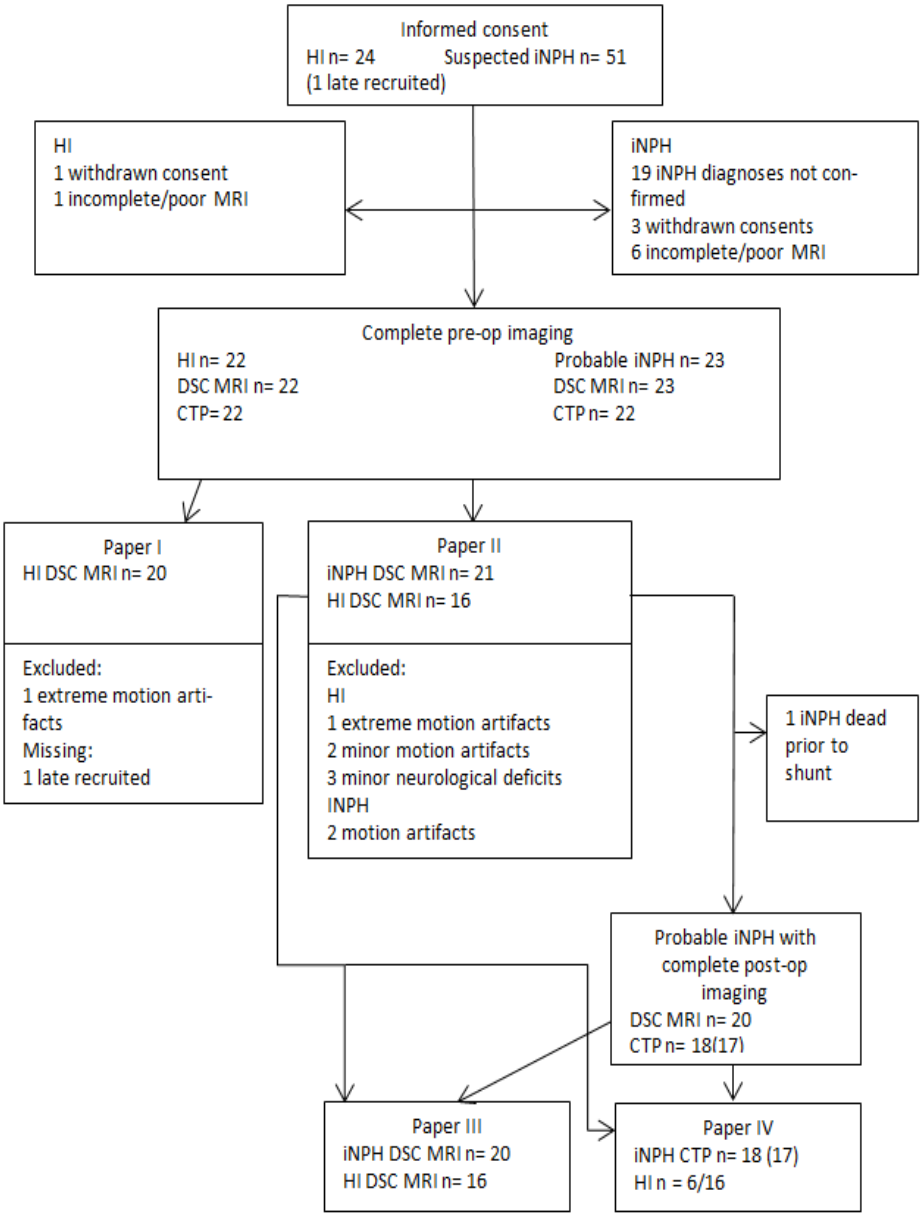

6.2 Grading of the clinical performance

A neurologist, a neuropsychologist and a physiotherapist shared the task of scoring patient performance. Grading was done according to the iNPH scale proposed by Hellström et al.[144], which assesses the four domains of neuropsychology, gait, balance and continence yielding separate scores as well as a total iNPH score. Domain scores and the total iNPH scale score range from 0 to 100. Zero represents the greatest impairment and the maximum score equals normal performance among 70-74 years old HI.

As gait disturbance is the main complaint of iNPH patients[255], the performance in this domain weighted twice in the estimation of the total iNPH score.

The Grooved pegboard test (Lafayette Instrument Co., Lafayette, IN, USA), the Rey Auditory Verbal Learning Test (RAVLT)[256] and the Swedish Stroop test [257] were used to measure the cognitive impairment.

During the grooved pegboard test the patients should as fast as possible fit 25 pegs into holes with randomly positioned slots, once with each hand. The test aims at the detection of deficits of hand and arm movements measuring the number of seconds of the fastest trial.

Verbal learning and memory, which are related to the medial temporal lobes, are evaluated by RAVLT[256], counting the total number of recalled words out of 15 concrete nouns during 5 trials.

Frontal-subcortical circuits mediate human behavior like executive function, working memory and wakefulness[223,258-260]. The Swedish Stroop test[257] grades this capacity by letting the patients name the colors (blue, red, green or yellow) of 100 rectangles as fast as possible and then to name the printed color of 100 incongruent color words (e.g. the word blue printed in red), measuring the number of seconds needed to complete the 2 tasks.

Evaluation of gait consisted of the assessment of the number of steps and time in seconds it takes to walk 10 m, at the patient's usual tempo, and of an ordinal rating of gait while the patient tried to walk heel-to-toe and to turn around 180°.

On an ordinal scale, balance was ranked according to the patients' ability to stand upright on one or both legs.

Continence was graded as follows:

1 Normal.

2 Urgency without incontinence.

3 Infrequent incontinence without napkin.

4 Frequent incontinence with napkin.

5 Bladder incontinence.

6.3 Imaging

At baseline, CBF was measured in all subjects using CTP and DSC MRI on two consecutive days at the same time of day to reduce diurnal fluctuations. Three months after shunt insertion CTP and DSC MRI were repeated in the patient group, again on two consecutive days at the same time of day.

On day one, MRI was performed on a 1.5T Gyroscan Intera 9.1 system (Philips Medical Systems, Best, The Netherlands). As part of the clinical routine protocol sagittal T2-weighted sequences were collected for anatomical evaluation of midline structures and inspection of flow-void effects along the cerebral aqueduct and the 4th ventricle. The morphological scan protocol further included a transverse fluid-attenuated inversion-recovery (FLAIR) sequence (TE 100ms, TR 9000ms, IR delay 2500ms, slice thickness 3mm, no slice gap, 44 slices, FOV 230mm, image acquisition matrix 192×192 reconstructed to 256×256) covering the entire brain. DSC MRI images were obtained each 1000 ms with a segmented k-space gradient-echo echo planar imaging (EPI) technique (TE 30ms, flip angle 40^{o}, slice thickness 5 mm, 12 slices, FOV 230 mm, matrix 128 x 128). At the tenth acquisition a rapid bolus (5 mL/s) of 0.1 mmol/kg body weight Gd-DTPA (0.5 mmol/mL, Magnevist, Schering, Berlin, Germany) was administered into the right antecubital vein, followed by a saline flush. The 12 slices of the DSC MRI perfusion were centered at the level of the posterior commissure, thus covering the superior part of the posterior fossa and the supratentorial region to the roof of the cella media.

For CTP on day two we used a CT unit with a 16-channel multi detector array (Lightspeed PRO 16; General Electric, Milwaukee, WI, USA). The bolus consisted of an injection of 50 ml iopromide (300mg iodine/ml, Ultravist, Schering, Berlin, Germany) at a rate of 4 ml/s, followed by a saline flush, into the same antecubital vein as during perfusion day one. Scanning was initiated 5 s after the start of the bolus injection. The examination covered 4 adjacent 5 mm sections immediately above the posterior commissure. Care was taken to ensure identical angulation as compared to the MRI scan, i.e., transverse slice orientation along a line between the posterior commissure and the root of the nose. The acquisition parameters were 80 kV, 200 mA, 99 scans, 4 images per cine scan, scan repetition time 0.5 s, acquisition time 50s, FOV 250 mm, and matrix 512 × 512.

6.4 Post-processing

Paper I

DSC MRI was post-processed using the software program ”Lupe”, developed at the University of Lund[261].

Two sets of parametric perfusion maps were calculated pixel-wise by oSVD[12], noise threshold 15%. One set was computed by use of a standard AIF and the other set was based on a rescaled AIF, according to Knutsson et al.[262], keeping all other variables unchanged.

As standard AIF we chose among semi-automatically suggested CTTC one voxel with the largest peak in the post-communicating segment of the anterior cerebral artery.

The areas under an AIF and a VOF that are free from PVE are equal[48], why the measured, standard AIF can be corrected for PVE by using the ratio of the areas under the VOF and the measured AIF. The PVE correction is a simple scaling factor.

AVOF, which was free from PVE but distorted secondary to signal saturation and signal relocation, was determined in the superior sagittal sinus/confluence sinuum. The distortion was removed by approximating the shape of a small venous CTTC to the form of the VOF.

CTP was analyzed on an Advantage Windows workstation 4.1 (GE Medical Systems, Milwaukee, WI, USA), using the software program CT-perfusion 3, Brain Stroke. The tissue impulse response function was determined in each pixel by deconvolution and the mean transit time (MTT) calculated as the ratio of the area (CBV) to the height (CBF) of the function.

Paper II

Post-processing was performed off-line using an in-house developed software running on MATLAB (Math Works, Natick, MD, USA), utilizing a batch processing framework (“pipeline”<) (Danish Research Centre for Magnetic Resonance, Copenhagen University Hospital Hvidovre, Danmark) and Statistical Parametric Mapping 2 (SPM2) (Wellcome Trust Centre for Neuroimaging, UCL, UK) for image co-registering and re-sampling.

In order to improve the SNR, the mean CTTC was obtained in each ROI (perfusion evaluation was based on ROI analysis as described in the below section) and, besides as common, in each voxel so that also perfusion maps could be created. ROI mean CBF was calculated by deconvolution according to oSVD[12], threshold 10%.

AIF were semi-automatically proposed in the post-communicating segment of the anterior cerebral artery. 1 to 4 voxels with the highest amplitude were selected manually to represent the global AIF.

Paper III

Post-processing was again done using "pipeline". The perfusion time series was co-registered and re-sampled to the first image. The signal-to-time curve was obtained as the average signal in each ROI. A model of the MR signal dip during bolus passage, described by the gamma variate function, was fitted to this curve. The fitted model was converted to the CTTC of the ROIs. In the same way also the signal-to-time curve of the voxel that determined the AIF was fitted and converted to a CTTC. For deconvolution we chose the FT method[9]. Noise was regularized with a Hanning (a.k.a Hann)[263] window setting that produced similar CBF estimates for the entire brain parenchyma compared to the results of a non-parametric oSVD[12] analysis of the same data in Paper II. The global AIF was placed in the distal M1 or proximal M2 segment of the left middle cerebral artery. Among semi-automatically preselected voxels, the narrowest voxel without signal saturation was manually picked.

Paper IV

Using "pipeline", the attenuation-to-time curve was built on the average CT-number of each ROI. The fit of a gamma variate function to the peak of the attenuation-to-time curves of the ROIs, the AIF and the VOF extracted the first pass of the contrast agent. According to the same criteria of shape and location as in Paper III, manually one voxel was selected as AIF. The average of four voxels in the center of the superior sagittal sinus or the confluence of sinuses determined the VOF. The AIF was scaled so that the area under the curve (AUC) was equaled to the AUC of the VOF. Deconvolution by oSVD[12] with a noise threshold of 0.05 was applied.

6.5 Evaluation

The perfusion evaluation was based on ROI analysis. ROIs were defined on all contiguous sections of the FLAIR sequence that contained the respective structure of interest.

In Paper I, 2D alignment of the functional maps and the transverse FLAIR-sequence was carried out manually by transverse translation and angulation. The DSC MRI and FLAIR sections that corresponded to the 4 CTP slices were chosen and the DSC MRI resized to the pixel size of the CTP. ROIs were automatically transferred from the FLAIR scan to the parametrical perfusion maps.

In Papers II-IV, the three stacks of the FLAIR scan were automatically aligned.

In Paper II and III, the FLAIR scan, including the ROIs, was co-registered with and re-sampled to the mean signal images of the perfusion scans, either DSC MRI or CTP. In Paper II and III this was performed automatically and in Paper IV manually.

By application of a parenchyma (Papers II, III) and a vessel mask (Papers II-IV), CSF and vessel signals were largely eliminated from the perfusion measurements. The thresholds for the parenchyma and CSF mask were empirically chosen on the histograms of the co-registered FLAIR. The vessel mask threshold was based on the histograms of the peak concentration images, calculated from the CTTC of the DSC MRI or CTP. Furthermore, the ROIs re-sampled to the perfusion series were trimmed such that only border voxels that contained more than 90% of the original FLAIR ROI were kept (Papers II-IV).

In Paper I manually drawn round or oval ROIs covered different kinds of tissue, e.g., representative areas of normal appearing white matter (NAWM), central GM, cortex without and with vessels as well as whole sections of the brain.

Anatomical regions that have been shown to be engaged in NPH[215-218,220,221] and that might be responsible for the generation of the symptoms [223,260,264-269] determined the choice of ROIs in Papers II-IV.

Detailed ROIs (Figure 5) were manually delineated and placed bilaterally in the basal, medial frontal cortex, the anterior cingulate gyrus, the occipital cortex, the caudate head, the lentiform nucleus, the thalamus, the hippocampus, the PVWM and the NAWM. PVWM ROIs had a cap like shape with a width of about 5mm, and cortical structures, basal ganglia ROIs and NAWM were irregularly outlined; remaining ROIs were rectangular or oval.

A parenchyma ROI was defined by the above mentioned parenchyma mask (Papers II, III) or computed on the voxel histogram of the filtered mean CT image of the CTP slabs by defining a threshold between the CSF and parenchyma peaks to excluded CSF from the parenchyma ROI (Paper IV).

Further, in Paper II perfusion profiles along straight lines through peri- and paraventricular frontal WM (WM-profile; 1-3 lines/frontal horn) and thalamic GM (Thalamus-profile; 5 lines/3rd ventricle) were analyzed. The profiles were aligned at the ventricular wall and average perfusion profiles were calculated.

Figure 5. Trans-axial FLAIR of a HI in Paper II at the level of the upper brainstem (a) and the level of the basal ganglia (b), illustrating the position of the manually drawn ROIs in these two of several contiguous slices. Figure 5c shows the slice of the CBF map that best corresponds to 5b.The parenchyma binary mask excludes the black pixels (CSF) and the slightly pink pixels are discarded by the vessel mask. Due to the effects of the masks, the trimming of the ROIs and the co-registration and re-sampling process, the contours of some ROIs in 5a and b differ from the ROIs in 5c.

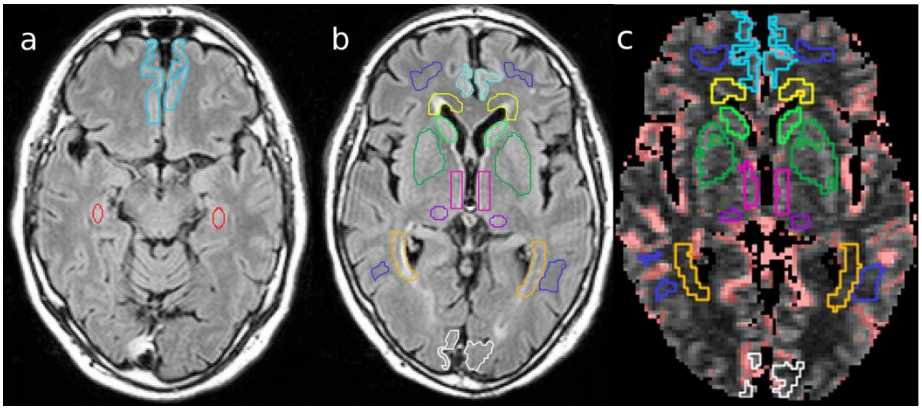

ROI-key on figure 1a: Basal, medial frontal cortex (light blue), hippocampus (red).

ROI-key on figure 1b and c: NAWM (dark blue), cingulate gyrus (turquoise), basal, medial frontal cortex (light blue), PVWM (yellow anteriorly, orange posteriorly), caudate head (light green), lentiform nucleus (dark green), periventricular thalamus (pink), central thalamus (purple), occipital cortex (white).

In Papers I-IV ROIs were also combined according to their tissue characterization.

Due to right-sided artifacts caused by metallic valve components of the shunt ROI analyses were limited to the left hemisphere in Paper III, except for the occipital ROI.

In Paper IV the basal, medial frontal cortex ROI and the hippocampus ROI were not sufficiently covered by the 2 cm wide CTP slab and omitted from the analyses. Even parts of the remaining ROIs were discarded to some extent in all subjects secondary to the limited spatial coverage of the perfusion sequence.

In Paper I and IV average absolute CBF and in Paper II and III mainly relative CBF (rCBF) estimates, calculated with the CBF of the occipital cortex as internal reference, were used for statistical testing.

On transaxial FLAIR images the EI was calculated and the extent of infra- and supratentorial WM changes was determined using the rating scale by Wahlund et al.[270].

6.6 Statistical methods

In Paper I, the relationship between the perfusion methods was studied by linear regression analysis and the Bland-Altman method, plotting the differences between the DSC MRI- and CTP-based CBF estimates against the average CBF from the two modalities

To select a potential preoperative rCBF threshold for outcome prediction in Paper II, receiver operating characteristic (ROC) analysis was carried out. The Youden's index, i.e. the difference between the true positive rate and the false positive rate, was maximized to find, from the ROC curve, an optimal cut-off point.

Wilcoxon's signed ranks test for related samples was used to compare groups with paired data in Papers I, III and IV.

Comparison of 2 unrelated groups was executed by the Mann-Whitney U test in Papers II, III and completed by the Independent sample median test in Paper III for comparison of medians across groups.

For the comparison of 3 unrelated groups we used the Kruskal-Wallis test in Paper IV.

Correlations were explored with the Spearman rank correlation test in Papers II, III and IV.

Significance was stated at $P < 0.05$.

P values were not adjusted for multiple comparisons, partly because of variations in sample sizes and partly to avoid type II errors when the results displayed consistent patterns.

6.7 Ethical approval

The Ethics Committee of Gothenburg and the Radiation Protection Committee of the Sahlgrenska University hospital approved all studies in this thesis. All participating patients signed a written informed consent form.

7 SUMMARY OF RESULTS

After CSF diversion 75% of the shunted patients improved (responders) and the clinical performance in 25% was unchanged or declined further (non-responders).

7.1 Paper I

The observed differences between the modalities were significant in all anatomical regions except for the CBF estimates of the whole brain comparing rescaled DSC MRI and CTP (Table 4).

Table 4. Absolute CBF estimates (mean ± SD) of the different ROIs for healthy elderly individuals. Significant differences between CTP and DSC MRI or rescaled DSC MRI are indicated by aterisks. = p<.05; ***= p<.001*

ROI	CBF [ml/(min·100g)]		
	CTP	DSC MRI	Rescaled DSC MRI
White matter	13 ± 2	51 ± 18***	25 ± 11***
Central grey matter	42 ± 7	115 ± 45***	57 ± 24*
Cortex without vessels	44 ± 7	153 ± 61***	75 ± 34***
Cortex with vessels	58 ± 13	161 ± 61***	72 ± 24*
Whole brain	49 ± 9	129 ± 47***	59 ± 21

The Bland –Altman plot (Figure 6) displayed that the difference between the modalities was larger than zero and that the difference was non-uniform, i.e. increasing in relationship to increasing average CBF values.

Figure 6. Bland-Altman graph.
Ovals represent DSC MRI (abbreviated MRP in Paper I) versus CTP. Triangles delineate rescaled DSC MRI (abbreviated Rescaled MRP in Paper I) versus CTP.

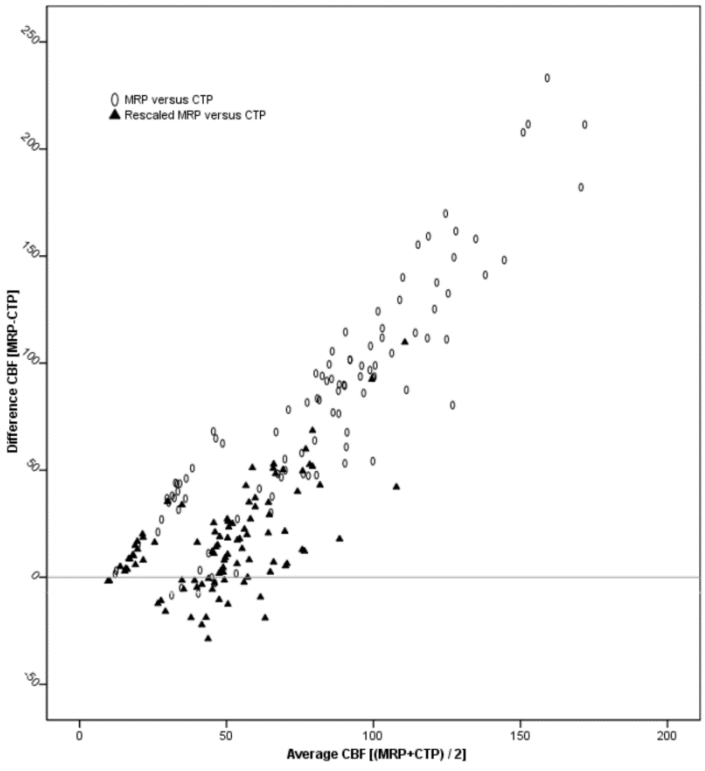

Regression analysis of the average CBF estimates of individual subjects proved an excellent correlation between DSC MRI with and without scaling (R^2 ~1) and good correlation between the different DSC MRI approaches and CTP (R^2 range rescaled DSC MRI/ CTP: 0.57-0.97; DSC MRI/ CTP: 0.65-0.98). Figure 7 is an example case.

In inter-subject comparison, linear regression resulted in no significant correlation in any anatomical region comparing DSC MRI- and CTP-based mean CBF values, but the rescaled DSC MRI and CTP correlated significantly in the central GM ($p=0.01$; $r=0.54$), and fairly in the whole parenchyma ($p=0.05$, $r= 0.44$) (Figure 8).

The rescaling brought the average CBF estimates closer to the identity line for all subjects and reduced the scattering.

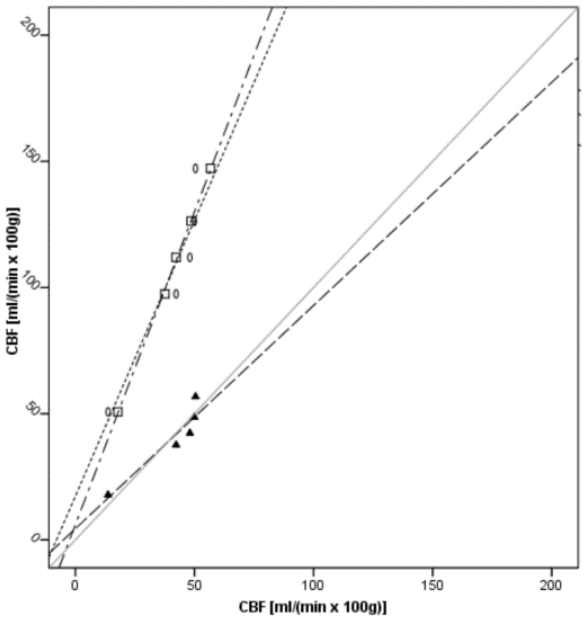

Figure 7. Scatter plot of all CBF estimates for case 1. DSC MRI (ovals) and rescaled DSC MRI (triangles) versus CTP are displayed with CTP along the x-axis. In the linear regression analysis of DSC MRI versus rescaled DSC MRI (squares) the x-axis instead represents rescaled DSC MRI.

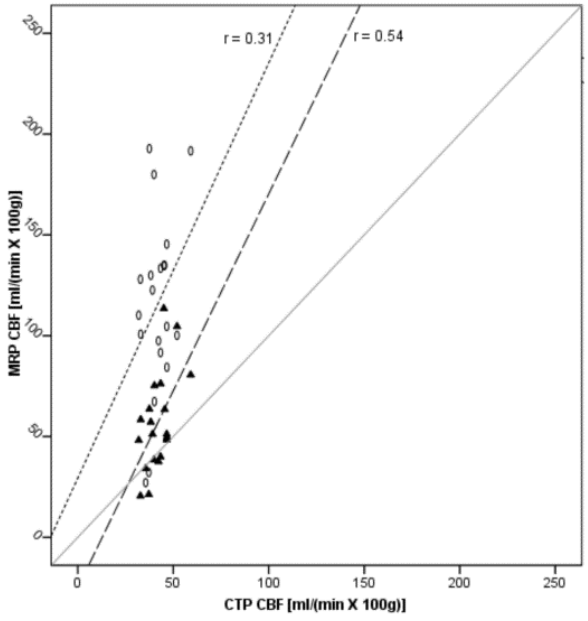

Figure 8. Scatter plot of mean CBF estimates for the central grey matter of all objects. DSC MRI (ovals) and rescaled DSC MRI (triangles) versus CTP are displayed with CTP along the x-axis. (In Paper I, DSC MRI was abbreviated MRP.) r = correlation coefficient

7.2 Paper II

Prior to surgery, rCBF in iNPH patients was significantly decreased in the basal, medial frontal cortex, the hippocampus, the lentiform nucleus, all PVWM regions, the central GM and the parenchyma as compared to HI. Along the WM-profile the mean rCBF of iNPH patients was reduced significantly at 2, 5 and 7 mm from the ventricular wall. Along the Thalamus-profile, an increased rCBF was observed in iNPH patients compared to HI, the differences reaching significance at 0 and 7-9 mm from the ventricular wall (Figure 9).

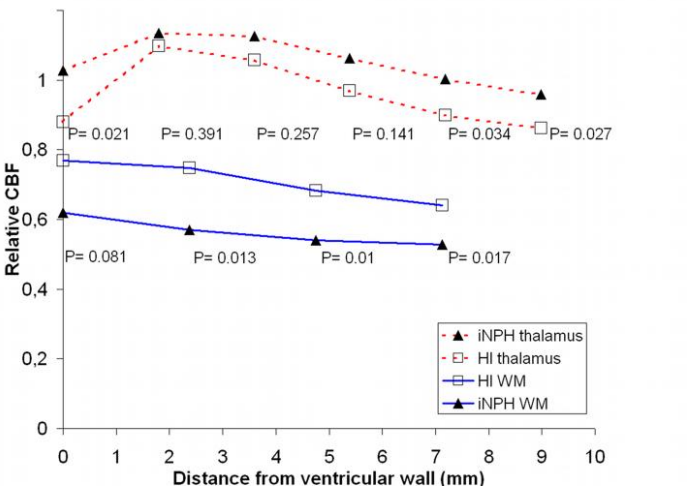

Figure 9. The mean rCBF values and p-values for each point of measurement along the WM-profiles (blue lines) and the Thalamus-profiles (dotted red lines) for the iNPH (triangles) and HI (squares) groups.

The rCBF along the WM-profile correlated at all points of measurement significantly and positively with the preoperative total iNPH score and the gait score and negatively with the degree of improvement after surgery in iNPH score points. Similar correlations, although not statistically significant at each point of measurement, were found along the 9 mm long Thalamus-profile.

In the iNPH group as a whole the rCBF in the various ROIs did not correlate with the pre- or postoperative clinical performance. On the other hand, the shunt responder subgroup presented a positive correlation between rCBF in the anterior, posterior and total PVWM and the preoperative total iNPH score, the gait score and the neuropsychological score. A negative, significant correlation was found between rCBF in GM and the degree of improvement.

The preoperative rCBF of the basal, medial frontal cortex in shunt responders was higher than in non-responders. Non-parametric ROC analysis for this rCBF variable versus outcome resulted in an area under the curve of 0.85. The basal, medial frontal rCBF cut off value of 0.798 showed the highest Youden's index (Figure 10).

Figure 10. ROC curve (a) of the relative CBF in basal, medial frontal cortex as predictor for good outcome after shunting and box plot (b) of the same perfusion estimate for non-responders and shunt responders (median, IQR, extreme values within 1.5 times the IQR).

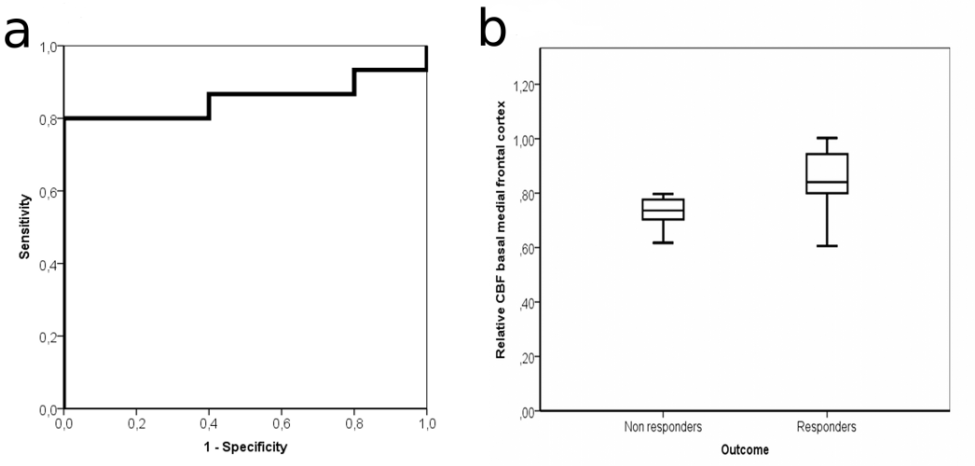

7.3 Paper III

The preoperative rCBF estimates for the responders and non-responders are illustrated in figure 11.

Responders showed an rCBF increase of 2-9% in all anatomical regions after shunting. Statistical significance was reached in the hippocampus ($p = 0.02$), the anterior PVWM ($p = 0.04$) and in the global parenchyma ($p = 0.004$) (Figure 12).

As the sample size of the non-responder was small, Wilcoxon´s signed ranks test for related samples was not performed in this subgroup.

Figure 11. Preoperative rCBF values (median ± SD) for the non-responder and the responder group. Statistically significant difference is indicated by the asterisk (p=0.04).

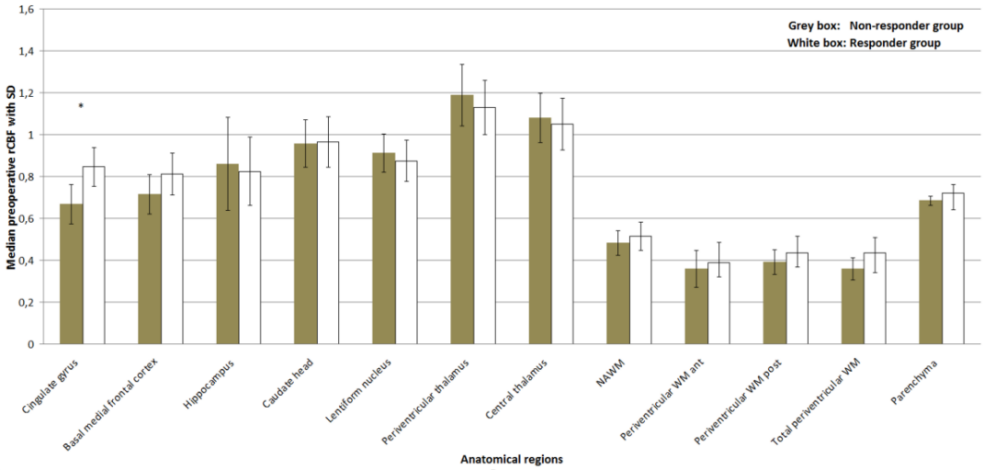

NAWM = normal appearing white matter; WM= white matter; ant= anterior, post= posterior

Figure 12. Postoperative rCBF changes in % (median ± SD) for the non-responder and the responder group. Statistically significant rCBF increases in the responder group are indicated by asterisks (p < .05).

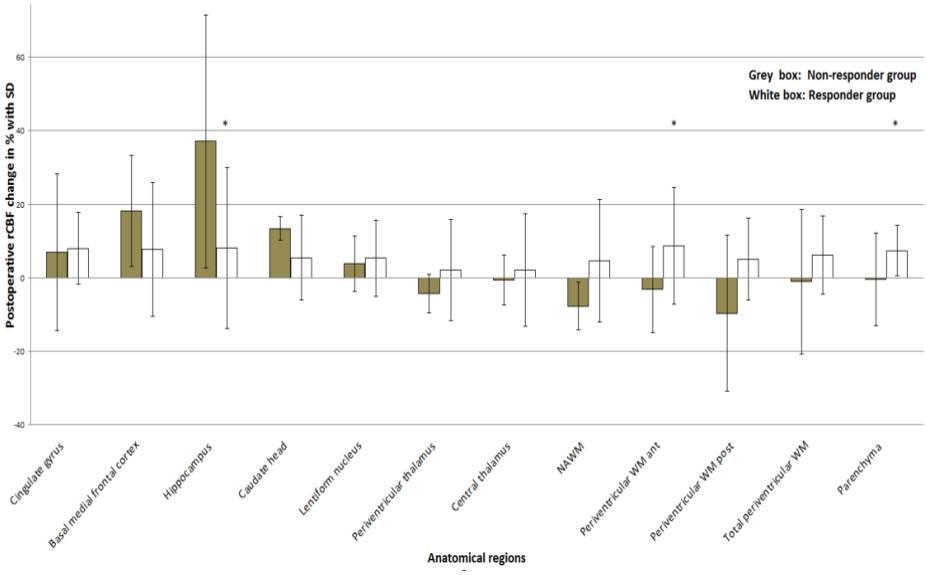

NAWM = normal appearing white matter; WM= white matter; ant= anterior, post= posterior

After CSF diversion, responders showed a positive correlation between the cingulate gyrus rCBF and the neuropsychology score, the gait domain score and the total iNPH scale score. Further, there was a positive relationship between perfusion in the anterior PVWM and the total iNPH scale score.

Analysis of the individual rCBF and clinical changes over time, comparing the pre-and the postoperative status, resulted in the correlations listed in table 5.

Table 5. Correlations (Spearman's rho) between changes in rCBF and changes in performance after shunting in shunt responders

Relative CBF	Neuropsychology score	Gait score	Balance score	Continence score	iNPH score
Cingulate gyrus	**0.55***	0.07	0.36	0.16	0.26
Basal, medial frontal cortex	0.37	0.31	0.31	0.05	0.33
Hippocampus	0.43	0.09	0.01	-0.16	0.08
Caudate head	0.19	**0.66***	**0.65***	-0.16	**0.56***
Lentiform nucleus	0.11	0.47	0.42	0.03	0.39
Periventricular thalamus	**0.66***	0.02	0.25	-0.10	0.13
Central thalamus	0.20	0.32	0.07	-0.20	0.07
NAWM	0.31	-0.00	0.34	0.14	0.25
PVWMant	0.48	0.14	0.22	0.30	0.40
PVWMpost	0.34	-0.07	0.22	0.41	0.37
Parenchyma	0.48	0.07	0.19	0.01	0.20

*NAWM= Normal appearing white matter; PVWMant = anterior periventricular white matter; PVWMpost = posterior periventricular white matter; * = p<.05*

7.4 Paper IV

In HI the mean CBF (± SD) was 13.7 (±2.7) ml/ (min ·100g) in central GM and 6.8 (±1) ml/ (min ·100g) in NAWM with a corresponding GM/WM ratio of 2.1 (±0.3).

Preoperatively, the iNPH group as a whole showed significantly decreased CBF in the PVWM (PVWMant p= 0.01, PVWMpost < 0.001 and TotalPVWM p= 0.001), in the lentiform nucleus (p< 0.05), the NAWM (p= 0.02) and the parenchyma (p= 0.01) compared to HI. Comparisons of the iNPH subgroups and HI (Figure 13) demonstrated no significant CBF differences between iNPH shunt responders and non-responders.

Figure 13. Preoperative CBF values (median, IQR) for the healthy individuals, the non-responders and the responders. Asterisks indicate significant CBF reduction as compared to HI (p < .05).

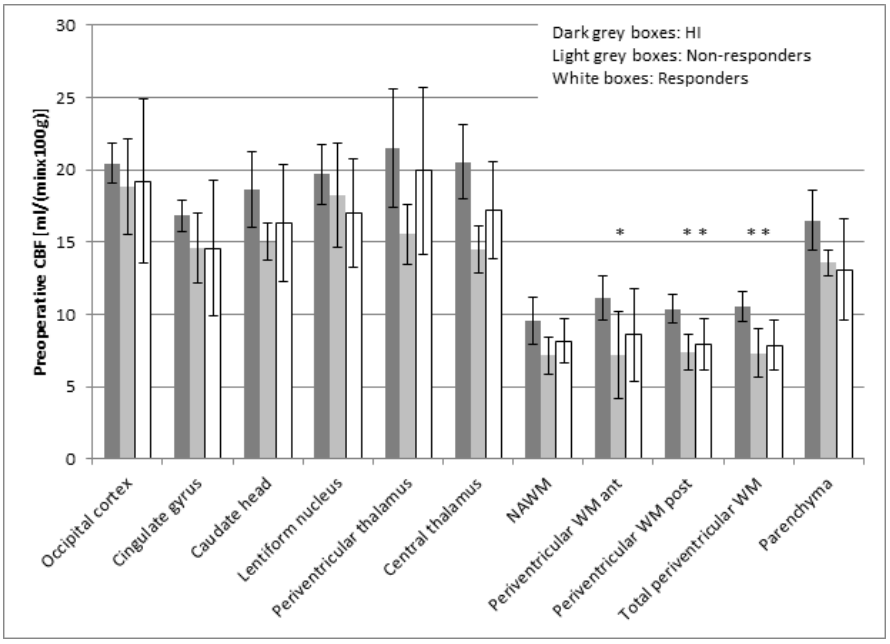

NAWM= normal appearing white matter; WM = white matter; ant= anterior; post= posterior

The CBF in responders increased postoperatively in all anatomical regions by 2.5-32 % (Figure 14).

The non-responders' CBF remained significantly reduced in the PVWM (PVWMant p= 0.02; PVWMpost p=0.002; total PVWM p= 0.008) (Figure 15).

Figure 14. Postoperative CBF changes in % (median, IQR) for the responders and non-responders. Statistically significant CBF increases in the responder group are indicated by asterisks ($p < .05$).

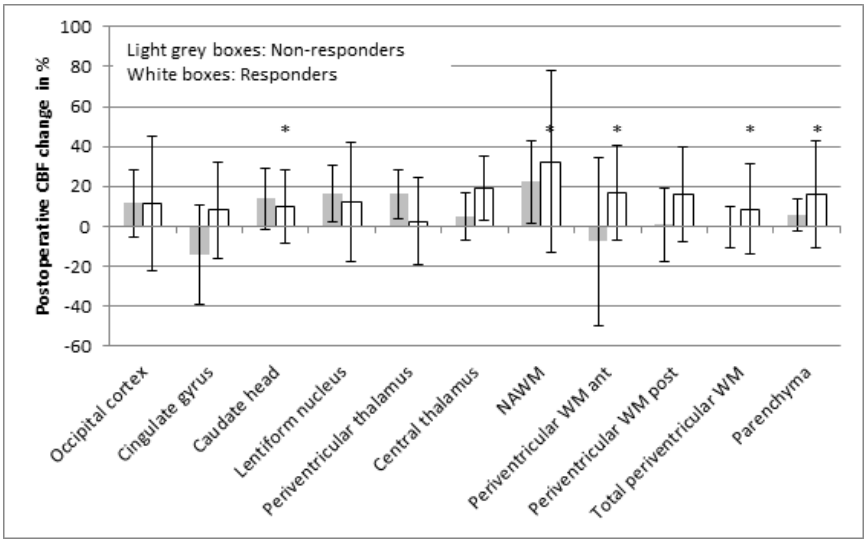

NAWM= normal appearing white matter; WM= white matter; ant = anterior; post = posterior

Figure 15. Postoperative CBF values (median, IQR) for the responders and non-responders. The corresponding preoperative values for the healthy individuals (HI) are displayed for comparison (same data as in figure 13). Asterisks indicate significant CBF reduction as compared to HI ($p < .05$).

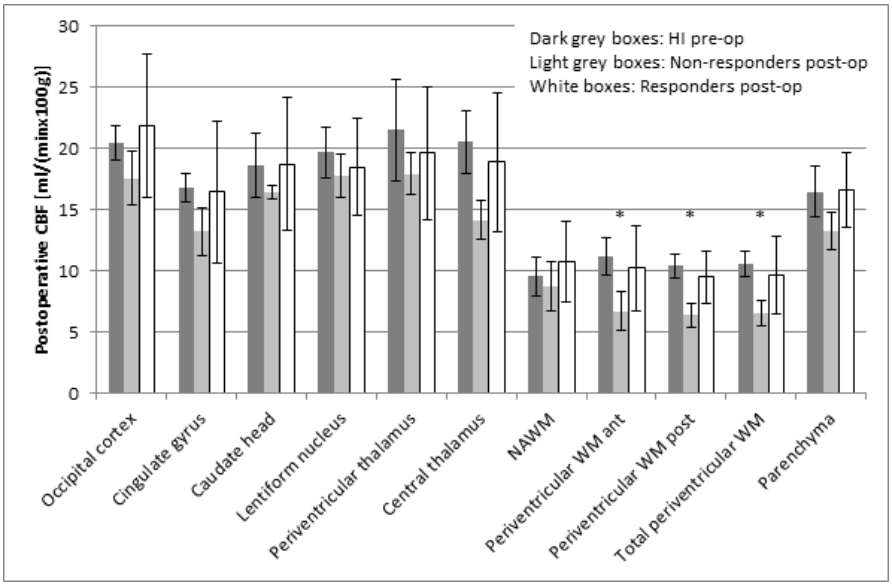

NAWM= normal appearing white matter; WM= white matter; ant = anterior; post = posterior

In responders, the preoperative CBF of the PVWM regions, the cingulate gyrus, the occipital cortex and the parenchyma correlated with the iNPH scale score and with several domain scores.

Postoperatively, responders demonstrated significant positive correlations between the CBF of the cingulate gyrus and the continence and total iNPH scale score. PVWM CBF displayed a positive relationship to the gait score, continence score and total iNPH scale score and continence was also positively related to perfusion of the occipital cortex. These correlations are summarized in table 6.

CBF changes and the improvement in clinical performance, i.e., the differences between pre- and postoperative results, correlated not.

There was no significant asymmetry of perfusion values between the hemispheres.

No visible shunt-induced metallic artefacts were detected on the CTP series.

Table 6. Correlations (Spearman's rho) between CBF and clinical performance in shunt responders

CBF[ml/ (min ·100g)]		Neuro-psychology score	Gait score	Balance score	Continence score	iNPH score
Occipital cortex	Preop	**.69***	.50	.48	**.69***	**.63***
	Postop	.19	.36	.14	**.73***	.52
Cingulate gyrus	Preop	**.68***	**.61***	.48	**.65***	**.67***
	Postop	.16	.57	.17	**.67***	**.61***
Caudate head	Preop	.44	.28	.02	.47	.28
	Postop	-.12	.39	.04	.49	.32
Lentiform nucleus	Preop	.52	.44	.25	.58	.46
	Postop	.17	.28	.23	.34	.35
Periventricular thalamus	Preop	.61	.49	.01	.53	.45
	Postop	.24	.57	.23	.55	.56
Central thalamus	Preop	**.76***	.54	.19	.53	.55
	Postop	.22	.48	.02	.38	.45
NAWM	Preop	.14	-.06	-.28	.28	.08
	Postop	-.10	.15	-.06	.19	.21
PVWMant	Preop	.45	**.69***	.23	.57	**.61***
	Postop	.43	**.78***	.27	.40	**.74***
PVWMpost	Preop	.45	**.69***	.23	.57	**.61***
	Postop	.09	.47	.17	**.59***	.52
Total PVWM	Preop	**.59***	**.72***	.27	**.60***	**.63***
	Postop	.23	**.60***	.14	**.62***	**.58***
Parenchyma	Preop	**.73***	**.57***	.34	**.66***	**.67***
	Postop	.16	.34	-.03	.43	.41

*Pre-op=preoperative; post-op=postoperative; NAWM= Normal appearing white matter; PVWMant = anterior periventricular white matter; PVWMpost = posterior periventricular white matter; TotalPVWM = PVWMant + PVWMpost; * = p<.05*

8 DISCUSSION

8.1 The perfusion techniques

8.1.1 Validity and reliability

A new technique must be demonstrated to produce valid and reliable results. The technique is valid if it measures the effect that we want to study and it is reliable if measurements are precise and reproducible. The precision and reproducibility of perfusion measurements can fail at different levels, e.g. during data collection, when post-processing the data or throughout the interpretation of the data. Validity is usually established by comparing the new method with a reference method. In the context of perfusion, the reference method in humans is considered to be ^{15}O-H_2O-PET and in animal studies the microsphere method is the reference.

Several studies have assessed the CTP-based perfusion quantification in healthy animals and animals with stroke or tumors against the microsphere method, reporting very good correlations (r: 0.78 -0.95; slope: 0.93- 1.05)[54-57,271,272]. In humans, CTP has been compared with PET and Xenon CT in healthy individuals, but also in patients with acute or chronic cerebrovascular disease. Deconvolution-based methods[17,58,59] seemed to produce perfusion estimates superior to the maximum slope method[273,274]. Based on linear regression and correlation analyses, CTP was described as accurate, especially when large vessels were excluded from the analysis (r: 0.69-0.89; slope: 0.87-1.05)[17,58,59], but agreement according to the Bland Altman method had not been investigated. Grüner et al.[275] used linear regression and the Bland Altman method and could not confirm the high accuracy of CTP in relation to PET. CTP repeatability studies on animals with the deconvolution approach demonstrated a 10% larger variability for CTP than for the microsphere method and higher variability for CBF than for CBV[54,272]. Nevertheless, the differences between the repeated CTP measurements were not significant[54]. The reported variability of perfusion measurements by CTP and the maximum slope model in humans was small (r: 0.884)[276].

The validity and reproducibility of DSC MRI was tested against PET by two groups. Agreement and reproducibility were defined as the 95% range for difference using the Bland Altman method, expressed also in percentage value. Carroll et al.[32], using SVD as deconvolution method, found a reproducibility of 10% for PET and 80% for DSC MRI in GM. The variability of DSC MRI was this large although a vessel mask had been applied. The agreement between the methods was considered reasonable,

provided that signals from large vessels were excluded in DSC MRI. Grandin et al.[33] calculated the DSC MRI-based perfusion measurement by FT deconvolution. They described a moderately and equally good repeatability for PET and DSC MRI. For CBF it was 18% with PET and 22% with DSC MRI. In individuals the DSC MRI- and PET-based perfusion estimates correlated well (R^2: 0.7 - 0.84), but the regional average CBF of all individual measurements showed a substantially lower correlation (R^2: 0.4-0.65). The limits of agreement between DSC MRI and PET according to the Bland Altman method were relatively large and DSC MRI estimates were systematically overestimated.
A direct comparison of the above results is difficult. The studies contain different and not always optimal statistical analyses and the different perfusion calculation processes have a confounding effect. Apparently, also the reference method PET displays varying reproducibility/repeatability, i.e. 10% in the study by Carroll et al.[32] and 18 % as reported by Grandin et al.[33]. This variability probably depends on different numbers of acquisitions and if global or regional CBF is assessed[33].

A group of experts for the different cerebral perfusion techniques published a comparative review in 2005[277]. CTP was accredited quantitative accuracy and a reproducibility of 10- 15%, but no reference was presented for the latter. The reproducibility of DSC MRI was likewise 10- 15%, referring to Grandin et al.[33], but the method was stated no to be quantitatively accurate in daily practice.

Xenon CT and ^{15}O-H_2O-PET rely on a diffusible tracer, while CTP and DSC MRI register the behavior of a non-diffusible intravascular contrast agent. These implicit differences might partly explain the varying results in studies of agreement and, in turn, it might seem reasonable to expect a good agreement between CTP and DSC MRI.

8.1.2 PVE

Of course also CTP and DSC MRI show obvious dissimilarities, for example regarding spatial resolution.

In DSC MRI, with a matrix of 128×128 and a FOV of 230mm, the voxel size is 1.8×1.8×5mm. For comparison, 5mm CTP sections with a 512×512 matrix and a FOV of 250mm result in a voxel size of 0.5×0.5×5mm. The average vessel diameter of the proximal anterior cerebral artery is 2.6± 0.3mm and that of a cortical branch ranges from 0.8± 0.3mm to 1.84±0.3mm[278]. In DSC MRI the placement of an AIF of one pixel can easily result in contamination of the vascular signal by signals from adjacent brain tissue, which is a major

cause of error in the absolute perfusion quantification[35]. An underestimation of the AIF leads to subsequent overestimation of CBF and CBV.

CTP allows the direct and routine registration of a VOF free from PVE, which can be used for scaling of the AIF[61]. In DSC MRI direct measurement of such a VOF is difficult, because of signal distortion[37] and saturation[36]. Distortion was minimized in this work by the use of a multi-shot EPI with a segmented k-space readout and parallel imaging. But as long as the TE is long to optimize the tissue signal, large vessel signal saturation cannot be avoided[36,46].

Proposed approaches to reduce or eliminate PVE in DSC MRI use the first pass or the "steady-state phase" of arterial and venous CTTC to scale the AIF[62,262,279-281]. The first method for PVE correction described in detail was published by Knutsson et al.[262] in 2007. They approximated the shape of a small venous CTTC to the saturated VOF to restore the true form of the latter. The ratio of the areas under the restored VOF and the measured AIF represented the proposed scaling factor.

This approach was implemented in Paper I, which, to our knowledge, was the first study to compare CTP and DSC MRI in HI.

The rescaling of the AIF improved the correlation between DSC MRI and CTP on group level in concordance with the findings by Knutsson et al.[262], who had tested the method at 3T against Xe-133-SPECT. The linear relationship between the modalities in individual subjects was good, independent of the scaling procedure. Yet, slope and intercept were far from unity and varied between subjects, which is a sign of large inter-individual differences of the AIF. Variations in vessel size presumably cause differences in the amount of interfering PVE, which the scaling accounts for. Further, at 1.5 T, in Paper I, the produced CBF values after rescaling were closer to the normal range, while the estimates at 3T had been highly overestimated, probably because the difference in transverse relaxation rate between large vessels and tissue, at a given contrast agent concentration, is larger at 3T.

However, the flow was still elevated compared with CTP and values from literature[31], suggesting that not all PVE were eliminated or that other factors contributed to the overestimation. For example, PVE can also affect the shape of small veins and/or the flanks of VOF.

A somewhat different approach to remove PVE[281] was also built on the ratio of the area under the AIF and the VOF, using trapezoidal integration, which increased precision, but resulted in negative bias of the measurements.

Recently, Knutsson et al.[280] proposed a new PVE correction concept, in which the AIF is scaled by a VOF obtained by a single slice pre-scan after injection of a fraction of the total contrast agent dose. The pre-scan is characterized by low geometric distortion and absence of large-vessel signal

saturation, which enables the direct registration of a VOF. This pre-bolus concept has produced flow estimates approaching those measured by PET, Xenon CT and arterial spin labeling and has shown good repeatability. It outperforms the PVE correction method of Paper I and also the tail-scaling technique by Björnerud et al.[62], which uses the ratio of the steady-state concentration levels of the AIF and the VOF to calculate a scale factor.

An alternative to rescaling the AIF to improve the accuracy and reproducibility of DSC MRI is to calibrate the CBF values with a T1-weighted steady-state CBV estimate[282,283], i.e. the book-end technique, which requires an additional "calibration" scan. Possible errors in the steady-state CBV calculation, due to water exchange between the intravascular- and extravascular space, and remaining AIF-related problems in the dynamic susceptibility sequence represent drawbacks of this method.

Individually tailored scaling of the perfusion parameters of DSC MRI improves the precision and reproducibility of the method. However, no scaling procedure has been proven to accurately and reliably quantify CBF, which would have been desirable for clinical use and in validation/ reliability studies. Thus, for inter-individual comparison or follow-up examinations, CBF and CBV values have to be normalized to an internal reference, rendering a scaling factor redundant.

8.1.3 Linear relationship and agreement of DSC MRI and CTP

Correlation and linear regression measure the strength of a linear relation between two variables but not their agreement. Agreement between two variables or methods can be assessed by plotting the mean difference between the variables against their mean. If the difference is zero, the methods/ variables agree completely, which is unusual. More important is to determine if the differences within the 95% limits of agreement are clinically important and if the difference varies systematically over the range of measurements, which indicates systematic bias[284].

Comparison of DSC MRI and CTP in Paper I showed both a poor linear relationship on group level for different ROIs and a CBF difference between the modalities that was substantially larger than zero and non-uniform even after PVE correction (Figure 6).

The overestimation of DSC MRI, which is the main cause for the large mean difference between the modalities, might be explained by remaining PVE even after rescaling of the AIF. However the large difference can also indicate a limited repeatability within each method as reported by several validation studies [32,33,54,272,275].

Further, some true, physiological variation of the CBF cannot be excluded as CTP and DSC MRI were performed on 2 consecutive days.

The fact that the CBF difference between the two modalities increased in relation to increasing average CBF values, was probably mainly caused by the concentration-dependent difference in T2* relaxivity between tissue and large vessels[43-45]. Other factors that might have contributed to the discrepancy between the modalities are smoothing effects incorporated in the commercial CTP post-processing software or other post-processing issues; different reductions in estimated tissue impulse response function peak value caused by differences in regularization during deconvolution, imperfect alignment of the perfusion scans and contribution of vessel signal/ attenuation to the tissue CTTC.

8.1.4 Pipeline

By gaining control over the post-processing steps of CTP and DSC MRI we wanted to reduce the amount of unknown bias of the perfusion measurements, which in turn would facilitate comparison of perfusion results. For this purpose we adopted in-house developed software, "pipeline", for Papers II-IV. This software is running on MATLAB, operates on a batch processing framework (Danish Research Centre for Magnetic Resonance, Copenhagen University Hospital Hvidovre, Danmark) and uses Statistical Parametric Mapping 2 for image co-registering and re-sampling.

Masks and ROIs

The removal of large vessels from CTP and DSC MRI has been shown to reduce the inter-subject variability[59,285]. In a CTP study Kudo et al.[59] eliminated vessel pixels based on their CBV value, choosing the best threshold by visual assessment. Ernst et al.[285] determined for DSC MRI the threshold of their vessel mask as 2.5 times the median of the CBF values on the histogram of a CBF map. Similarly to Ernst et al.[285], the vessel mask in Papers II-IV was empirically chosen on the histograms of the peak concentration images, calculated from the CTTC of the DSC MRI or CTP. Concentrations greater than 3.0 times the position of the single peak in the histogram defined voxels containing vessels. The susceptibility effect in DSC MRI is not constrained to the vasculature but influences also the tissue adjacent to the vessels. To remove vessel signals without eliminating tissue pixels can therefore be more difficult in DSC MRI than in CTP.

In Paper II and III a parenchyma mask was used, which discarded CSF voxels. Further, the ROIs on the perfusion maps were trimmed such that only border voxels that contained more than 90% of the original ROI were kept.

The application of masks in combination with much more detailed ROIs than in Paper I, promised CBF measurements in exact anatomical regions with minimized contamination by adjacent tissues/ structures. The major disadvantage of this ROI-analysis is that it is time consuming and to some degree operator dependent. As only one operator placed all ROIs, merely the intra-observer reliability might have been an issue. Spatial normalization of the perfusion maps to a template defined in a standard space and application of standard ROIs was not an option, as normalization programs have difficulties to warp hydrocephalic brains.

Alignment

Instead of the manual 2D alignment in Paper I, in Papers II-IV, FLAIR scans with ROIs were co-registered with and re-sampled to the mean images of the perfusion scans in all 3 dimensions. In Paper II and III this was performed automatically. In Paper IV manual co-registration was necessary, because the CTP data was limited to four 5 mm thick sections, which NiftyReg[286,287], SPM2 and other tested software packages could not handle satisfactory. Although more time-consuming, the manual co-registration was much more reliable than the automatic methods, which was checked by inspecting the placement of the ROIs on the mean CT-image after co-registering and subsequent re-sampling.

SNR

A low SNR affects the accuracy of perfusion techniques and is a major problem of CTP. In Papers II-IV some steps were taken to increase the SNR. Perfusion was not calculated pixel-wise but based on the mean signal-to-time/ concentration-to-time curve of each ROI, which was drawn as large as possible. Further, the use of a model-based deconvolution method (Papers III, IV) limited noise propagation in the calculation of the perfusion, which is especially important in low SNR regions like the PVWM.

Reformatting the four 5 mm sections of the CTP slab into two 10mm sections would also have increased the SNR but at the expense of undesirably increased PVE regarding the ROI evaluation and AIF placement [288]. Spatial smoothing was avoided as it was essential to confine the CBF measurements to within the borders of the ROIs. Due to a fixed imaging study protocol a higher contrast agent concentration, resulting in an increased maximum enhancement of vessels and parenchyma and an improved SNR, was not an alternative solution[23,70]. Neither was an increase of tube voltage or current an option in CTP, as this would have generated a higher radiation dose.

DSC MRI and SVD/oSVD (Papers I, II)

Considering the published literature, the most widely spread deconvolution method is the non-parametric SVD. Since Östergaard et al.[3,4] presented the theoretical basis of CBF measurements by DSC MRI and the results of a simulation- and a pilot-study, SVD has been largely accepted as the most robust and accurate method to reproduce flow independent of the underlying vascular structure and volume. Östergaard et al.[3,4] described the FT approach as especially sensitive to noise and yielding underestimated CBF values at high flow rates with short MTT (2-3s).

However, also SVD and the delay insensitive oSVD[12] produce less accurate CBF values in regions with short MTT, because of the AIF being relatively long compared to the short residue function [4,289].

In Paper I, commercially or freely available post-processing software products were used and these apply for the most part deconvolution with SVD and oSVD. In Paper II we also chose to implement the oSVD method into pipeline, because of its robustness and insensitivity for delay.

DSC MRI and Model dependent FT (Paper III)

During data analysis we noticed that the signal-to-time curves of DSC MRI displayed oscillations on pixel level, exemplified in figure 16. These oscillations were probably secondary to bulk movement during systole and diastole, aggravated by the applied EPI technique with segmented k-space.

To minimize the motion artefacts on pixel level in Paper III it seemed adequate to use a model dependent FT approach.

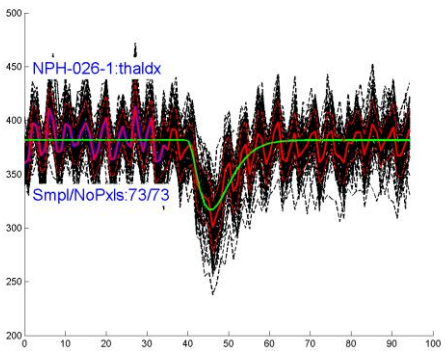

Figure 16. DSC MRI signal-to-time curve, measured in 73 pixels within a ROI placed in the right thalamus of a HI. Note the quite regular oscillations of the signal-to-time curve in each pixel. Outlined in green is a model of the MR signal dip during bolus passage, described by the gamma variate function.

The FT is delay insensitive and exact if the measured CTTCs are periodic[290], implying that the CTTs should return to their baseline level, which usually is not the case in bolus tracking due to recirculation effects. If this condition is

not fulfilled, the curves have to be corrected by extrapolation[9] or fitting[10,279]. The FT in Paper III was combined with the use of a gamma variate fitting which also removed the oscillations. The fitting operation is robust when applied to ROIs instead of single pixel data[11].

Publications that followed the studies by Östergaard et al.[3,4], in which they had raised concerns regarding FT deconvolution, showed parametric SVD and FT to produce similar CBF values[290] and demonstrated that the oSVD and FT deconvolution methods are mathematically identical apart from how regularization is applied[289,291].

In all forms of deconvolution noise suppression is required to produce stable results. In the frequency domain, noise dominates at high and physiological information at lower frequencies. Thus, by the application of a filter for regularization, noise dependent alterations of the CBF estimates can be avoided in FT[9,10]. The frequency cut off does not add information to the tissue impulse response function and regularization is stable[289].

In SVD, the smallest singular values hold the highest noise representation. Determination of a cut-off threshold for the singular values of the matrix that describes the deconvolution reduces the noise. This cut-off threshold varies in DSC MRI between 10 and 20% depending on the SNR[4,27]. An optimal cut-off value has not yet been defined for CTP. Higher thresholds, excluding more singular values, tend to lead to CBF underestimation[292]. Further, the number of singular values that pass the threshold and contribute to the tissue impulse response function varies between deconvolution processes in spite of identical thresholds[289]. Another factor that bias the SVD is that noise can enlarge or diminish signals, which then are falsely accepted or discarded in the search for the largest singular value[11].

In Paper III the noise filter of the FT was set to match the oSVD perfusion estimates of the parenchyma, as measured in Paper II. As a consequence of FT and oSVD being mathematically identical, this matching of the levels of regularization led to a good correspondence of the HI´s mean CBF estimates comparing Paper II and III.

CTP and Model dependent oSVD (Paper IV)

The straightforward comparison of CTP- and DSC MRI-based perfusion results requires the evaluation processes to be as similar as possible. The application of a model dependent FT to the CTP data was, however, not feasible. To our knowledge there are no studies that have investigated the performance of FT in CTP and an online-search for a CTP software using FT has been fruitless. An attempt to calculate CBF from our CTP data by FT resulted in more pronounced CBF underestimation and variance than by oSVD (data not shown).

As it has been shown that model dependent FT and SVD correlate very well[290], in Paper IV a model dependent oSVD was used.

Truncation, i.e. the CTP scan is too short to fully sample the venous passage of the injected tracer, was noted in some of the scans, but was compensated for by fitting of a gamma variate function to the peak of all measured attenuation-to-time curves. Truncation in non-ischemic patients can be caused by reduced injection rates, large patient stature or reduced cardiac output, and has been shown to generate perfusion errors, the extent of which depends on the post-processing algorithm[71].

Further, the model limited movement artifacts and noise propagation in the calculation of the perfusion, especially important in low SNR regions like the PVWM. Recirculation effects were also eliminated, which ensured one of the assumptions of bolus tracking, namely to measure the first pass.

The performance of different deconvolution methods has been an object of intensive research in DSC MRI but not in CTP. The few existing CTP studies of deconvolution methods indicated that adaption of the oSVD[12] to CTP data is possible and results in the reduction of tracer delay induced effects[85,293,294]. Yet, the same studies reported remarkable variations of the absolute CBF values among the tested algorithms with the lowest estimates for oSVD[293]. Thus, the sub-physiological CBF estimates of Paper IV are not unique after oSVD of CTP data, but the underlying cause is not clear.

One possible explanation is the noise regularization of the deconvolution process, which in our study at 5% allowed on average only 5 to 7 singular values to determine the form of the tissue impulse response function, which probably reduced the maximum height of this curve and thereby the estimated CBF. The higher the chosen noise threshold, the more pronounced this effect will be.

Further, the bolus injection time in CTP (12.5 s) is substantially longer than in DSC MRI (3s), because of the larger volume of contrast agent. As a result the arterial and tissue CTTCs are broad and relatively flat. The tissue impulse response function, convoluted over such a long time, will be very hard to estimate via deconvolution. For the context of DSC MRI Östergaard et al.[4] explained that CBF inaccuracy increases with shorter MTT because AIF varies slowly compared with MTT, the time scale of the residue function that is to be sampled. The only possibility to circumvent this limitation is the use of rapid bolus injections with very narrow AIF[4]; a recommendation that is definitely not fulfilled in CTP.

In spite of the deviance of the CBF values, the absolute estimates were used for statistical analyses within and between groups, as the underlying methodological bias was supposed to affect all subjects in an equivalent manner. Also, the GM/ WM ratio was within the expected range[11], indicating

a proportional and systematic effect of the bias on GM and WM. The use of relative CBF values was not an option, as relative estimates would confound the interpretation of the observed CBF changes.

8.2 Clinical aspects

8.2.1 Material

The majority of earlier perfusion studies of NPH has been performed on sNPH patients or mixed groups of iNPH/ sNPH. Non-uniformity of the patient groups complicates the comparison of study results and the interpretation of the findings from a pathophysiological point of view[212]. The patient group in this work was diagnosed with probable iNPH according to the current EA-diagnostic guidelines[125] and the clinical improvement rate of 75% after CSF diversion indicated the validity of the diagnosis[241].

iNPH patients suffered to a larger extent of hypertension[111] than HI, which can raise concerns about hypertension confounding the CBF measurements. However, a group comparison of the regional rCBF values of our iNPH patients with hypertension and those without elevated blood pressure did not reveal any statistically significant differences in Paper II.

On trend level, the non-responder group exhibited a higher frequency of hypertension and cardio-vascular disease and higher scores for WM changes, which might indicate a larger degree of negative influence from small vessel disease in this subgroup. However, the presence of cerebrovascular risk factors and WM changes normally associated with vascular encephalopathy does not predict negative outcome after shunt insertion[140,179,238]. On average the reported mean duration of symptoms was shorter and the preoperative performance better in non-responders than in responders. Considering that iNPH is a progressive disease over time, the inverse relationship would have been expected. Yet, the large inter-individual variability of the natural history of iNPH[251] in combination with the small size of the non-responder group might explain the described distribution of the clinical variables.

Patients were classified into shunt responders and non-responders based on an arbitrary chosen limit on the iNPH scale[144]. Improvement after shunt surgery was defined as an increment of $\geq$5 points, which corresponds to an increase by 25 points in one of the domains neuropsychology, balance and continence or 12.5 points in the gait domain, the weight of which is doubled. Twenty-five points on the domain score of the iNPH scale equals one quarter of the accessible points in that domain and implies a substantially improved clinical performance. The choice of limit can obviously influence the

statistical results in the comparative analyses of the subgroups, a challenge that all scales that are in use have to face. The distribution of outcome rates, i.e. 75% responders and 25% non-responders, is within the expected range[241], which indicates that the chosen limit is consistent with the limits of other, previously used scales.

8.2.2 Global and regional CBF

By DSC MRI and CTP, which are new perfusion techniques in the context of iNPH, we were able to demonstrate preoperative regional and global CBF reductions that, after shunt insertion, were restored in responders to approximately the perfusion levels of HI.

With few exceptions the results of the perfusion measurements of DSC MRI and CTP corresponded well and were further in accordance with earlier perfusion reports. Each of the following comparisons of the DSC MRI- and CTP-based results is accompanied by references to some of the corresponding SPECT- or PET- or Xenon CT- findings.

Significant preoperative perfusion deficits in the iNPH group were seen with DSC MRI and CTP in the parenchyma ROI, in the PVWM and the lentiform nucleus prior to shunting[208,212,215-217]. CTP revealed also significant NAWM hypoperfusion[218,219,295]. Due to the limited spatial coverage of the perfusion slab in CTP, the basal, medial frontal cortex and the hippocampus could not be evaluated; regions that had shown low rCBF in DSC MRI[220,223,296].

After shunting the CBF increased in all ROIs in responders by 2-9% measured in relative (DSC MRI) and by 2.5-32% in absolute values (CTP).The increases were significant in the parenchyma ROI[224,226] and the PVWM[221], for both techniques, but in the NAWM and the caudate head only for the CTP-based analysis[221]. Again, the hippocampus was not included in the CTP evaluation. Consequently, the perfusion increase in this structure as seen by DSC MRI[223,296] could not be confirmed.

In iNPH multiple cortical and subcortical anatomical regions as well as their connections seem to be affected and the PVWM may have a central role. Many investigations, like histopathologic surveys, metabolic studies and morphological as well as functional imaging reports, have shown pathophysiological changes that involve the periventricular region.

In an MRI co-registered PET study[217], an induced rise in CSF pressure resulted in CBF reductions in the basal ganglia, thalami and in the WM. A finite element analysis indicated that the mean stress and the shear stress were most pronounced in regions closest to the ventricles and lowest in the cortical regions. A ROI evaluation further suggested the existence of a relationship between the proximity to the ventricles and the observed CBF

decrease. As the CBF reductions correlated poorly with changes in ICP, perfusion pressure or mean arterial blood pressure, a direct compression of the cerebral parenchyma was unlikely to be the cause. Instead, the suggested mechanism was an increased transependymal CSF flow into the interstitial space. This reversed flow of interstitial fluid might lead to stagnation of vasoactive and/ or toxic metabolites, which in turn influence the cerebral perfusion[297,298], causing the subcortical symptomatology.

In Papers II-IV the PVWM was the anatomical region that in percentage showed the largest preoperative CBF/ rCBF reduction and together with NAWM the most pronounced restoration ratio after shunt surgery in responders. In non-responders the PVWM CBF/ rCBF remained reduced after shunt surgery, while the CBF/ rCBF in several GM structures increased. The recovery of these GM structures, even when it in percentage and in absolute terms equaled or exceeded the postoperative perfusion increase of the responders, effected no clinical improvement.

This might indicate that the improvement of the GM perfusion is insufficient in non-responders or that improved GM CBF/ rCBF is irrelevant as long as the WM regions do not recover, maybe because of permanent damage[191,197,208,218,240,299].

8.2.3 CBF and symptoms

The expected positive relationship between the level of cortical and subcortical perfusion and the severity of symptoms in the domains cognition, gait, balance and continence has previously not been shown for a homogenous iNPH group.

Earlier studies that investigated this correlation were either performed on sNPH or mixed sNPH/iNPH groups[218,223,296,300-302] , assessed either only the total clinical performance[216,220,221] or one single symptom[222], or observed a negative correlation between CBF, gait and cognition[303], or no correlation at all[304].

The correlations for responders shown in Paper IV were largely in agreement with the findings of Paper II and III. Paper IV, in responders, revealed also relationships between perfusion and clinical performance for the parenchyma and the central thalamus preoperatively, and the occipital cortex pre-and postoperatively. However, the analysis of the individual changes of CBF and clinical performance after shunting in Paper IV resulted in no significant linear relationships, which contrasts to Paper III. This inconsistency can either be due to a type I error in the DSC MRI study or a type II error in the CTP study. The somewhat lower sample size and power of the CTP study might favor the latter.

The negative correlation between PVWM, thalamus and total GM rCBF and the postoperative improvement in iNPH score points, seen in Paper II, was not evaluated in Paper III or IV. This relationship is interpreted as a more obvious recovery after shunt insertion in patients with a lower overall preoperative function, which was also reported in the European multicenter study on iNPH [145].

Clusters of positive correlations were found pre- and postoperatively for the perfusion in PVWM and cingulate gyrus on one hand, and gait performance, cognition, continence and the total iNPH scale score on the other.

The WM tracts linked to gait velocity, stride length and stride width are located close to the lateral ventricles[305] which might explain the linear relationship between PVWM CBF/ rCBF and the severity of the gait disturbance.

The PVWM perfusion is probably also of significance for the functioning of the bidirectional frontal-subcortical circuits and association pathways that travel by next to the ventricular walls. These pathways are responsible for the neural transmission that maintains different aspects of cognition[260,306] and might account for the finding of a positive correlation between PVWM CBF/ rCBF and the neuropsychology score.

Also the relationship between incontinence and reduced CBF in the cingulate gyrus or the PVWM demonstrated in this study might be illustrated by neuroanatomical observations. The voluntary, inhibitory control of micturition is dependent on connections between the frontal cortex and the hypothalamus as well as between the paracentral lobule and the brainstem. Further, tonic suppression of the micturition reflex pathway seems to be exerted by the medial frontal cortex and the basal ganglia and CBF is increased in the dorsolateral prefrontal cortex and the anterior cingulate gyrus during voiding [307].

The anterior cingulate gyrus and the thalamus, being parts of the above mentioned frontal-subcortical circuits, convey behavior and are engaged in the regulation of overall cortical arousal[223,258-260] in line with the correlation between CBF in these areas and cognitive performance.

In responders, in Paper III, the post-surgical rCBF restoration ratio of the caudate head, the cingulate gyrus and the periventricular thalamus correlated with the clinical improvement in several domains and overall. However, the significant perfusion recovery in the PVWM and parenchyma showed no relationship to the relief of symptoms. Possibly, when the functioning of PVWM tracts in the responder group is restored or improved, GM structures regain importance in the frontal-subcortical circuits. Similar findings were made by Mataro et al.[221]. Postoperative CBF increase was demonstrated in several regions of both frontal lobes including the frontal right WM and the

right parietal lobe and only regions with improved CBF in GM structures, e.g. the left frontal insula and the anterior cingulate gyrus, correlated with post-surgical clinical improvement.

The importance of the association, commissural and projection tracts in the pathophysiology of iNPH is underlined by the DTI findings. An increased, but reversible FA has been reported along the corticospinal tract and loss of directionality (decreased FA) has been found in the corpus callosum and the PVWM[198,199,201-206]. The lower the FA values in the corpus callosum the more severe were the observed gait disturbances[205].

Comparing the neuropsychological performance of iNPH patients and HI, Hellström et al.[123] found that different, seemingly unrelated neuropsychological tests were associated with each other and with the level of disturbance of gait, balance and continence. These associations indicated that widely distributed and interrelated cortical and subcortical regions participate in the generation of symptoms and signs in iNPH. A hypoperfused PVWM might represent the functional neuroanatomical region with a potential of influencing multiple other areas simultaneously.

8.2.4 Relative versus absolute CBF values

As discussed earlier, absolute perfusion quantification by DSC MRI is still not established. Inter-subject comparisons must therefore be performed using an internal reference that is supposed to have little inter-subject variability[47]. For Papers II and III the occipital cortex was chosen as internal reference as there are only a few studies[218,219,304] that have reported a mild hypoperfusion in this area. Because of the unexpected result of a preoperatively elevated rCBF in the thalami (Paper II), a second comparative statistical analysis of the data with the global parenchyma as internal reference was performed without changing the finding.

Yet, the analysis of the CTP-based absolute CBF estimates (Paper IV) revealed CBF reductions in the thalamic and occipital regions in iNPH when compared with HI, which, however, were not statistically significant. In light of this CTP observation, the thalamic DSC MRI finding was probably caused by the use of relative CBF values. An internal reference, that is hypoperfused to an equal or more pronounced extent than the thalami, would mask the CBF reduction of the latter.

A variable internal reference can certainly also lead to overestimation of the CBF ratio.

Further, variability of the internal reference over time might be a problem in repeated measurements. If the CSF diversion does not affect the cerebral

parenchyma uniformly, calculated differences between the pre-and postoperative level of perfusion, like those in Paper III, might be distorted.

It would be desirable to have reliable, absolute CBF estimates in the statistical context, but also in the search for a prognostic imaging marker.

Also with regards to CTP, absolute perfusion values cannot be compared among different post-processing programs. Slope and intercept in linear regression analysis of absolute perfusion estimates varied significantly in a phantom study by Kudo et al.[84], examining the accuracy and reliability of various perfusion software solutions.

8.2.5 Prognostic imaging marker

The decision about which iNPH patients one should offer CSF diversion is, today, guided by the patients' general health condition, clinical performance, age and sometimes by supplementary test results. The intention is to reduce the risks for complications and to increase the percentage of patients that improve after shunting, which, today, on average is >80%[145,241]. If we presume, that the diagnosis and the outcome assessment of the 20% without improvement are correct, these patients probably have already developed irreversible brain damage at the time of the CSF diversion. Perfusion studies have to date either not identified a prognostic pattern [208,212,220,224,308] or reported contradictory findings[220,225,299,309-311].

In Paper II we found that a preoperative basal, medial frontal rCBF $\geq$0.798 predicted good outcome after shunt insertion. Approximately the same anatomical region was pointed out as an area of interest in predicting outcome by Klinge et al. [311] and Murakami et al.[225]. Other investigations reported, in line with our results, that patients with higher global or regional preoperative CBF showed the most consistent clinical improvement after shunt therapy[299,309,310].

However, in Paper III, did the rCBF of the basal, medial frontal cortex not differ significantly between responders and non-responders, but this was the case with the cingulate gyrus. In Paper IV, the basal, medial frontal cortex was not sufficiently covered by the CTP slab to allow analysis, but the cingulate gyrus was evaluated. None of the assessed ROIs demonstrated a significant CBF difference between iNPH subgroups.

Thus, the finding of Paper II regarding a predictive rCBF value might be erroneous. One possible explanation is that susceptibility artefacts from the skull base have influenced the perfusion sequence. Other sources of error are the use of relative CBF values and the multiple comparisons that increase the risk of falsely rejecting the null hypothesis.

8.3 Main limitations

Due to the complex imaging and data collection protocol, which stretched over several days, both pre- and postoperatively, it was not an easy task to find willing participants, and for ethical reasons (patients and healthy individuals were exposed to radiation during the CT scan) we did not want to include too many subjects and closed the recruitment when 24 controls and 51 patients were enrolled. Moreover, the study design required the omission of patients and HI who had not a complete set of 4 successful perfusion imaging series leaving fewer subjects in the study than intended. These factors resulted in small sample sizes and limited statistical power.

Contemporary single center reports on iNPH in general also struggle with gathering larger sample sizes as the disease still is underdiagnosed and also because of the frail nature of the patients. As the present study aimed at investigating the application of a new imaging methodology, it was performed as a single center study with its limitations, and our results need to be confirmed in future studies, including larger number of patients.

The perfusion data showed quite large variances, which most likely were related to technique inherent problems, e.g. the PVE and the SNR, but probably also secondary to the small sample size.

In Paper III the metallic valve artefacts necessitated a unilateral ROI evaluation, which decreased the number of voxels contributing to the signal and probably influenced the variance negatively.

The relatively low SNR of DSC MRI improves at higher field strength, but at 3T the metallic valve artefacts in Paper III would probably have compromised also the evaluation of the contralateral hemisphere. Shunt devices with valves that do not contain metallic parts, but instead for example a silicone diaphragm, should be used to enable bilateral perfusion measurements in the future.

Due to the limited spatial coverage of the CTP and some variation of the placement of the perfusion slab, ROIs corresponded to parts of, instead of entire, specific anatomical regions and showed some intra- and inter-individual variance, which supposedly increased the variance of the data. Unfortunately, at the time of the data collection no CT-scanner with a more extended coverage was available at our center.

Depending on the software used, post-processing of DSC MRI and CTP is performed in a manual, semiautomatic or fully automatic way. In general semiautomatic or automatic programs are preferred as they can be expected to improve accuracy and repeatability of the measurements.

Studies of the inter-observer variability of commercial, semiautomatic CTP software have shown coefficients of variation ranging from 2.5 to 33%[77,80]. One study that did not allow for a manual correction of the automatically chosen variables reported greater inter-observer variability for fully automated perfusion calculation[77]. Another study found the fully automated version to generate smaller coefficients of variability, but had permitted manual correction of obvious misplaced AIF or VOF[80].

In the studies for this thesis only one experienced observer selected the post-processing variables.

The intra-observer variability regarding the CTP software used in Paper I was tested by Sanelli et al.[77]. The coefficient of variation was low, ranging between 0.3 and 11%. The more experienced the observer, the lower the variability.

In the DSC MRI part of Paper I, the manual selection of a small vein for rescaling purpose of the AIF introduces a potential source of inaccuracy. Yet, the user-interaction dependency was examined by Knutsson et al.[312], who found a very good correlation (r=0.87) between 2 measurements at least one week apart.

In a simulation study, Kjølby et al. [313] used a model of an AIF voxel including the relaxation properties of blood and tissue and different locations of the artery relative to the main magnetic field. They found that PVE induced broadening and fluctuations of the AIF and lead, in a nonlinear way, to overestimation of the CBF, irrespective of vessel orientation. In contrast to AIF from arteries perpendicular to the main magnetic field, the amplitudes of AIF in arteries parallel to the main magnetic field expressed to some extent the amount of PVE in the voxels. They concluded, in concordance with van Osch et al. [314], that a global AIF is best chosen from an artery parallel with the main magnetic field using high amplitude as sign of small PVE. Fully automated AIF placement and also placement of local AIF near ROIs can usually not guarantee that the chosen vessels run parallel to the magnetic field. Thus, semiautomatic post-processing, that allows the active choice of a target artery might be of advantage.

The criteria for AIF selection defined by Kjølby et al.[313] were, as far as possible, adopted in Paper II and III. The intra-observer variability for semiautomatic AIF selection in DSC MRI according to their criteria has not been studied. Our impression is, however, that the variance of the perfusion results is dependent on the variable appearance of the AIF due to PVE, saturation and patient motion, rather than on the intra-observer variability.

8.4 Scientific and clinical value

The methodology of Papers III-IV was explorative and the statistical analyses contained multiple comparisons, both regarding perfusion levels and correlations between perfusion and clinical performance. Significant results have to be interpreted with caution as the risk of rejecting the null hypothesis by chance is increased. However, the fact that the CTP measurements (Paper IV) are a replication of the DSC MRI-based assessments (Papers II, III) on the same material, one day apart, increases the scientific value of the results. It seems very unlikely that two different perfusion techniques and calculation processes would result in incidental findings of such high similarity. Reversing this thought, we can also assume that both techniques contain perfusion information and are reliable.

Thus, DSC MRI and CTP have been shown to be applicable for research purposes in iNPH.

However, as long as a definite CBF-based imaging marker for the prediction of outcome after shunting or a diagnostic marker differentiating iNPH from SAE and AD has not been identified, the implementation of DSC MRI or CTP into the routine work up of iNPH is not indicated.

9 MAIN FINDINGS

Paper I

- CBF estimates, obtained by rescaled DSC MRI, were closer to the normal range and correlated better with CTP values than uncorrected DSC MRI estimates.
- DSC MRI and CTP showed a poor linear relationship inter-individually and a CBF difference between the modalities that was substantially larger than zero and non-uniform even after PVE correction, indicating poor agreement.

Paper II

- DSC MRI demonstrated in iNPH a preoperative reduction of the rCBF in the basal, medial frontal cortex, the hippocampus, the lentiform nucleus, PVWM regions and the parenchyma.
- The preoperative rCBF of the PVWM, the thalamus and the total grey matter, measured by DSC MRI, correlated positively with the clinical overall performance, the gait and cognition.
- The same regional rCBF correlated negatively with the level of improvement after shunting.
- Higher frontal rCBF seemed to predict good outcome after shunting.

Paper III

- DSC MRI-based measurements showed after shunting an rCBF increase of 2-9% in all anatomical regions in responders. Statistical significance was reached in the hippocampus, the anterior PVWM and in the parenchyma.
- The improved postoperative perfusion in the cingulate gyrus, caudate head and periventricular thalamus correlated with the degree of clinical improvement after shunting in responders. The significant CBF increase in the hippocampus, the anterior PVWM and the parenchyma, however, showed no correlation with better postoperative clinical performance.

Paper IV

- Preoperatively CTP-based measurements displayed regional and global CBF reductions, including the occipital cortex and the thalamus in iNPH patients compared to HI. The CBF decrease was significant in the PVWM, the lentiform nucleus, the NAWM and the parenchyma compared to HI.
- No significant CBF differences were found between responders and non-responders at baseline.

- After CSF diversion the CBF recovered in responders by 2.5-32% to approximately to the perfusion levels of HI, but remained significantly decreased in the PVWM of non-responders.
- The PVWM demonstrated the largest percentage preoperative CBF reduction and together with NAWM the most pronounced recovery after shunt surgery in responders.
- The pre- and postoperative global and regional CBF of the responders correlated with the overall clinical performance and the severity of the symptoms in the different domains.
- There was no significant linear relationship related to individual changes of CBF and clinical performance after shunting.

10 CONCLUSIONS

- PVE correction in DSC MRI by rescaling the AIF using the VOF increased the accuracy of the CBF estimates at 1.5 T. The method might improve inter-subject comparison and patient follow up.
- DSC MRI and CTP demonstrated limited correlation and agreement.
- DSC MRI can measure relative global and regional pre- and postoperative CBF changes in iNPH patients, although metallic valve artefacts after shunting limit the perfusion evaluation to one hemisphere.
- In spite of a limited spatial coverage, CTP can be used to measure CBF changes in iNPH patients pre- and postoperatively.
- The good overall agreement of the results of CTP- and DSC MRI-based measurements of the same material indicates reliability of both perfusion methods. The methods might be used as investigational perfusion techniques in iNPH.
- At baseline the CBF/ rCBF of iNPH patients is reduced in cortical and subcortical regions as well as globally. The reduction is most pronounced in the PVWM.
- After shunting the CBF/ rCBF of responders recovers.
- In non-responders the CBF/ rCBF in the PVWM remains significantly reduced.
- Regional and global CBF/ rCBF correlate with symptoms and signs of iNPH.
- Patients with higher preoperative perfusion generally perform better in clinical tests.
- Patients with a lower overall preoperative function, show a more obvious clinical recovery after CSF diversion.
- As no definite CBF threshold for prediction of outcome after shunting has been identified, the incorporation of DSC MRI or CTP into the routine work up of iNPH is not yet indicated.

11 FUTURE PERSPECTIVES

As both CTP and DSC MRI appear to be useful research tools in the context of iNPH, further investigations should be performed using CTP and DSC MRI.

Larger sample sizes of both responders and especially non-responders are needed to increase the power of these investigations, most likely by including patients from other centers.

Because of the multitude of findings that point to the periventricular region as central in the pathophysiology of iNPH, future studies might concentrate on confirming that the PVWM perfusion is restored in responders but remains decreased/ further decreases in non-responders. As SAE represents the major differential diagnosis of iNPH and possibly even shares the pathophysiological pattern[114], patients with SAE should be included as control subjects.

This confirmative approach could be combined by an explorative multiple regression analysis incorporating the possible prognostic changes on morphological MRI[157] and DTI[202]. If a single imaging marker cannot be found, we should try to predict outcome by a model that incorporates several imaging features and possibly even iNPH relevant clinical variables.

Whether the hypoperfusion of the PVWM is secondary to low perfusion pressure or to metabolic down regulation is unclear. Studies that combine the assessment of CBF and metabolism are therefore warranted.

Newer CT scanners offer larger spatial coverage of the CTP sequence, which is of advantage. Larger ROIs can be evaluated, and interesting anatomical regions, which were not included in the 2 cm CTP slab in this work, could be analyzed. Of course, the temporal resolution must be kept reasonably short to avoid inaccurate perfusion values. To increase the SNR further, reconstructing the CTP data to a lower matrix resolution prior to the perfusion calculation might be a way to go in future studies.

A relatively new type of deconvolution, the Bayesian method, seems to produce more accurate DSC MRI- and CTP-based perfusion parameters in vivo and in phantoms than delay insensitive SVD approaches[7,8,60]. One can hope that this method or some other approach may show results that are convincingly accurate to become a standard of perfusion analysis, which would facilitate the comparison of perfusion studies between hospitals and modalities.

Moreover, international agreement and uniformity in definitions of the disease criteria, both clinical and image-related, are needed to allow comparisons of results from different research groups.

ACKNOWLEDGEMENTS

During the work on this thesis many people have helped, supported an encouraged me. I want to thank them all, especially:

Professor Mikael Hellström, my supervisor, for providing calm advice, fresh criticism of this thesis that is far from his main research interests, and for regularly allowing me a share of his research funds.

Associate professor Göran Starck, my co-supervisor, for his scientific thoroughness, his ability and patience when explaining physics to a physician and for sometimes having been my "Wailing Wall".

Professor Carsten Wikkelsø, my second co-supervisor, who knows everything about iNPH, for inviting me into the NPH team and for his optimistic attitude.

Prof. Sven Ekholm, the most generous person my husband and I know, for introducing me to research, for his interest and help in the production of this thesis and, most of all, for our year in Rochester, NY.

Prof. Stig Holtås, my initial main supervisor, for organizing my registration as a PhD student, the project plan, the basic financing and valuable contacts.

Irene K. Mikkelsen, PhD, Maria Hultenmo and Jonathan Arvidsson, for all their time and effort that went into "Pipeline".

Associate Professor Mats Tullberg and Per Hellström, PhD, for friendly and constructive discussions, pointing out the essentials and, last but not least, for statistical advice.

All my co-authors not already mentioned, Mikael Edsbagge, Professor Eva Forsell-Aronson, Associate Professor Linda Knutsson, David Kristiansen and Martin Jakobsson, for their commitment and their contribution.

Marios Mitsis, my colleague, for switching rooms with me. What a blessing to escape the alarm system at the “Obama house”!

All my other dear colleagues at the neuroradiology department, Birgitte Berthelsen, PhD, Åke Bovaller, Pavlos Chrisanis, Dennis Dunker, Nickoleta Hoefling, Christer Jensen, Lars Jönsson, Anders Johansson, Angelika Kouti, Mats Laesser, PhD, Matilda Lanne, Birgitta Leiram, Mia Ljevak, Inger Nilsson, Anas Rashid, Alexandros Rentzos, Gundi Schnabel and Luisella Sibilla for friendship, cheerful coffee breaks and for covering during my research leave.

Gudrun Barrows and Gunilla Ahl Börjesson for keeping track of the database and all other members of the Hydrocephalus Unit for taking care of the clinical aspects of this work and for excellent publications to rely on

The CT- and MRI staff, for performing the scans and burning CDs for archiving purposes.

My father in law, Traian, for being a role model as he is one of these doctors who really loves the job.

Lucia, my mother in law, who always found the time to help with the laundry.

Our children, Clara, Julius and Anna, for patiently waiting this thesis out, and my husband, Radu, for looking after things at home.

REFERENCES

1. Wintermark M, Maeder P, Thiran JP, Schnyder P, Meuli R. Quantitative assessment of regional cerebral blood flows by perfusion CT studies at low injection rates: a critical review of the underlying theoretical models. *European radiology.* 2001;11(7):1220-1230.
2. Meier P, Zierler KL. On the theory of the indicator-dilution method for measurement of blood flow and volume. *J Appl Physiol.* Jun 1954;6(12):731-744.
3. Ostergaard L, Sorensen AG, Kwong KK, Weisskoff RM, Gyldensted C, Rosen BR. High resolution measurement of cerebral blood flow using intravascular tracer bolus passages. Part II: Experimental comparison and preliminary results. *Magn Reson Med.* Nov 1996;36(5):726-736.
4. Ostergaard L, Weisskoff RM, Chesler DA, Gyldensted C, Rosen BR. High resolution measurement of cerebral blood flow using intravascular tracer bolus passages. Part I: Mathematical approach and statistical analysis. *Magn Reson Med.* Nov 1996;36(5):715-725.
5. Zierler KL. Theoretical basis of indicator-dilution methods for measuring flow and volume. *Circ Res.* 1962;10:393-407.
6. Zierler KL. Equations for Measuring Blood Flow by External Monitoring of Radioisotopes. *Circ Res.* Apr 1965;16:309-321.
7. Mouridsen K, Friston K, Hjort N, Gyldensted L, Ostergaard L, Kiebel S. Bayesian estimation of cerebral perfusion using a physiological model of microvasculature. *NeuroImage.* Nov 1 2006;33(2):570-579.
8. Boutelier T, Kudo K, Pautot F, Sasaki M. Bayesian hemodynamic parameter estimation by bolus tracking perfusion weighted imaging. *IEEE transactions on medical imaging.* Jul 2012;31(7):1381-1395.
9. Gobbel GT, Fike JR. A deconvolution method for evaluating indicator-dilution curves. *Phys Med Biol.* Nov 1994;39(11):1833-1854.
10. Rempp KA, Brix G, Wenz F, Becker CR, Guckel F, Lorenz WJ. Quantification of regional cerebral blood flow and volume with dynamic susceptibility contrast-enhanced MR imaging. *Radiology.* Dec 1994;193(3):637-641.
11. Wirestam R, Andersson L, Ostergaard L, et al. Assessment of regional cerebral blood flow by dynamic susceptibility contrast MRI using different deconvolution techniques. *Magn Reson Med.* May 2000;43(5):691-700.

12. Wu O, Ostergaard L, Weisskoff RM, Benner T, Rosen BR, Sorensen AG. Tracer arrival timing-insensitive technique for estimating flow in MR perfusion-weighted imaging using singular value decomposition with a block-circulant deconvolution matrix. *Magn Reson Med.* Jul 2003;50(1):164-174.

13. Andersen IK, Szymkowiak A, Rasmussen CE, et al. Perfusion quantification using Gaussian process deconvolution. *Magn Reson Med.* Aug 2002;48(2):351-361.

14. Vonken EJ, van Osch MJ, Bakker CJ, Viergever MA. Measurement of cerebral perfusion with dual-echo multi-slice quantitative dynamic susceptibility contrast MRI. *Journal of magnetic resonance imaging : JMRI.* Aug 1999;10(2):109-117.

15. Vonken EP, Beekman FJ, Bakker CJ, Viergever MA. Maximum likelihood estimation of cerebral blood flow in dynamic susceptibility contrast MRI. *Magn Reson Med.* Feb 1999;41(2):343-350.

16. Valentinuzzi ME, Montaldo Volachec EM. Discrete deconvolution. *Medical & biological engineering.* Jan 1975;13(1):123-125.

17. Wintermark M, Thiran JP, Maeder P, Schnyder P, Meuli R. Simultaneous measurement of regional cerebral blood flow by perfusion CT and stable xenon CT: a validation study. *AJNR. American journal of neuroradiology.* May 2001;22(5):905-914.

18. Rosen BR, Belliveau JW, Vevea JM, Brady TJ. Perfusion imaging with NMR contrast agents. *Magn Reson Med.* May 1990;14(2):249-265.

19. Boxerman JL, Hamberg LM, Rosen BR, Weisskoff RM. MR contrast due to intravascular magnetic susceptibility perturbations. *Magn Reson Med.* Oct 1995;34(4):555-566.

20. Fisel CR, Ackerman JL, Buxton RB, et al. MR contrast due to microscopically heterogeneous magnetic susceptibility: numerical simulations and applications to cerebral physiology. *Magn Reson Med.* Feb 1991;17(2):336-347.

21. Guckel F, Brix G, Rempp K, Deimling M, Rother J, Georgi M. Assessment of cerebral blood volume with dynamic susceptibility contrast enhanced gradient-echo imaging. *Journal of computer assisted tomography.* May-Jun 1994;18(3):344-351.

22. Thilmann O, Larsson EM, Bjorkman-Burtscher IM, Stahlberg F, Wirestam R. Comparison of contrast agents with high molarity and with weak protein binding in cerebral perfusion imaging at 3 T. *Journal of magnetic resonance imaging : JMRI.* Nov 2005;22(5):597-604.

23. Benner T, Reimer P, Erb G, et al. Cerebral MR perfusion imaging: first clinical application of a 1 M gadolinium chelate (Gadovist 1.0) in a double-blinded randomized dose-finding study. *Journal of magnetic resonance imaging : JMRI.* Sep 2000;12(3):371-380.

24. Tombach B, Benner T, Reimer P, et al. Do highly concentrated gadolinium chelates improve MR brain perfusion imaging? Intraindividually controlled randomized crossover concentration comparison study of 0.5 versus 1.0 mol/L gadobutrol. *Radiology.* Mar 2003;226(3):880-888.

25. Thomsen HS, Morcos SK, Almen T, et al. Nephrogenic systemic fibrosis and gadolinium-based contrast media: updated ESUR Contrast Medium Safety Committee guidelines. *European radiology.* Feb 2013;23(2):307-318.

26. Boxerman JL, Rosen BR, Weisskoff RM. Signal-to-noise analysis of cerebral blood volume maps from dynamic NMR imaging studies. *Journal of magnetic resonance imaging : JMRI.* May-Jun 1997;7(3):528-537.

27. Knutsson L, Stahlberg F, Wirestam R. Aspects on the accuracy of cerebral perfusion parameters obtained by dynamic susceptibility contrast MRI: a simulation study. *Magn Reson Imaging.* Jul 2004;22(6):789-798.

28. van Osch MJ, Vonken EJ, Wu O, Viergever MA, van der Grond J, Bakker CJ. Model of the human vasculature for studying the influence of contrast injection speed on cerebral perfusion MRI. *Magn Reson Med.* Sep 2003;50(3):614-622.

29. Perkio J, Aronen HJ, Kangasmaki A, et al. Evaluation of four postprocessing methods for determination of cerebral blood volume and mean transit time by dynamic susceptibility contrast imaging. *Magn Reson Med.* May 2002;47(5):973-981.

30. Thompson HK, Jr., Starmer CF, Whalen RE, McIntosh HD. Indicator Transit Time Considered as a Gamma Variate. *Circ Res.* Jun 1964;14:502-515.

31. Leenders KL, Perani D, Lammertsma AA, et al. Cerebral blood flow, blood volume and oxygen utilization. Normal values and effect of age. *Brain.* Feb 1990;113 (Pt 1):27-47.

32. Carroll TJ, Teneggi V, Jobin M, et al. Absolute quantification of cerebral blood flow with magnetic resonance, reproducibility of the method, and comparison with H2(15)O positron emission tomography. *J Cereb Blood Flow Metab.* Sep 2002;22(9):1149-1156.

33. Grandin CB, Bol A, Smith AM, Michel C, Cosnard G. Absolute CBF and CBV measurements by MRI bolus tracking before and after acetazolamide challenge: repeatabilily and comparison with PET in humans. *NeuroImage.* Jun 2005;26(2):525-535.

34. van Osch MJ, Vonken EJ, Bakker CJ, Viergever MA. Correcting partial volume artifacts of the arterial input function in quantitative cerebral perfusion MRI. *Magn Reson Med.* Mar 2001;45(3):477-485.

35. Wirestam R, Ryding E, Lindgren A, Geijer B, Holtas S, Stahlberg F. Absolute cerebral blood flow measured by dynamic susceptibility contrast MRI: a direct comparison with Xe-133 SPECT. *Magma.* Dec 2000;11(3):96-103 Erratum in: MAGMA 2001;2013:2060.

36. Ellinger R, Kremser C, Schocke MF, et al. The impact of peak saturation of the arterial input function on quantitative evaluation of dynamic susceptibility contrast-enhanced MR studies. *Journal of computer assisted tomography.* Nov-Dec 2000;24(6):942-948.

37. Rausch M, Scheffler K, Rudin M, Radu EW. Analysis of input functions from different arterial branches with gamma variate functions and cluster analysis for quantitative blood volume measurements. *Magn Reson Imaging.* Dec 2000;18(10):1235-1243.

38. Carroll TJ, Rowley HA, Haughton VM. Automatic calculation of the arterial input function for cerebral perfusion imaging with MR imaging. *Radiology.* May 2003;227(2):593-600.

39. Murase K, Kikuchi K, Miki H, Shimizu T, Ikezoe J. Determination of arterial input function using fuzzy clustering for quantification of cerebral blood flow with dynamic susceptibility contrast-enhanced MR imaging. *Journal of magnetic resonance imaging : JMRI.* May 2001;13(5):797-806.

40. Calamante F, Morup M, Hansen LK. Defining a local arterial input function for perfusion MRI using independent component analysis. *Magn Reson Med.* Oct 2004;52(4):789-797.

41. Knutsson L, Larsson EM, Thilmann O, Stahlberg F, Wirestam R. Calculation of cerebral perfusion parameters using regional arterial input functions identified by factor analysis. *Journal of magnetic resonance imaging : JMRI.* Apr 2006;23(4):444-453.

42. Mouridsen K, Christensen S, Gyldensted L, Ostergaard L. Automatic selection of arterial input function using cluster analysis. *Magn Reson Med.* Mar 2006;55(3):524-531.

43. Kiselev VG. On the theoretical basis of perfusion measurements by dynamic susceptibility contrast MRI. *Magn Reson Med.* Dec 2001;46(6):1113-1122.

44. Kjolby BF, Ostergaard L, Kiselev VG. Theoretical model of intravascular paramagnetic tracers effect on tissue relaxation. *Magn Reson Med.* Jul 2006;56(1):187-197.

45. van Osch MJ, Vonken EJ, Viergever MA, van der Grond J, Bakker CJ. Measuring the arterial input function with gradient echo sequences. *Magn Reson Med.* Jun 2003;49(6):1067-1076.

46. Knutsson L. Optimisation and validiation of dynamic susceptibility contrast MRI perfusion measurements. *Thesis for the Degree of Doctor of Philosophy*. 2006;University of Lund.

47. Ostergaard L. Principles of cerebral perfusion imaging by bolus tracking. *Journal of magnetic resonance imaging : JMRI.* Dec 2005;22(6):710-717.

48. Axel L. Cerebral blood flow determination by rapid-sequence computed tomography: theoretical analysis. *Radiology*. Dec 1980;137(3):679-686.

49. Koenig M, Klotz E, Luka B, Venderink DJ, Spittler JF, Heuser L. Perfusion CT of the brain: diagnostic approach for early detection of ischemic stroke. *Radiology*. Oct 1998;209(1):85-93.

50. Reichenbach JR, Rother J, Jonetz-Mentzel L, et al. Acute stroke evaluated by time-to-peak mapping during initial and early follow-up perfusion CT studies. *AJNR. American journal of neuroradiology.* Nov-Dec 1999;20(10):1842-1850.

51. Konig M. Brain perfusion CT in acute stroke: current status. *Eur J Radiol*. Mar 2003;45 Suppl 1:S11-22.

52. Eastwood JD, Lev MH, Azhari T, et al. CT perfusion scanning with deconvolution analysis: pilot study in patients with acute middle cerebral artery stroke. *Radiology.* Jan 2002;222(1):227-236.

53. Eastwood JD, Provenzale JM, Hurwitz LM, Lee TY. Practical injection-rate CT perfusion imaging: deconvolution-derived hemodynamics in a case of stroke. *Neuroradiology.* Mar 2001;43(3):223-226.

54. Cenic A, Nabavi DG, Craen RA, Gelb AW, Lee TY. Dynamic CT measurement of cerebral blood flow: a validation study. *AJNR. American journal of neuroradiology.* Jan 1999;20(1):63-73.

55. Cenic A, Nabavi DG, Craen RA, Gelb AW, Lee TY. A CT method to measure hemodynamics in brain tumors: validation and application of cerebral blood flow maps. *AJNR. American journal of neuroradiology*. Mar 2000;21(3):462-470.

56. Nabavi DG, Cenic A, Craen RA, et al. CT assessment of cerebral perfusion: experimental validation and initial clinical experience. *Radiology*. Oct 1999;213(1):141-149.

57. Nabavi DG, Cenic A, Henderson S, Gelb AW, Lee TY. Perfusion mapping using computed tomography allows accurate prediction of cerebral infarction in experimental brain ischemia. *Stroke; a journal of cerebral circulation.* Jan 2001;32(1):175-183.

58. Bisdas S, Donnerstag F, Berding G, Vogl TJ, Thng CH, Koh TS. Computed tomography assessment of cerebral perfusion using a distributed parameter tracer kinetics model: validation with

H(2)((15))O positron emission tomography measurements and initial clinical experience in patients with acute stroke. *J Cereb Blood Flow Metab.* Feb 2008;28(2):402-411.

59. Kudo K, Terae S, Katoh C, et al. Quantitative cerebral blood flow measurement with dynamic perfusion CT using the vascular-pixel elimination method: comparison with H2(15)O positron emission tomography. *AJNR. American journal of neuroradiology.* Mar 2003;24(3):419-426.

60. Sasaki M, Kudo K, Boutelier T, et al. Assessment of the accuracy of a Bayesian estimation algorithm for perfusion CT by using a digital phantom. *Neuroradiology.* Oct 2013;55(10):1197-1203.

61. Lee TY. Scientific basis and validation. *In: Miles K.A., Charnsangavej C., Cuenod C.A., eds. Multidetector Computed Tomography in Oncology: CT Perfusion Imaging. Albingdon, UK: Informa Healthcare.* 2007:13-27.

62. Bjornerud A, Emblem KE. A fully automated method for quantitative cerebral hemodynamic analysis using DSC-MRI. *J Cereb Blood Flow Metab.* May 2010;30(5):1066-1078.

63. Weisskoff RM, Chesler D, Boxerman JL, Rosen BR. Pitfalls in MR measurement of tissue blood flow with intravascular tracers: which mean transit time? *Magn Reson Med.* Apr 1993;29(4):553-558.

64. Axel L. Tissue mean transit time from dynamic computed tomography by a simple deconvolution technique. *Investigative radiology.* Jan-Feb 1983;18(1):94-99.

65. Roberts HC, Roberts TP, Smith WS, Lee TJ, Fischbein NJ, Dillon WP. Multisection dynamic CT perfusion for acute cerebral ischemia: the "toggling-table" technique. *AJNR. American journal of neuroradiology.* Jun-Jul 2001;22(6):1077-1080.

66. Youn SW, Kim JH, Weon YC, Kim SH, Han MK, Bae HJ. Perfusion CT of the brain using 40-mm-wide detector and toggling table technique for initial imaging of acute stroke. *AJR. American journal of roentgenology.* Sep 2008;191(3):W120-126.

67. Klingebiel R, Siebert E, Diekmann S, et al. 4-D Imaging in cerebrovascular disorders by using 320-slice CT: feasibility and preliminary clinical experience. *Academic radiology.* Feb 2009;16(2):123-129.

68. Mori S, Obata T, Nakajima N, Ichihara N, Endo M. Volumetric perfusion CT using prototype 256-detector row CT scanner: preliminary study with healthy porcine model. *AJNR. American journal of neuroradiology.* Nov-Dec 2005;26(10):2536-2541.

69. Stacul F, van der Molen AJ, Reimer P, et al. Contrast induced nephropathy: updated ESUR Contrast Media Safety Committee guidelines. *European radiology.* Dec 2011;21(12):2527-2541.

70. Silvennoinen HM, Hamberg LM, Valanne L, Hunter GJ. Increasing contrast agent concentration improves enhancement in first-pass CT perfusion. *AJNR. American journal of neuroradiology.* Aug 2007;28(7):1299-1303.

71. Copen WA, Deipolyi AR, Schaefer PW, Schwamm LH, Gonzalez RG, Wu O. Exposing Hidden Truncation-Related Errors in Acute Stroke Perfusion Imaging. *AJNR. American journal of neuroradiology.* Dec 11 2014.

72. Knollmann F, Schimpf K, Felix R. [Iodine delivery rate of different concentrations of iodine-containing contrast agents with rapid injection]. *RoFo : Fortschritte auf dem Gebiete der Rontgenstrahlen und der Nuklearmedizin.* Jun 2004;176(6):880-884.

73. Konig M, Bultmann E, Bode-Schnurbus L, Koenen D, Mielke E, Heuser L. Image quality in CT perfusion imaging of the brain. The role of iodine concentration. *European radiology.* Jan 2007;17(1):39-47.

74. Wintermark M, Smith WS, Ko NU, Quist M, Schnyder P, Dillon WP. Dynamic perfusion CT: optimizing the temporal resolution and contrast volume for calculation of perfusion CT parameters in stroke patients. *AJNR. American journal of neuroradiology.* May 2004;25(5):720-729.

75. Wintermark M, Maeder P, Verdun FR, et al. Using 80 kVp versus 120 kVp in perfusion CT measurement of regional cerebral blood flow. *AJNR. American journal of neuroradiology.* Nov-Dec 2000;21(10):1881-1884.

76. Ferreira RM, Lev MH, Goldmakher GV, et al. Arterial input function placement for accurate CT perfusion map construction in acute stroke. *AJR. American journal of roentgenology.* May 2010;194(5):1330-1336.

77. Sanelli PC, Lev MH, Eastwood JD, Gonzalez RG, Lee TY. The effect of varying user-selected input parameters on quantitative values in CT perfusion maps. *Academic radiology.* Oct 2004;11(10):1085-1092.

78. Wintermark M, Lau BC, Chien J, Arora S. The anterior cerebral artery is an appropriate arterial input function for perfusion-CT processing in patients with acute stroke. *Neuroradiology.* Mar 2008;50(3):227-236.

79. Kealey SM, Loving VA, Delong DM, Eastwood JD. User-defined vascular input function curves: influence on mean perfusion

parameter values and signal-to-noise ratio. *Radiology.* May 2004;231(2):587-593.

80. Soares BP, Dankbaar JW, Bredno J, et al. Automated versus manual post-processing of perfusion-CT data in patients with acute cerebral ischemia: influence on interobserver variability. *Neuroradiology.* Jul 2009;51(7):445-451.

81. Konstas AA, Goldmakher GV, Lee TY, Lev MH. Theoretic basis and technical implementations of CT perfusion in acute ischemic stroke, part 2: technical implementations. *AJNR. American journal of neuroradiology.* May 2009;30(5):885-892.

82. San Millan Ruiz D, Murphy K, Gailloud P. 320-multidetector row whole-head dynamic subtracted CT angiography and whole-brain CT perfusion before and after carotid artery stenting: technical note. *Eur J Radiol.* Jun 2010;74(3):413-419.

83. Shankar JJ, Lum C, Sharma M. Whole-brain perfusion imaging with 320-MDCT scanner: Reducing radiation dose by increasing sampling interval. *AJR. American journal of roentgenology.* Nov 2010;195(5):1183-1186.

84. Kudo K, Christensen S, Sasaki M, et al. Accuracy and reliability assessment of CT and MR perfusion analysis software using a digital phantom. *Radiology.* Apr 2013;267(1):201-211.

85. Kudo K, Sasaki M, Ogasawara K, Terae S, Ehara S, Shirato H. Difference in tracer delay-induced effect among deconvolution algorithms in CT perfusion analysis: quantitative evaluation with digital phantoms. *Radiology.* Apr 2009;251(1):241-249.

86. Yamada K, Wu O, Gonzalez RG, et al. Magnetic resonance perfusion-weighted imaging of acute cerebral infarction: effect of the calculation methods and underlying vasculopathy. *Stroke; a journal of cerebral circulation.* Jan 2002;33(1):87-94.

87. Afifi AK, Bergman RA. Functional Neuroanatomy Text and Atlas, Mc Graw Hill, USA. 1998.

88. Sakka L, Coll G, Chazal J. Anatomy and physiology of cerebrospinal fluid. *European annals of otorhinolaryngology, head and neck diseases.* Dec 2011;128(6):309-316.

89. Bulat M, Lupret V, Orehkovic D, Klarica M. Transventricular and transpial absorption of cerebrospinal fluid into cerebral microvessels. *Collegium antropologicum.* Jan 2008;32 Suppl 1:43-50.

90. Rubenstein E. Relationship of senescence of cerebrospinal fluid circulatory system to dementias of the aged. *Lancet.* Jan 24 1998;351(9098):283-285.

91. Kapoor KG, Katz SE, Grzybowski DM, Lubow M. Cerebrospinal fluid outflow: an evolving perspective. *Brain research bulletin.* Dec 16 2008;77(6):327-334.

92. Hasegawa M, Yamashima T, Kida S, Yamashita J. Membranous ultrastructure of human arachnoid cells. *J Neuropathol Exp Neurol.* Nov 1997;56(11):1217-1227.

93. Yamashima T. Functional ultrastructure of cerebrospinal fluid drainage channels in human arachnoid villi. *Neurosurgery.* Apr 1988;22(4):633-641.

94. Edsbagge M, Tisell M, Jacobsson L, Wikkelso C. Spinal CSF absorption in healthy individuals. *Am J Physiol Regul Integr Comp Physiol.* Dec 2004;287(6):R1450-1455.

95. Deo-Narine V, Gomez DG, Vullo T, et al. Direct in vivo observation of transventricular absorption in the hydrocephalic dog using magnetic resonance imaging. *Investigative radiology.* Mar 1994;29(3):287-293.

96. Greitz D. Cerebrospinal fluid circulation and associated intracranial dynamics. A radiologic investigation using MR imaging and radionuclide cisternography. *Acta radiologica. Supplementum.* 1993;386:1-23.

97. Tourdias T, Dragonu I, Fushimi Y, et al. Aquaporin 4 correlates with apparent diffusion coefficient and hydrocephalus severity in the rat brain: a combined MRI-histological study. *NeuroImage.* Aug 15 2009;47(2):659-666.

98. Iliff JJ, Lee H, Yu M, et al. Brain-wide pathway for waste clearance captured by contrast-enhanced MRI. *The Journal of clinical investigation.* Mar 2013;123(3):1299-1309.

99. Iliff JJ, Nedergaard M. Is there a cerebral lymphatic system? *Stroke; a journal of cerebral circulation.* Jun 2013;44(6 Suppl 1):S93-95.

100. Greitz D. Radiological assessment of hydrocephalus: new theories and implications for therapy. *Neurosurgical review.* Jul 2004;27(3):145-165; discussion 166-147.

101. Di Rocco C, Di Trapani G, Pettorossi VE, Caldarelli M. On the pathology of experimental hydrocephalus induced by artificial increase in endoventricular CSF pulse pressure. *Child's brain.* 1979;5(2):81-95.

102. O´Connel JEA. The vascular factor in intracranial pressure and the maintenance of the CSF circulation. *Brain.* 1943;66:204-228.

103. Avezaat CJ, van Eijndhoven JH, Wyper DJ. Cerebrospinal fluid pulse pressure and intracranial volume-pressure relationships. *Journal of neurology, neurosurgery, and psychiatry.* Aug 1979;42(8):687-700.

104. Bateman GA. Vascular compliance in normal pressure hydrocephalus. *AJNR. American journal of neuroradiology.* Oct 2000;21(9):1574-1585.

105. Bateman GA. Pulse-wave encephalopathy: a comparative study of the hydrodynamics of leukoaraiosis and normal-pressure hydrocephalus. *Neuroradiology.* Sep 2002;44(9):740-748.

106. Bateman GA. The pathophysiology of idiopathic normal pressure hydrocephalus: cerebral ischemia or altered venous hemodynamics? *AJNR. American journal of neuroradiology.* Jan 2008;29(1):198-203.

107. Bateman GA, Loiselle AM. Can MR measurement of intracranial hydrodynamics and compliance differentiate which patient with idiopathic normal pressure hydrocephalus will improve following shunt insertion? *Acta neurochirurgica.* 2007;149(5):455-462; discussion 462.

108. Bateman GA. The reversibility of reduced cortical vein compliance in normal-pressure hydrocephalus following shunt insertion. *Neuroradiology.* Feb 2003;45(2):65-70.

109. Czosnyka M, Czosnyka ZH, Whitfield PC, Donovan T, Pickard JD. Age dependence of cerebrospinal pressure-volume compensation in patients with hydrocephalus. *J Neurosurg.* Mar 2001;94(3):482-486.

110. Bradley WG, Jr., Whittemore AR, Watanabe AS, Davis SJ, Teresi LM, Homyak M. Association of deep white matter infarction with chronic communicating hydrocephalus: implications regarding the possible origin of normal-pressure hydrocephalus. *AJNR. American journal of neuroradiology.* Jan-Feb 1991;12(1):31-39.

111. Graff-Radford NR, Godersky JC. Idiopathic normal pressure hydrocephalus and systemic hypertension. *Neurology.* May 1987;37(5):868-871.

112. Krauss JK, Regel JP, Vach W, Droste DW, Borremans JJ, Mergner T. Vascular risk factors and arteriosclerotic disease in idiopathic normal-pressure hydrocephalus of the elderly. *Stroke; a journal of cerebral circulation.* Jan 1996;27(1):24-29.

113. Krauss JK, Regel JP, Vach W, et al. White matter lesions in patients with idiopathic normal pressure hydrocephalus and in an age-matched control group: a comparative study. *Neurosurgery.* Mar 1997;40(3):491-495; discussion 495-496.

114. Tullberg M, Hultin L, Ekholm S, Mansson JE, Fredman P, Wikkelso C. White matter changes in normal pressure hydrocephalus and Binswanger disease: specificity, predictive value and correlations to axonal degeneration and demyelination. *Acta Neurol Scand.* Jun 2002;105(6):417-426.

115. Fisher CM. The clinical picture in occult hydrocephalus. *Clinical neurosurgery*. 1977;24:270-284.

116. Stolze H, Kuhtz-Buschbeck JP, Drucke H, et al. Gait analysis in idiopathic normal pressure hydrocephalus--which parameters respond to the CSF tap test? *Clin Neurophysiol.* Sep 2000;111(9):1678-1686.

117. Blomsterwall E, Bilting M, Stephensen H, Wikkelso C. Gait abnormality is not the only motor disturbance in normal pressure hydrocephalus. *Scandinavian journal of rehabilitation medicine.* Dec 1995;27(4):205-209.

118. Krauss JK, Regel JP, Droste DW, Orszagh M, Borremans JJ, Vach W. Movement disorders in adult hydrocephalus. *Movement disorders : official journal of the Movement Disorder Society*. Jan 1997;12(1):53-60.

119. Wikkelso C, Blomsterwall E, Frisen L. Subjective visual vertical and Romberg's test correlations in hydrocephalus. *J Neurol.* Jun 2003;250(6):741-745.

120. Sakakibara R, Kanda T, Sekido T, et al. Mechanism of bladder dysfunction in idiopathic normal pressure hydrocephalus. *Neurourology and urodynamics.* 2008;27(6):507-510.

121. Hellstrom P, Edsbagge M, Archer T, Tisell M, Tullberg M, Wikkelso C. The neuropsychology of patients with clinically diagnosed idiopathic normal pressure hydrocephalus. *Neurosurgery.* Dec 2007;61(6):1219-1226; discussion 1227-1218.

122. Lindqvist G, Malmgren H. Organic mental disorders as hypothetical pathogenetic processes. *Acta Psychiatr Scand Suppl.* 1993;373:5-17.

123. Hellström P. The neuropsychology of idiopathic normal pressure hydrocephalus. *Thesis for the Degree of Doctor of Philosophy*. 2011;University of Gothenburg.

124. Jaraj D, Rabiei K, Marlow T, Jensen C, Skoog I, Wikkelso C. Prevalence of idiopathic normal-pressure hydrocephalus. *Neurology.* Apr 22 2014;82(16):1449-1454.

125. Relkin N, Marmarou A, Klinge P, Bergsneider M, Black PM. Diagnosing idiopathic normal-pressure hydrocephalus. *Neurosurgery.* Sep 2005;57(3 Suppl):S4-16; discussion ii-v.

126. Brean A, Eide PK. Prevalence of probable idiopathic normal pressure hydrocephalus in a Norwegian population. *Acta Neurol Scand.* Jul 2008;118(1):48-53.

127. Hiraoka K, Meguro K, Mori E. Prevalence of idiopathic normal-pressure hydrocephalus in the elderly population of a Japanese rural community. *Neurologia medico-chirurgica.* May 2008;48(5):197-199; discussion 199-200.

128. Iseki C, Kawanami T, Nagasawa H, et al. Asymptomatic ventriculomegaly with features of idiopathic normal pressure hydrocephalus on MRI (AVIM) in the elderly: a prospective study in a Japanese population. *Journal of the neurological sciences.* Feb 15 2009;277(1-2):54-57.

129. Tanaka N, Yamaguchi S, Ishikawa H, Ishii H, Meguro K. Prevalence of possible idiopathic normal-pressure hydrocephalus in Japan: the Osaki-Tajiri project. *Neuroepidemiology.* 2009;32(3):171-175.

130. Trenkwalder C, Schwarz J, Gebhard J, et al. Starnberg trial on epidemiology of Parkinsonism and hypertension in the elderly. Prevalence of Parkinson's disease and related disorders assessed by a door-to-door survey of inhabitants older than 65 years. *Archives of neurology.* Oct 1995;52(10):1017-1022.

131. Ishikawa M. Clinical guidelines for idiopathic normal pressure hydrocephalus. *Neurologia medico-chirurgica.* Apr 2004;44(4):222-223.

132. Marmarou A, Bergsneider M, Relkin N, Klinge P, Black PM. Development of guidelines for idiopathic normal-pressure hydrocephalus: introduction. *Neurosurgery.* Sep 2005;57(3 Suppl):S1-3; discussion ii-v.

133. Ishikawa M, Hashimoto M, Kuwana N, et al. Guidelines for management of idiopathic normal pressure hydrocephalus. *Neurologia medico-chirurgica.* 2008;48 Suppl:S1-23.

134. Mori E, Ishikawa M, Kato T, et al. Guidelines for management of idiopathic normal pressure hydrocephalus: second edition. *Neurologia medico-chirurgica.* 2012;52(11):775-809.

135. Czosnyka M, Pickard JD. Monitoring and interpretation of intracranial pressure. *Journal of neurology, neurosurgery, and psychiatry.* Jun 2004;75(6):813-821.

136. Marmarou A, Bergsneider M, Klinge P, Relkin N, Black PM. The value of supplemental prognostic tests for the preoperative assessment of idiopathic normal-pressure hydrocephalus. *Neurosurgery.* Sep 2005;57(3 Suppl):S17-28; discussion ii-v.

137. Malm J, Jacobsson J, Birgander R, Eklund A. Reference values for CSF outflow resistance and intracranial pressure in healthy elderly. *Neurology.* Mar 8 2011;76(10):903-909.

138. Gilland O, Tourtellotte WW, O'Tauma L, Henderson WG. Normal cerebrospinal fluid pressure. *J Neurosurg.* May 1974;40(5):587-593.

139. Boon AJ, Tans JT, Delwel EJ, et al. Dutch normal pressure hydrocephalus study: baseline characteristics with emphasis on clinical findings. *European journal of neurology : the official journal*

of the European Federation of Neurological Societies. Jan 1997;4(1):39-47.

140. Krauss JK, Droste DW, Vach W, et al. Cerebrospinal fluid shunting in idiopathic normal-pressure hydrocephalus of the elderly: effect of periventricular and deep white matter lesions. *Neurosurgery.* Aug 1996;39(2):292-299; discussion 299-300.
141. Kubo Y, Kazui H, Yoshida T, et al. Validation of grading scale for evaluating symptoms of idiopathic normal-pressure hydrocephalus. *Dementia and geriatric cognitive disorders.* 2008;25(1):37-45.
142. Rankin J. Cerebral vascular accidents in patients over the age of 60. II. Prognosis. *Scottish medical journal.* May 1957;2(5):200-215.
143. Stein SC, Langfitt TW. Normal-pressure hydrocephalus. Predicting the results of cerebrospinal fluid shunting. *J Neurosurg.* Oct 1974;41(4):463-470.
144. Hellstrom P, Klinge P, Tans J, Wikkelso C. A new scale for assessment of severity and outcome in iNPH. *Acta Neurol Scand.* Oct 2012;126(4):229-237.
145. Klinge P, Hellstrom P, Tans J, Wikkelso C. One-year outcome in the European multicentre study on iNPH. *Acta Neurol Scand.* Sep 2012;126(3):145-153.
146. Katzman R, Hussey F. A simple constant-infusion manometric test for measurement of CSF absorption. I. Rationale and method. *Neurology.* Jun 1970;20(6):534-544.
147. Marmarou A, Shulman K, Rosende RM. A nonlinear analysis of the cerebrospinal fluid system and intracranial pressure dynamics. *J Neurosurg.* Mar 1978;48(3):332-344.
148. Andersson K, Sundstrom N, Malm J, Eklund A. Effect of resting pressure on the estimate of cerebrospinal fluid outflow conductance. *Fluids and barriers of the CNS.* 2011;8(1):15.
149. Czosnyka Z, Owler B, Keong N, et al. Impact of duration of symptoms on CSF dynamics in idiopathic normal pressure hydrocephalus. *Acta Neurol Scand.* Jun 2011;123(6):414-418.
150. Wikkelso C, Hellstrom P, Klinge PM, Tans JT. The European iNPH Multicentre Study on the predictive values of resistance to CSF outflow and the CSF Tap Test in patients with idiopathic normal pressure hydrocephalus. *Journal of neurology, neurosurgery, and psychiatry.* May 2013;84(5):562-568.
151. Eide PK, Sorteberg W. Diagnostic intracranial pressure monitoring and surgical management in idiopathic normal pressure hydrocephalus: a 6-year review of 214 patients. *Neurosurgery.* Jan 2010;66(1):80-91.

152. Chiewvit S, Nuntaaree S, Kanchaanapiboon P, Chiewvit P. Assessment lumboperitoneal or ventriculoperitoneal shunt patency by radionuclide technique: a review experience cases. *World journal of nuclear medicine.* May 2014;13(2):75-84.

153. Malm J, Lundkvist B, Eklund A, Koskinen LO, Kristensen B. CSF outflow resistance as predictor of shunt function. A long-term study. *Acta Neurol Scand.* Sep 2004;110(3):154-160.

154. Evans WAJ. An encephalographic ratio for estimating ventricular enlargement and cerebral atrophy. *Arch Neurol Psychiatry.* 1942;47(6):931-937.

155. Toma AK, Holl E, Kitchen ND, Watkins LD. Evans' index revisited: the need for an alternative in normal pressure hydrocephalus. *Neurosurgery.* Apr 2011;68(4):939-944.

156. Kazui H, Mori E, Ohkawa S, et al. Predictors of the disappearance of triad symptoms in patients with idiopathic normal pressure hydrocephalus after shunt surgery. *Journal of the neurological sciences.* May 15 2013;328(1-2):64-69.

157. Virhammar J, Laurell K, Cesarini KG, Larsson EM. Preoperative Prognostic Value of MRI Findings in 108 Patients with Idiopathic Normal Pressure Hydrocephalus. *AJNR. American journal of neuroradiology.* Jul 10 2014.

158. Holodny AI, Waxman R, George AE, Rusinek H, Kalnin AJ, de Leon M. MR differential diagnosis of normal-pressure hydrocephalus and Alzheimer disease: significance of perihippocampal fissures. *AJNR. American journal of neuroradiology.* May 1998;19(5):813-819.

159. Kurihara Y, Simonson TM, Nguyen HD, et al. MR imaging of ventriculomegaly--a qualitative and quantitative comparison of communicating hydrocephalus, central atrophy, and normal studies. *Journal of magnetic resonance imaging : JMRI.* Jul-Aug 1995;5(4):451-456.

160. Meier U, Paris S, Grawe A, Stockheim D, Hajdukova A, Mutze S. Is there a correlation between operative results and change in ventricular volume after shunt placement? A study of 60 cases of idiopathic normal-pressure hydrocephalus. *Neuroradiology.* Jun 2003;45(6):377-380.

161. Anderson RC, Grant JJ, de la Paz R, Frucht S, Goodman RR. Volumetric measurements in the detection of reduced ventricular volume in patients with normal-pressure hydrocephalus whose clinical condition improved after ventriculoperitoneal shunt placement. *J Neurosurg.* Jul 2002;97(1):73-79.

162. Bradley WG. Normal pressure hydrocephalus: new concepts on etiology and diagnosis. *AJNR. American journal of neuroradiology.* Oct 2000;21(9):1586-1590.

163. Krauss JK, Regel JP, Vach W, Jungling FD, Droste DW, Wakhloo AK. Flow void of cerebrospinal fluid in idiopathic normal pressure hydrocephalus of the elderly: can it predict outcome after shunting? *Neurosurgery.* Jan 1997;40(1):67-73; discussion 73-64.

164. Bradley WG, Jr., Whittemore AR, Kortman KE, et al. Marked cerebrospinal fluid void: indicator of successful shunt in patients with suspected normal-pressure hydrocephalus. *Radiology.* Feb 1991;178(2):459-466.

165. Algin O, Hakyemez B, Taskapilioglu O, Ocakoglu G, Bekar A, Parlak M. Morphologic features and flow void phenomenon in normal pressure hydrocephalus and other dementias: are they really significant? *Academic radiology.* Nov 2009;16(11):1373-1380.

166. Ishii K, Kanda T, Harada A, et al. Clinical impact of the callosal angle in the diagnosis of idiopathic normal pressure hydrocephalus. *European radiology.* Nov 2008;18(11):2678-2683.

167. Tarnaris A, Toma AK, Kitchen ND, Watkins LD. Ongoing search for diagnostic biomarkers in idiopathic normal pressure hydrocephalus. *Biomarkers in medicine.* Dec 2009;3(6):787-805.

168. Algin O, Hakyemez B, Parlak M. The efficiency of PC-MRI in diagnosis of normal pressure hydrocephalus and prediction of shunt response. *Academic radiology.* Feb 2010;17(2):181-187.

169. Scollato A, Tenenbaum R, Bahl G, Celerini M, Salani B, Di Lorenzo N. Changes in aqueductal CSF stroke volume and progression of symptoms in patients with unshunted idiopathic normal pressure hydrocephalus. *AJNR. American journal of neuroradiology.* Jan 2008;29(1):192-197.

170. Scollato A, Gallina P, Gautam B, et al. Changes in aqueductal CSF stroke volume in shunted patients with idiopathic normal-pressure hydrocephalus. *AJNR. American journal of neuroradiology.* Sep 2009;30(8):1580-1586.

171. Benson DF, LeMay M, Patten DH, Rubens AB. Diagnosis of normal-pressure hydrocephalus. *The New England journal of medicine.* Sep 17 1970;283(12):609-615.

172. LeMay M, New PF. Radiological diagnosis of occult normal-pressure hydrocephalus. *Radiology.* Aug 1970;96(2):347-358.

173. Virhammar J, Laurell K, Cesarini KG, Larsson EM. The callosal angle measured on MRI as a predictor of outcome in idiopathic normal-pressure hydrocephalus. *J Neurosurg.* Jan 2014;120(1):178-184.

174. Del Bigio MR. Neuropathological changes caused by hydrocephalus. *Acta neuropathologica.* 1993;85(6):573-585.

175. Tamaki N, Shirakuni T, Ehara K, Matsumoto S. Characterization of periventricular edema in normal-pressure hydrocephalus by measurement of water proton relaxation times. *J Neurosurg.* Dec 1990;73(6):864-870.

176. Aygok G, Marmarou A, Fatouros P, Young H. Brain tissue water content in patients with idiopathic normal pressure hydrocephalus. *Acta neurochirurgica. Supplement.* 2006;96:348-351.

177. Sahuquillo J, Rubio E, Codina A, et al. Reappraisal of the intracranial pressure and cerebrospinal fluid dynamics in patients with the so-called "normal pressure hydrocephalus" syndrome. *Acta neurochirurgica.* 1991;112(1-2):50-61.

178. Zimmerman RD, Fleming CA, Lee BC, Saint-Louis LA, Deck MD. Periventricular hyperintensity as seen by magnetic resonance: prevalence and significance. *AJR. American journal of roentgenology.* Mar 1986;146(3):443-450.

179. Tullberg M, Jensen C, Ekholm S, Wikkelso C. Normal pressure hydrocephalus: vascular white matter changes on MR images must not exclude patients from shunt surgery. *AJNR. American journal of neuroradiology.* Oct 2001;22(9):1665-1673.

180. Ishii K, Kawaguchi T, Shimada K, et al. Voxel-based analysis of gray matter and CSF space in idiopathic normal pressure hydrocephalus. *Dementia and geriatric cognitive disorders.* 2008;25(4):329-335.

181. Kitagaki H, Mori E, Ishii K, Yamaji S, Hirono N, Imamura T. CSF spaces in idiopathic normal pressure hydrocephalus: morphology and volumetry. *AJNR. American journal of neuroradiology.* Aug 1998;19(7):1277-1284.

182. Hashimoto M, Ishikawa M, Mori E, Kuwana N. Diagnosis of idiopathic normal pressure hydrocephalus is supported by MRI-based scheme: a prospective cohort study. *Cerebrospinal Fluid Res.* 2010;7:18.

183. Iseki C, Takahashi Y, Wada M, Kawanami T, Adachi M, Kato T. Incidence of idiopathic normal pressure hydrocephalus (iNPH): a 10-year follow-up study of a rural community in Japan. *Journal of the neurological sciences.* Apr 15 2014;339(1-2):108-112.

184. Akiguchi I, Shirakashi Y, Budka H, et al. Disproportionate subarachnoid space hydrocephalus-outcome and perivascular space. *Annals of clinical and translational neurology.* Aug 2014;1(8):562-569.

185. Adachi M, Kawanami T, Ohshima F, Kato T. Upper midbrain profile sign and cingulate sulcus sign: MRI findings on sagittal images in idiopathic normal-pressure hydrocephalus, Alzheimer's disease, and progressive supranuclear palsy. *Radiation medicine.* Oct 2006;24(8):568-572.

186. Lee PH, Yong SW, Ahn YH, Huh K. Correlation of midbrain diameter and gait disturbance in patients with idiopathic normal pressure hydrocephalus. *J Neurol.* Aug 2005;252(8):958-963.

187. Mocco J, Tomey MI, Komotar RJ, et al. Ventriculoperitoneal shunting of idiopathic normal pressure hydrocephalus increases midbrain size: a potential mechanism for gait improvement. *Neurosurgery.* Oct 2006;59(4):847-850; discussion 850-841.

188. Wikkelso C, Andersson H, Blomstrand C, Matousek M, Svendsen P. Computed tomography of the brain in the diagnosis of and prognosis in normal pressure hydrocephalus. *Neuroradiology.* 1989;31(2):160-165.

189. Lundin F, Tisell A, Dahlqvist Leinhard O, et al. Reduced thalamic N-acetylaspartate in idiopathic normal pressure hydrocephalus: a controlled 1H-magnetic resonance spectroscopy study of frontal deep white matter and the thalamus using absolute quantification. *Journal of neurology, neurosurgery, and psychiatry.* Jul 2011;82(7):772-778.

190. Lundin F, Tisell A, Leijon G, et al. Preoperative and postoperative 1H-MR spectroscopy changes in frontal deep white matter and the thalamus in idiopathic normal pressure hydrocephalus. *Journal of neurology, neurosurgery, and psychiatry.* Feb 2013;84(2):188-193.

191. Lenfeldt N, Hauksson J, Birgander R, Eklund A, Malm J. Improvement after cerebrospinal fluid drainage is related to levels of N-acetyl-aspartate in idiopathic normal pressure hydrocephalus. *Neurosurgery.* Jan 2008;62(1):135-141, discussion 141-132.

192. Shiino A, Nishida Y, Yasuda H, Suzuki M, Matsuda M, Inubushi T. Magnetic resonance spectroscopic determination of a neuronal and axonal marker in white matter predicts reversibility of deficits in secondary normal pressure hydrocephalus. *Journal of neurology, neurosurgery, and psychiatry.* Aug 2004;75(8):1141-1148.

193. del Mar Matarin M, Pueyo R, Poca MA, et al. Post-surgical changes in brain metabolism detected by magnetic resonance spectroscopy in normal pressure hydrocephalus: results of a pilot study. *Journal of neurology, neurosurgery, and psychiatry.* Jul 2007;78(7):760-763.

194. Braun KP, Gooskens RH, Vandertop WP, Tulleken CA, van der Grond J. 1H magnetic resonance spectroscopy in human hydrocephalus. *Journal of magnetic resonance imaging : JMRI.* Mar 2003;17(3):291-299.

195. Kizu O, Yamada K, Nishimura T. Proton chemical shift imaging in normal pressure hydrocephalus. *AJNR. American journal of neuroradiology.* Oct 2001;22(9):1659-1664.

196. Kubas B, Kulak W, Sobaniec W, Walecki J, Lewko J. Proton magnetic resonance spectroscopy in patients with normal pressure hydrocephalus. *The neuroradiology journal.* Nov 30 2006;19(5):597-602.

197. Lenfeldt N, Larsson A, Nyberg L, et al. Idiopathic normal pressure hydrocephalus: increased supplementary motor activity accounts for improvement after CSF drainage. *Brain.* Nov 2008;131(Pt 11):2904-2912.

198. Assaf Y, Ben-Sira L, Constantini S, Chang LC, Beni-Adani L. Diffusion tensor imaging in hydrocephalus: initial experience. *AJNR. American journal of neuroradiology.* Sep 2006;27(8):1717-1724.

199. Hattingen E, Jurcoane A, Melber J, et al. Diffusion tensor imaging in patients with adult chronic idiopathic hydrocephalus. *Neurosurgery.* May 2010;66(5):917-924.

200. Hattori T, Yuasa T, Aoki S, et al. Altered microstructure in corticospinal tract in idiopathic normal pressure hydrocephalus: comparison with Alzheimer disease and Parkinson disease with dementia. *AJNR. American journal of neuroradiology.* Oct 2011;32(9):1681-1687.

201. Jang SH, Ho Kim S. Diffusion tensor imaging following shunt in a patient with hydrocephalus. *Journal of neuroimaging : official journal of the American Society of Neuroimaging.* Jan 2011;21(1):69-72.

202. Jurcoane A, Keil F, Szelenyi A, Pfeilschifter W, Singer OC, Hattingen E. Directional diffusion of corticospinal tract supports therapy decisions in idiopathic normal-pressure hydrocephalus. *Neuroradiology.* Jan 2014;56(1):5-13.

203. Scheel M, Diekhoff T, Sprung C, Hoffmann KT. Diffusion tensor imaging in hydrocephalus--findings before and after shunt surgery. *Acta neurochirurgica.* Sep 2012;154(9):1699-1706.

204. Kanno S, Abe N, Saito M, et al. White matter involvement in idiopathic normal pressure hydrocephalus: a voxel-based diffusion tensor imaging study. *J Neurol.* Nov 2011;258(11):1949-1957.

205. Koyama T, Marumoto K, Domen K, Miyake H. White matter characteristics of idiopathic normal pressure hydrocephalus: a diffusion tensor tract-based spatial statistic study. *Neurologia medico-chirurgica.* 2013;53(9):601-608.

206. Lenfeldt N, Larsson A, Nyberg L, Birgander R, Eklund A, Malm J. Diffusion tensor imaging reveals supplementary lesions to frontal

white matter in idiopathic normal pressure hydrocephalus. *Neurosurgery.* Jun 2011;68(6):1586-1593; discussion 1593.

207. Bradley WG, Jr., Bahl G, Alksne JF. Idiopathic normal pressure hydrocephalus may be a "two hit" disease: benign external hydrocephalus in infancy followed by deep white matter ischemia in late adulthood. *Journal of magnetic resonance imaging : JMRI.* Oct 2006;24(4):747-755.

208. Corkill RG, Garnett MR, Blamire AM, Rajagopalan B, Cadoux-Hudson TA, Styles P. Multi-modal MRI in normal pressure hydrocephalus identifies pre-operative haemodynamic and diffusion coefficient changes in normal appearing white matter correlating with surgical outcome. *Clin Neurol Neurosurg.* Jul 2003;105(3):193-202.

209. Gideon P, Sorensen PS, Thomsen C, Stahlberg F, Gjerris F, Henriksen O. Increased brain water self-diffusion in patients with idiopathic intracranial hypertension. *AJNR. American journal of neuroradiology.* Feb 1995;16(2):381-387.

210. Tullberg M, Ziegelitz D, Ribbelin S, Ekholm S. White matter diffusion is higher in Binswanger disease than in idiopathic normal pressure hydrocephalus. *Acta Neurol Scand.* Oct 2009;120(4):226-234.

211. Greitz D, Hannerz J, Rahn T, Bolander H, Ericsson A. MR imaging of cerebrospinal fluid dynamics in health and disease. On the vascular pathogenesis of communicating hydrocephalus and benign intracranial hypertension. *Acta radiologica (Stockholm, Sweden : 1987).* May 1994;35(3):204-211.

212. Owler BK, Pickard JD. Normal pressure hydrocephalus and cerebral blood flow: a review. *Acta Neurol Scand.* Dec 2001;104(6):325-342.

213. Hertel F, Walter C, Schmitt M, et al. Is a combination of Tc-SPECT or perfusion weighted magnetic resonance imaging with spinal tap test helpful in the diagnosis of normal pressure hydrocephalus? *Journal of neurology, neurosurgery, and psychiatry.* Apr 2003;74(4):479-484.

214. Walter C, Hertel F, Naumann E, Morsdorf M. Alteration of cerebral perfusion in patients with idiopathic normal pressure hydrocephalus measured by 3D perfusion weighted magnetic resonance imaging. *J Neurol.* Dec 2005;252(12):1465-1471.

215. Momjian S, Owler BK, Czosnyka Z, Czosnyka M, Pena A, Pickard JD. Pattern of white matter regional cerebral blood flow and autoregulation in normal pressure hydrocephalus. *Brain.* May 2004;127(Pt 5):965-972.

216. Owler BK, Momjian S, Czosnyka Z, et al. Normal pressure hydrocephalus and cerebral blood flow: a PET study of baseline values. *J Cereb Blood Flow Metab.* Jan 2004;24(1):17-23.

217. Owler BK, Pena A, Momjian S, et al. Changes in cerebral blood flow during cerebrospinal fluid pressure manipulation in patients with normal pressure hydrocephalus: a methodological study. *J Cereb Blood Flow Metab.* May 2004;24(5):579-587.

218. Kimura M, Tanaka A, Yoshinaga S. Significance of periventricular hemodynamics in normal pressure hydrocephalus. *Neurosurgery.* May 1992;30(5):701-704; discussion 704-705.

219. Meyer JS, Kitagawa Y, Tanahashi N, et al. Pathogenesis of normal-pressure hydrocephalus--preliminary observations. *Surg Neurol.* Feb 1985;23(2):121-133.

220. Klinge PM, Brooks DJ, Samii A, et al. Correlates of local cerebral blood flow (CBF) in normal pressure hydrocephalus patients before and after shunting--A retrospective analysis of [(15)O]H(2)O PET-CBF studies in 65 patients. *Clin Neurol Neurosurg.* Apr 2008;110(4):369-375.

221. Mataro M, Poca MA, Salgado-Pineda P, et al. Postsurgical cerebral perfusion changes in idiopathic normal pressure hydrocephalus: a statistical parametric mapping study of SPECT images. *J Nucl Med.* Dec 2003;44(12):1884-1889.

222. Sakakibara R, Uchida Y, Ishii K, et al. Correlation of right frontal hypoperfusion and urinary dysfunction in iNPH: a SPECT study. *Neurourology and urodynamics.* Jan 2012;31(1):50-55.

223. Tullberg M, Hellstrom P, Piechnik SK, Starmark JE, Wikkelso C. Impaired wakefulness is associated with reduced anterior cingulate CBF in patients with normal pressure hydrocephalus. *Acta Neurol Scand.* Nov 2004;110(5):322-330.

224. Chang CC, Asada H, Mimura T, Suzuki S. A prospective study of cerebral blood flow and cerebrovascular reactivity to acetazolamide in 162 patients with idiopathic normal-pressure hydrocephalus. *J Neurosurg.* Sep 2009;111(3):610-617.

225. Murakami M, Hirata Y, Kuratsu JI. Predictive assessment of shunt effectiveness in patients with idiopathic normal pressure hydrocephalus by determining regional cerebral blood flow on 3D stereotactic surface projections. *Acta neurochirurgica.* Oct 2007;149(10):991-997.

226. Takeuchi T, Goto H, Izaki K, et al. Pathophysiology of cerebral circulatory disorders in idiopathic normal pressure hydrocephalus. *Neurologia medico-chirurgica.* Jul 2007;47(7):299-306; discussion 306.

227. Klinge P, Berding G, Brinker T, et al. The role of cerebral blood flow and cerebrovascular reserve capacity in the diagnosis of chronic hydrocephalus--a PET-study on 60 patients. *Acta neurochirurgica. Supplement.* 2002;81:39-41.

228. Miyamoto J, Tatsuzawa K, Inoue Y, Imahori Y, Mineura K. Oxygen metabolism changes in patients with idiopathic normal pressure hydrocephalus before and after shunting operation. *Acta Neurol Scand.* Sep 2007;116(3):137-143.

229. Klinge P, Berding G, Brinker T, Schuhmann M, Knapp WH, Samii M. PET-studies in idiopathic chronic hydrocephalus before and after shunt-treatment: the role of risk factors for cerebrovascular disease (CVD) on cerebral hemodynamics. *Acta neurochirurgica. Supplement.* 2002;81:43-45.

230. Bateman GA, Siddique SH. Cerebrospinal fluid absorption block at the vertex in chronic hydrocephalus: obstructed arachnoid granulations or elevated venous pressure? *Fluids and barriers of the CNS.* 2014;11:11.

231. Agren-Wilsson A, Lekman A, Sjoberg W, et al. CSF biomarkers in the evaluation of idiopathic normal pressure hydrocephalus. *Acta Neurol Scand.* Nov 2007;116(5):333-339.

232. Jeppsson A, Zetterberg H, Blennow K, Wikkelso C. Idiopathic normal-pressure hydrocephalus: pathophysiology and diagnosis by CSF biomarkers. *Neurology.* Apr 9 2013;80(15):1385-1392.

233. Tullberg M, Blennow K, Mansson JE, Fredman P, Tisell M, Wikkelso C. Ventricular cerebrospinal fluid neurofilament protein levels decrease in parallel with white matter pathology after shunt surgery in normal pressure hydrocephalus. *European journal of neurology : the official journal of the European Federation of Neurological Societies.* Mar 2007;14(3):248-254.

234. Tullberg M, Mansson JE, Fredman P, et al. CSF sulfatide distinguishes between normal pressure hydrocephalus and subcortical arteriosclerotic encephalopathy. *Journal of neurology, neurosurgery, and psychiatry.* Jul 2000;69(1):74-81.

235. Kapaki EN, Paraskevas GP, Tzerakis NG, et al. Cerebrospinal fluid tau, phospho-tau181 and beta-amyloid1-42 in idiopathic normal pressure hydrocephalus: a discrimination from Alzheimer's disease. *European journal of neurology : the official journal of the European Federation of Neurological Societies.* Feb 2007;14(2):168-173.

236. Silverberg GD, Mayo M, Saul T, Rubenstein E, McGuire D. Alzheimer's disease, normal-pressure hydrocephalus, and senescent changes in CSF circulatory physiology: a hypothesis. *Lancet Neurol.* Aug 2003;2(8):506-511.

237. Hakim S, Adams RD. The special clinical problem of symptomatic hydrocephalus with normal cerebrospinal fluid pressure. Observations on cerebrospinal fluid hydrodynamics. *Journal of the neurological sciences.* Jul-Aug 1965;2(4):307-327.

238. Tisell M, Tullberg M, Hellstrom P, Edsbagge M, Hogfeldt M, Wikkelso C. Shunt surgery in patients with hydrocephalus and white matter changes. *J Neurosurg.* May 2011;114(5):1432-1438.

239. Bergsneider M, Black PM, Klinge P, Marmarou A, Relkin N. Surgical management of idiopathic normal-pressure hydrocephalus. *Neurosurgery.* Sep 2005;57(3 Suppl):S29-39; discussion ii-v.

240. Kondziella D, Sonnewald U, Tullberg M, Wikkelso C. Brain metabolism in adult chronic hydrocephalus. *J Neurochem.* Aug 2008;106(4):1515-1524.

241. Toma AK, Papadopoulos MC, Stapleton S, Kitchen ND, Watkins LD. Systematic review of the outcome of shunt surgery in idiopathic normal-pressure hydrocephalus. *Acta neurochirurgica.* Oct 2013;155(10):1977-1980.

242. Malm J, Kristensen B, Stegmayr B, Fagerlund M, Koskinen LO. Three-year survival and functional outcome of patients with idiopathic adult hydrocephalus syndrome. *Neurology.* Aug 22 2000;55(4):576-578.

243. Lemcke J, Meier U. Idiopathic normal pressure hydrocephalus (iNPH) and co-morbidity: an outcome analysis of 134 patients. *Acta neurochirurgica. Supplement.* 2012;114:255-259.

244. Brean A, Fredo HL, Sollid S, Muller T, Sundstrom T, Eide PK. Five-year incidence of surgery for idiopathic normal pressure hydrocephalus in Norway. *Acta Neurol Scand.* Nov 2009;120(5):314-316.

245. Tisell M, Hoglund M, Wikkelso C. National and regional incidence of surgery for adult hydrocephalus in Sweden. *Acta Neurol Scand.* Aug 2005;112(2):72-75.

246. Stein SC, Burnett MG, Sonnad SS. Shunts in normal-pressure hydrocephalus: do we place too many or too few? *J Neurosurg.* Dec 2006;105(6):815-822.

247. Mitchell P, Mathew B. Third ventriculostomy in normal pressure hydrocephalus. *British journal of neurosurgery.* Aug 1999;13(4):382-385.

248. Pinto FC, Saad F, Oliveira MF, et al. Role of endoscopic third ventriculostomy and ventriculoperitoneal shunt in idiopathic normal pressure hydrocephalus: preliminary results of a randomized clinical trial. *Neurosurgery.* May 2013;72(5):845-853; discussion 853-844.

249. Aimard G, Vighetto A, Gabet JY, Bret P, Henry E. [Acetazolamide: an alternative to shunting in normal pressure hydrocephalus? Preliminary results]. *Revue neurologique.* 1990;146(6-7):437-439.

250. Alperin N, Oliu CJ, Bagci AM, et al. Low-dose acetazolamide reverses periventricular white matter hyperintensities in iNPH. *Neurology.* Apr 15 2014;82(15):1347-1351.

251. Andren K, Wikkelso C, Tisell M, Hellstrom P. Natural course of idiopathic normal pressure hydrocephalus. *Journal of neurology, neurosurgery, and psychiatry.* Jul 2014;85(7):806-810.

252. Razay G, Vreugdenhil A, Liddell J. A prospective study of ventriculo-peritoneal shunting for idiopathic normal pressure hydrocephalus. *Journal of clinical neuroscience : official journal of the Neurosurgical Society of Australasia.* Sep 2009;16(9):1180-1183.

253. Agren-Wilsson A, Eklund A, Koskinen LO, Bergenheim AT, Malm J. Brain energy metabolism and intracranial pressure in idiopathic adult hydrocephalus syndrome. *Journal of neurology, neurosurgery, and psychiatry.* Aug 2005;76(8):1088-1093.

254. Agren-Wilsson A, Roslin M, Eklund A, Koskinen LO, Bergenheim AT, Malm J. Intracerebral microdialysis and CSF hydrodynamics in idiopathic adult hydrocephalus syndrome. *Journal of neurology, neurosurgery, and psychiatry.* Feb 2003;74(2):217-221.

255. Toma AK, Tarnaris A, Kitchen ND, Watkins LD. Working towards patient oriented outcome assessment in normal pressure hydrocephalus, what is the most important? *Acta neurochirurgica.* Jan 2011;153(1):177-180.

256. Schmidt M. Rey auditory verbal learning test: a handbook (RAVLT). *Los Angeles, CA: Western Psychological Services.* 1996 1996.

257. Hellström P. Stroop, the bewildering effect (in Swedish). *Svensk Neuropsykologi.* 2001;13:12-15.

258. Hofle N, Paus T, Reutens D, et al. Regional cerebral blood flow changes as a function of delta and spindle activity during slow wave sleep in humans. *The Journal of neuroscience : the official journal of the Society for Neuroscience.* Jun 15 1997;17(12):4800-4808.

259. Paus T. Functional anatomy of arousal and attention systems in the human brain. *Progress in brain research.* 2000;126:65-77.

260. Tekin S, Cummings JL. Frontal-subcortical neuronal circuits and clinical neuropsychiatry: an update. *Journal of psychosomatic research.* Aug 2002;53(2):647-654.

261. Thilmann O. LUPE: an extensible modular framework for evaluation of DSC-acquired perfusion images. *Magma.* 2004;16 (elecronic suppl. 1):537.

262. Knutsson L, Borjesson S, Larsson EM, et al. Absolute quantification of cerebral blood flow in normal volunteers: correlation between Xe-133 SPECT and dynamic susceptibility contrast MRI. *Journal of magnetic resonance imaging : JMRI.* Oct 2007;26(4):913-920.

263. Harris FJ. On the use of windows for harmonic analysis with the discrete Fourier transform. . *Proceedings of the IEEE.* 1978;66(1):51-83.

264. Curran T, Lang AE. Parkinsonian syndromes associated with hydrocephalus: case reports, a review of the literature, and pathophysiological hypotheses. *Movement disorders : official journal of the Movement Disorder Society.* Sep 1994;9(5):508-520.

265. Denays R, Tondeur M, Noel P, Ham HR. Bilateral cerebral mediofrontal hypoactivity in Tc-99m HMPAO SPECT imaging. *Clinical nuclear medicine.* Oct 1994;19(10):873-876.

266. Iddon JL, Pickard JD, Cross JJ, Griffiths PD, Czosnyka M, Sahakian BJ. Specific patterns of cognitive impairment in patients with idiopathic normal pressure hydrocephalus and Alzheimer's disease: a pilot study. *Journal of neurology, neurosurgery, and psychiatry.* Dec 1999;67(6):723-732.

267. Nowak DA, Gumprecht H, Topka H. CSF drainage ameliorates the motor deficit in normal pressure hydrocephalus: evidence from the analysis of grasping movements. *J Neurol.* May 2006;253(5):640-647.

268. Rossor MN, Tyrrell PJ, Warrington EK, Thompson PD, Marsden CD, Lantos P. Progressive frontal gait disturbance with atypical Alzheimer's disease and corticobasal degeneration. *Journal of neurology, neurosurgery, and psychiatry.* Sep 1999;67(3):345-352.

269. Stolze H, Kuhtz-Buschbeck JP, Drucke H, Johnk K, Illert M, Deuschl G. Comparative analysis of the gait disorder of normal pressure hydrocephalus and Parkinson's disease. *Journal of neurology, neurosurgery, and psychiatry.* Mar 2001;70(3):289-297.

270. Wahlund LO, Barkhof F, Fazekas F, et al. A new rating scale for age-related white matter changes applicable to MRI and CT. *Stroke; a journal of cerebral circulation.* Jun 2001;32(6):1318-1322.

271. Gobbel GT, Cann CE, Iwamoto HS, Fike JR. Measurement of regional cerebral blood flow in the dog using ultrafast computed tomography. Experimental validation. *Stroke; a journal of cerebral circulation.* Jun 1991;22(6):772-779.

272. Nabavi DG, Cenic A, Dool J, et al. Quantitative assessment of cerebral hemodynamics using CT: stability, accuracy, and precision studies in dogs. *Journal of computer assisted tomography.* Jul-Aug 1999;23(4):506-515.

273. Gillard JH, Minhas PS, Hayball MP, et al. Assessment of quantitative computed tomographic cerebral perfusion imaging with H2(15)O positron emission tomography. *Neurological research.* Jul 2000;22(5):457-464.

274. Sase S, Honda M, Machida K, Seiki Y. Comparison of cerebral blood flow between perfusion computed tomography and xenon-enhanced computed tomography for normal subjects: territorial analysis. *Journal of computer assisted tomography.* Mar-Apr 2005;29(2):270-277.

275. Gruner JM, Paamand R, Hojgaard L, Law I. Brain perfusion CT compared with15O-H2O-PET in healthy subjects. *EJNMMI research.* 2011;1(1):28.

276. Gillard JH, Antoun NM, Burnet NG, Pickard JD. Reproducibility of quantitative CT perfusion imaging. *The British journal of radiology.* Jun 2001;74(882):552-555.

277. Wintermark M, Sesay M, Barbier E, et al. Comparative overview of brain perfusion imaging techniques. *Journal of neuroradiology. Journal de neuroradiologie.* Dec 2005;32(5):294-314.

278. Stefani MA, Schneider FL, Marrone AC, Severino AG, Jackowski AP, Wallace MC. Anatomic variations of anterior cerebral artery cortical branches. *Clin Anat.* 2000;13(4):231-236.

279. Hagen T, Bartylla K, Piepgras U. Correlation of regional cerebral blood flow measured by stable xenon CT and perfusion MRI. *Journal of computer assisted tomography.* Mar-Apr 1999;23(2):257-264.

280. Knutsson L, Lindgren E, Ahlgren A, et al. Dynamic susceptibility contrast MRI with a prebolus contrast agent administration design for improved absolute quantification of perfusion. *Magn Reson Med.* Oct 2014;72(4):996-1006.

281. Zaharchuk G, Bammer R, Straka M, et al. Improving dynamic susceptibility contrast MRI measurement of quantitative cerebral blood flow using corrections for partial volume and nonlinear contrast relaxivity: A xenon computed tomographic comparative study. *Journal of magnetic resonance imaging : JMRI.* Oct 2009;30(4):743-752.

282. Shin W, Horowitz S, Ragin A, Chen Y, Walker M, Carroll TJ. Quantitative cerebral perfusion using dynamic susceptibility contrast MRI: evaluation of reproducibility and age- and gender-dependence with fully automatic image postprocessing algorithm. *Magn Reson Med.* Dec 2007;58(6):1232-1241.

283. Wirestam R, Knutsson L, Risberg J, et al. Attempts to improve absolute quantification of cerebral blood flow in dynamic susceptibility contrast magnetic resonance imaging: a simplified T1-

weighted steady-state cerebral blood volume approach. *Acta radiologica (Stockholm, Sweden : 1987).* Jun 2007;48(5):550-556.

284. Bland JM, Altman DG. Statistical methods for assessing agreement between two methods of clinical measurement. *Lancet.* Feb 8 1986;1(8476):307-310.

285. Ernst T, Chang L, Itti L, Speck O. Correlation of regional cerebral blood flow from perfusion MRI and spect in normal subjects. *Magn Reson Imaging.* Apr 1999;17(3):349-354.

286. Ourselin S, Roche A, Subsol G, Pennec X, Ayache N. Reconstructing a 3D structure from serial histological sections. *Image and Vision Computing.* 2001;19(1-2):25-31.

287. Ourselin S, Stefanescu R, Pennec X. Robust registration of multi-modal images: towards real-time clinical applications. *Medical Image Computing and Computer-Assisted Intervention.* 2002;2489:140-147.

288. van der Schaaf I, Vonken EJ, Waaijer A, Velthuis B, Quist M, van Osch T. Influence of partial volume on venous output and arterial input function. *AJNR. American journal of neuroradiology.* Jan 2006;27(1):46-50.

289. Salluzzi M, Frayne R, Smith MR. An alternative viewpoint of the similarities and differences of SVD and FT deconvolution algorithms used for quantitative MR perfusion studies. *Magn Reson Imaging.* Apr 2005;23(3):481-492.

290. Smith AM, Grandin CB, Duprez T, Mataigne F, Cosnard G. Whole brain quantitative CBF and CBV measurements using MRI bolus tracking: comparison of methodologies. *Magn Reson Med.* Apr 2000;43(4):559-564.

291. Sirovich L. Introduction to applied mathmatics. *Springer, Berlin.* 1988.

292. Liu HL, Pu Y, Liu Y, et al. Cerebral blood flow measurement by dynamic contrast MRI using singular value decomposition with an adaptive threshold. *Magn Reson Med.* Jul 1999;42(1):167-172.

293. Sasaki M, Kudo K, Ogasawara K, Fujiwara S. Tracer delay-insensitive algorithm can improve reliability of CT perfusion imaging for cerebrovascular steno-occlusive disease: comparison with quantitative single-photon emission CT. *AJNR. American journal of neuroradiology.* Jan 2009;30(1):188-193.

294. Wittsack HJ, Wohlschlager AM, Ritzl EK, et al. CT-perfusion imaging of the human brain: advanced deconvolution analysis using circulant singular value decomposition. *Computerized medical imaging and graphics : the official journal of the Computerized Medical Imaging Society.* Jan 2008;32(1):67-77.

295. Takaya M, Kazui H, Tokunaga H, et al. Global cerebral hypoperfusion in preclinical stage of idiopathic normal pressure hydrocephalus. *Journal of the neurological sciences.* Nov 15 2010;298(1-2):35-41.

296. Larsson A, Bergh AC, Bilting M, et al. Regional cerebral blood flow in normal pressure hydrocephalus: diagnostic and prognostic aspects. *Eur J Nucl Med.* Feb 1994;21(2):118-123.

297. Marmarou A, Takagi H, Shulman K. Biomechanics of brain edema and effects on local cerebral blood flow. *Advances in neurology.* 1980;28:345-358.

298. Whittle IR, Piper IR, Miller JD. The role of bradykinin in the etiology of vasogenic brain edema and perilesional brain dysfunction. *Acta neurochirurgica.* 1992;115(1-2):53-59.

299. Tanaka A, Kimura M, Nakayama Y, Yoshinaga S, Tomonaga M. Cerebral blood flow and autoregulation in normal pressure hydrocephalus. *Neurosurgery.* Jun 1997;40(6):1161-1165; discussion 1165-1167.

300. Lying-Tunell U, Lindblad BS, Malmlund HO, Persson B. Cerebral blood flow and metabolic rate of oxygen, glucose, lactate, pyruvate, ketone bodies and amino acids in patients with normal pressure hydrocephalus before and after shunting and in normal subjects. *Acta neurologica Scandinavica. Supplementum.* 1977;64:338-339.

301. Lying-Tunell U, Lindblad BS, Malmlund HO, Persson B. Cerebral blood flow and metabolic rate of oxygen, glucose, lactate, pyruvate, ketone bodies and amino acids. *Acta Neurol Scand.* Jun 1981;63(6):337-350.

302. Meyer JS, Kitagawa Y, Tanahashi N, et al. Evaluation of treatment of normal-pressure hydrocephalus. *J Neurosurg.* Apr 1985;62(4):513-521.

303. Klinge P, Ruckert N, Schuhmann M, et al. Neuropsychological sequels to changes in global cerebral blood flow and cerebrovascular reserve capacity after shunt treatment in chronic hydrocephalus--a quantitative PET-study. *Acta neurochirurgica. Supplement.* 2002;81:55-57.

304. Vorstrup S, Christensen J, Gjerris F, Sorensen PS, Thomsen AM, Paulson OB. Cerebral blood flow in patients with normal-pressure hydrocephalus before and after shunting. *J Neurosurg.* Mar 1987;66(3):379-387.

305. de Laat KF, Tuladhar AM, van Norden AG, Norris DG, Zwiers MP, de Leeuw FE. Loss of white matter integrity is associated with gait disorders in cerebral small vessel disease. *Brain.* Jan 2011;134(Pt 1):73-83.

306. Kennedy KM, Raz N. Aging white matter and cognition: differential effects of regional variations in diffusion properties on memory, executive functions, and speed. *Neuropsychologia.* Feb 2009;47(3):916-927.

307. de Groat WC. A neurologic basis for the overactive bladder. *Urology.* Dec 1997;50(6A Suppl):36-52; discussion 53-36.

308. Kushner M, Younkin D, Weinberger J, Hurtig H, Goldberg H, Reivich M. Cerebral hemodynamics in the diagnosis of normal pressure hydrocephalus. *Neurology.* Jan 1984;34(1):96-99.

309. Hayashi M, Kobayashi H, Kawano H, Yamamoto S, Maeda T. Cerebral blood flow and ICP patterns in patients with communicating hydrocephalus after aneurysm rupture. *J Neurosurg.* Jul 1984;61(1):30-36.

310. Mathew NT, Meyer JS, Hartmann A, Ott EO. Abnormal cerebrospinal fluid-blood flow dynamics. Implications in diagnosis, treatment, and prognosis in normal pressure hydrocephalus. *Archives of neurology.* Oct 1975;32(10):657-664.

311. Klinge P, Berding G, Brinker T, Weckesser E, Knapp WH, Samii M. Regional cerebral blood flow profiles of shunt-responder in idiopathic chronic hydrocephalus--a 15-O-water PET-study. *Acta neurochirurgica. Supplement.* 2002;81:47-49.

312. Knutsson L, Wirestam R, Petersen ET, et al. Absolute quantification of cerebral blood flow using dynamic susceptibility contrast MRI: a comparison with model-free arterial spin labeling. *25th Annual Meeting of the European Society for Magnetic Resonance in Medicine and Biology* 2008;318.

313. Kjolby BF, Mikkelsen IK, Pedersen M, Ostergaard L, Kiselev VG. Analysis of partial volume effects on arterial input functions using gradient echo: a simulation study. *Magn Reson Med.* Jun 2009;61(6):1300-1309.

314. van Osch MJ, van der Grond J, Bakker CJ. Partial volume effects on arterial input functions: shape and amplitude distortions and their correction. *Journal of magnetic resonance imaging : JMRI.* Dec 2005;22(6):704-709.

315. Sasaki H, Ishii K, Kono AK, et al. Cerebral perfusion pattern of idiopathic normal pressure hydrocephalus studied by SPECT and statistical brain mapping. *Annals of nuclear medicine.* Jan 2007;21(1):39-45.

316. Chen YF, Wang YH, Hsiao JK, et al. Normal pressure hydrocephalus: cerebral hemodynamic, metabolism measurement, discharge score, and long-term outcome. *Surg Neurol.* Dec 2008;70 Suppl 1:S1:69-77; discussion S61:77.

317. Kobayashi S, Tateno M, Utsumi K, Takahashi A, Morii H, Saito T. Two-layer appearance on brain perfusion SPECT in idiopathic normal pressure hydrocephalus: a qualitative analysis by using easy Z-score imaging system, eZIS. *Dementia and geriatric cognitive disorders.* 2009;28(4):330-337.

318. Yoon B, Yang DW, Shim YS, et al. Voxel-based analysis of Tc-99m ECD brain perfusion SPECT in patients with normal pressure hydrocephalus. *Applied radiation and isotopes : including data, instrumentation and methods for use in agriculture, industry and medicine.* Jul-Aug 2009;67(7-8):1377-1381.

319. El Sankari S, Gondry-Jouet C, Fichten A, et al. Cerebrospinal fluid and blood flow in mild cognitive impairment and Alzheimer's disease: a differential diagnosis from idiopathic normal pressure hydrocephalus. *Fluids and barriers of the CNS.* 2011;8(1):12.

320. Ishii K, Hashimoto M, Hayashida K, et al. A multicenter brain perfusion SPECT study evaluating idiopathic normal-pressure hydrocephalus on neurological improvement. *Dementia and geriatric cognitive disorders.* 2011;32(1):1-10.

321. Kuriyama N, Tokuda T, Yamada K, et al. Flow velocity of the superior sagittal sinus is reduced in patients with idiopathic normal pressure hydrocephalus. *Journal of neuroimaging : official journal of the American Society of Neuroimaging.* Oct 2011;21(4):365-369.

322. Yamada SM, Masahira N, Kawanishi Y, Fujimoto Y, Shimizu K. Preoperative acetazolamide SPECT is useful for predicting outcome of shunt operation in idiopathic normal pressure hydrocephalus patients. *Clinical nuclear medicine.* Sep 2013;38(9):671-676.

323. Mori K, Maeda M, Asegawa S, Iwata J. Quantitative local cerebral blood flow change after cerebrospinal fluid removal in patients with normal pressure hydrocephalus measured by a double injection method with N-isopropyl-p-[(123)I] iodoamphetamine. *Acta neurochirurgica.* Mar 2002;144(3):255-262; discussion 262-253.

324. Dumarey NE, Massager N, Laureys S, Goldman S. Voxel-based assessment of spinal tap test-induced regional cerebral blood flow changes in normal pressure hydrocephalus. *Nuclear medicine communications.* Sep 2005;26(9):757-763.

325. Virhammar J, Laurell K, Ahlgren A, Cesarini KG, Larsson EM. Idiopathic normal pressure hydrocephalus: cerebral perfusion measured with pCASL before and repeatedly after CSF removal. *J Cereb Blood Flow Metab.* Nov 2014;34(11):1771-1778.

12 APPENDIX

Table 7. Preoperative CBF studies in NPH, performed since 2000. Methods and baseline findings.

Reference	Diagnosis	Method	Main parameter	Subgroups	Baseline findings
Bateman [103] 2002	NPH	Phase contrast MRI	arterial, venous CBF	18 NPH, 60 idiopathic dementia wo/w leukoaraiosis, 18 HI	CBF reduced in NPH and idiopathic dementia, no CBF difference between dementia groups; mild to moderate LA: increased cortical vein compliance; severe LA and NPH: decreased compliance
Klinge et al.[311] 2002	iNPH	15-O-H2OPET, at rest/after acetazolamide	reg CBF, CVR	5 responders, 6 non-responders	CBF reduced in fronto-basal cortex in responders; CVR decreased in various cortical regions in responders (temporo-dorsal, limbic, fronto-basal)
Owler et al.[216] 2004	iNPH/NPH	15-O-H2OPET, MRI co-registration	g and reg CBF	12 iNPH, 5 sNPH, 12 HI	gCBF reduced in cerebellum and cerebrum; reg CBF not reduced in WM, but in thalamus, putamen, caudate head; positive correlation in iNPH: CBF in thalamus and putamen to clinical performance
Owler et al.[217] 2004	NPH	15-O-H2OPET, at rest/after CSF infusion, MRI co- registration	g and reg CBF	12 iNPH, 3 sNPH	After infusion test: gCBF reduced in cerebrum and cerebellum; reg CBF reduced in WM, caudate head, thalamus
Momjian et al.[115] 2004	iNPH	15-O-H2OPET, at rest/after CSF infusion, MRI co- registration	g and reg CBF	12 iNPH, 10 HI	At rest global CBF reduced, reduced reg CBF in WM increasing w distance from ventricles; after infusion: impaired autoregulation, particularly in paraventricular watershed WM
Sasaki et al.[315] 2007	iNPH	(123I)-IMP SPECT, 3D-SSP	CBF z-scores	30 iNPH, 30 AD, 15 HI	CBF reduced in frontal and parieto-temporal lobes as compared to HI; reduced CBF in corpus callosum and Sylvian fissures as compared to HI and AD based on dilated subarachnoidal space/ventriculomegaly
Bateman, Loiselle[207] 2007	iNPH	Phase -contrast MRI	arterial, venous CBF, ASV	20 responders, 12 non-responders, 12 AD, 12 HI	No difference between responders and non-responders; reduced arterial and venous CBF, AVD, compliance ratio, increased ASV as compared to HI; as compared to AD reduced venous CBF, compliance ratio
Bateman[206] 2008	iNPH	Phase -contrast MRI	arterial, venous CBF, ASV	20 NPH w arterial CBF above normal, 12 HI	No difference in total venous outflow, but superficial venous sinus outflow in % of inflow reduced, reduced AVD and increased ASV
Chen et al.[316] 2008	NPH	Stable Xenon CT, at rest/after acteazolamide	reg CBF, CVR	23 responders, 5 non-responders	CBF, CVR, NAA/Cr in centrum semiovale not different between groups; post ACT CBF and CVR higher in responders in the anterior centrum semiovale; positive correlation: pre-op CBF, post ACT CBF, CVR to post-op clinical performance
Kobayashi et al.[317] 2009	iNPH	99m TC-ECD SPECT, eZIS	CBF z-scores	12 iNPH, 10 AD	iNPH: 2 layers w reduced CBF around corpus callosum, increased CBF outside cingulus; AD: reduced CBF in precuneus and/or posterior cingulus
Yoon et al.[318] 2009	iNPH	99m TC-ECD SPECT, SPM and SPAM	CBF z-scores	10 iNPH, 13 HI	Decreased CBF mainly in prefrontal and subcortical areas (bilateral thalami, right prefrontal, bilateral cingulate gyrus, right caudate head, left parahippocampus)
Takaya et al.[285] 2010	iNPH	(123I)-IMP SPECT, ARG	reg CBF	7 iNPH w few symptoms, 7 iNPH w triad (34 HI)	CBF reduced in 35 ROI compared to HI; CBF in frontal WM lower in iNPH w triad than in iNPH w few symptoms; no other differences between iNPH subgroups
ElSankari et al.[319] 2011	iNPH	Phase -contrast MRI	arterial, venous CBF, ASV	13 iNPH, 10 MCI, 9 AD, 12 HI	Arterial and venous CBF reduced as compared to MCI, but not to HI or AD; aqueductal stroke volume increased compared to AD, HI but not MCI; AVD reduced as compared to HI, but not MCI, AD
Ishii et al.[320] 2011	iNPH	(123I)-IMP SPECT, 3-D SSP	CBF z-scores	71 responders, 13 non-responders, 38 HI	iNPH CBF reduction patterns: anterior, mixed, posterior; compared to HI reduced CBF frontal, parieto-temporal lobes and "2 layer" appearance around corpus callosum and cingulus; no difference between responders and non-responders
Sakakibara et al.[222] 2012	iNPH	(123I)-IMP SPECT, 3-D SSP	CBF z-scores	97 iNPH w severe or mild urinary dysfunction	Severe urinary dysfunction: decreased CBF in the frontal, mainly right cortex and left inferior temporal gyrus
Bateman, Siddiqe[208] 2014	chronic communi-cating HC	Phase-contrast MRI, 2D-TOF MRI venography	venous CBF, area of transverse sinus	20 HC, 10 young HI, 20 elderly HI	Venous CBF reduced, cross-sectional area reduced, venous pressure increased as compared to elderly HI

Table 8. Postoperative CBF studies in NPH, performed since 2000. Methods and findings.

Reference	Diagnosis	Method	Main parameter	Follow-up	Subgroups	Baseline findings	Post-op changes
Bateman[104] 2000	NPH	Phase contrast MRI	arterial, venous flow	?	5 responders, 5 NPH wo op, 20 ischemia/ atrophy, 7 HI	Superficial venous sinus compliance in NPH decreased and superficial venous CBF reduced as compared to HI, ischemia/ atrophy	Superficial venous sinus compliance and CBF increase
Klinge et al.[227] 2002	NPH?	15-O-H2OPET, at rest/after acetazolamide	g cortical CBF, CVR	7d, 7m	31 responders, 29 non-responders	CBF lower in responders, CVR not different	No CBF change; CVR increase in responders, decrease in non-responders
Klinge et al.[229] 2002	iNPH	15-O-H2OPET, at rest/after acetazolamide	g cortical CBF, CVR	7d, 7m	27 responders, 26 non-responders (vascular high risk 26, low risk 27)	High vascular risk factor group: CBF lower in responders, CVR marginal in both groups; Low risk group: CBF not different, CVR lower in responders	No CBF change; high vascular risk factor group: CVR increase in responders; low risk group: CVR decrease in non-responders
Klinge et al.[103] 2002	iNPH	15-O-H2OPET, at rest/after acetazolamide	g cortical CBF, CVR	7d, 7m	27 patients; 26 shunted, 1 ETV (response not stated)	No correlation between neuropsychology and hemodynamics	7d: Positive correlation gait to CVR, negative to CBF; 7m: Positive correlation visual attention and verbal memory to CVR, negative to CBF
Mataro et al.[221] 2003	iNPH	(99mTc)-HMPAO SPECT, SPM	CBF z-scores	6m	14 responders, 1 non-responder	Not evaluated	CBF increase: left prefrontal dorsolateral, right frontal premotor, right frontal WM, right frontal medial, right basal ganglia, right inferior parietal lobule; positive correlation: CBF in anterior cingulus and left insula to clinical performance
Corkill et al.[208] 2003	iNPH	DSC MRI, DWI	rrCBV, ADC	7-42ws	5 responders, 6 non-responders	Periventricular rCBV reduced, not different between groups; periventricular ADC elevated in non-responders	No CBV change; no post-op DWI performed
Tullberg et al.[223] 2004	NPH	(99mTc)-HMPAO SPECT	rrCBF	3m	21 responders, 7 non-responders, 21 HI	rrCBF reduced in mesencephalon, hippocampus, basal frontal cortex, anterior cingulus; patients without impaired wakefulness: No rrCBF reduction in anterior cingulus	rrCBF increase 4-7% in thalamus, frontal association cortex, hippocampus; negative correlation: rrCBF frontal association cortex to impaired wakefulness
Takeuchi et al.[226] 2007	iNPH	(123I)-IMP SPECT	g and reg CBF	1m	40 responders, 4 non-responders	CBF reduced in cortex or thalamus-basal ganglia or both	CBF increase 60-85%: in cortex, thalamus- basal ganglia or both
Murakami et al.[225] 2007	iNPH	(123I)-IMP SPECT, 3D-SSP	CBF z-scores	10-36m	14 responders, 10 non-responders	CBF reduced in basal frontal lobes and anterior cingulus in responders	CBF increase in basal frontal lobe and anterior cingulus in responders
Miyamoto et al.[228] 2007	iNPH	15-O-H2O PET	reg CBF, reg CBV, rOEF, rCMRO2	5-60m	5 responders, 3 non-responders	Not evaluated	rCMRO2 increase in responders in frontal WM, thalamus, putamen; rOEF decrease in same regions in non-responders; no CBF or CBV changes in subgroups

Klinge et al.[220] 2008	iNPH	15-O-H2O PET, SPM	g and reg CBF	7-10d	36 responders, 29 non-responders	CBF not different between groups; positive correlation: uptake in basal, anterior, mesial frontal area or anterior, left temporal cortex to clinical performance	No change in mean global CBF; CBF decrease in superior mesial frontal area in non-responders; CBF increase in superior (mesial) frontal cortex in responders
Chang et al.[224] 2009	iNPH	(99mTc)-HMPAO SPECT, at rest/ after acetazolamide, ARG and 3D-SSP	g CBF, CVR	3-6m	146 responders, 16 non-responders, 13 HI	CBF not different between groups; CVR impaired in responders	CBF and CVR increase in responders
Kuriyama et al.[321] 2011	iNPH	Phase -contrast MRI venography	venous flow velocity	3-4ws	11 responders, 9 iNPH wo op, 24 HI	iNPH: Maximum venous velocity lower and more extensive decrease of velocity during valsalva	Improved venous velocity
Yamada et al.[322] 2013	iNPH	99m TC-ECD SPECT after acetazolamide	reg CBF, CVR	1m	25 iNPH, 10 ventriculomegaly, 30 HI	iNPH: same CBF reduction as in ventriculomegaly; if CVR less than 20% the postop cognitive improvement is better than if CVR > 40%; CVR normal in HI, ventriculomegaly	No CBF increase at rest; CVR normalizes if pre-op CVR <20%

Table 9. Studies of CBF in NPH since 2000: results of spinal tap test

Reference	Diagnosis	Method	Main parameter	Follow-up	Subgroups	Baseline findings	Post STT changes
Mori et al.[323] 2002	NPH	(123I)-IMP SPECT before/after STT	g and reg CBF	1m	15 responders, 7 non-responders	CBF not different between groups	reg and g CBF increase significantly in responders; less than 20% CBF change indicate non-responder
Hertel et al.[213] 2003	iNPH	(99mTc)-bicisate SPECT DSC MRI, before/after STT	rrCBF, NI	3m	27 iNPH, 15 op, 15 responders	Not evaluated	Increase of CBF (SPECT), NI (DSC MRI) in 18 pat., clinical improvement in 9; good post-op outcome even in pat. selected for op based only on imaging
Dumarey et al.[324] 2005	NPH	(99mTc)-HMPAO SPECT, SPM, before/after STT	rrCBF	3m	40 NPH,14 op, 13 responders	Not evaluated	CBF increase in middle frontal gyrus and left parahippocampus in pat. with improved gait
Walter et al.[214] 2005	iNPH	DSC MRI, before/after STT	NI, IM, TTP, T0, MTT	3m	28 iNPH, 14 op, 14 responders	NI lower in pat who show NI increase after STT	Increased NI, TTP-T0 in 16 pat., clinical improvement in 7; good post-op outcome even in pat. selected for op based only on imaging
Virhammar et al.[325] 2014	iNPH	pCASL, before/after STT	CBF	/	20 iNPH	No correlation CBF to clinical performance	No significant CBF increase; no correlation CBF to clinical performance

Abbreviations tables 7-9: ACT: acetazolamide, AD: Alzheimer´s disease, ARG: autoradiography, ASV: aqueductal stroke volume, AVD: ateriovenous delay, CBF: absolute cerebral blood flow, Cr: creatine, CVR: cerebrovascular reactivity, d: day, ETV: Endoscopic third ventriculostomy, eZIS: easy Z score imaging system, g: global, HC: hydrocephalus , HI: healthy individuals, IM: index map representing rCBF, LA: leukoaraiosis, MCI: mild cognitive impairment, m: month, NAA: N-acetylaspartate, NI: negative interval representing rCBV, rCMRO2: regional cerebral metabolic rate of oxygen, reg: regional, rOEF: regional oxygen extraction fraction, rr: relative regional, SPAM: statistical probabilistic brain anatomic map, SPM: statistical parametric mapping, STT: spinal tap test, TO: time of arrival, TOF: time of flight, Triad: triad of symptoms (disturbed gait, cognition, continence), TTP: time to peak, Pat.: patient, pCASL: pseudo-continuous arterial spin labeling, ws: week, w: with, WM: white matter, wo: without, z-score: standard score, [123I]IMP SPECT: N-isopropyl-(123I)-P-iodo-amphetamine SPECT, 3D-SSP: 3D stereotactic surface projection, 99m TC-ECD SPECT: 99m Technetium- ethylcysteinate SPECT, 99mTc-HMPAO SPECT: 99 technetium-hexamethylpropyleneamine oxime SPECT